

Statistical Study of the *Swift* X-ray Flash and X-ray Rich Gamma-Ray Bursts

Xiongwei Bi^{1,2}, Jirong Mao^{3,4,2}, Chuanxi Liu^{3,4,5}, and Jin-Ming Bai^{3,4,2}

jirongmao@mail.ynao.ac.cn

ABSTRACT

We build a comprehensive sample to statistically describe the properties of X-ray flashes (XRFs) and X-ray riches (XRRs) from the latest third *Swift* Burst Alert Telescope (BAT3) catalog of Gamma-ray bursts (GRBs). We obtain 81 XRFs, 540 XRRs, and 394 classical GRBs (C-GRBs). We statistically explore the different properties of the γ -ray prompt emission, the X-ray emission, the X-ray lightcurve type, the association with supernovae (SNe), and the host galaxy properties for these sources. We confirm that most XRFs/XRRs are long GRBs with low values of peak energy E_{peak}^{obs} and they are low-luminosity GRBs. XRFs, XRRs, and C-GRBs follow the same $E_{X,iso}-E_{\gamma,iso}-E_{peak,z}$ correlations. Compared to the classical GRBs, XRFs are favorable to have the association with SN explosions. We do not find any significant differences of redshift distribution and host galaxy properties among XRFs, XRRs, and C-GRBs. We also discuss some observational biases and selection effects that may affect on our statistical results. The GRB detectors with wide energy range and low energy threshold are expected for the XRF/XRR research in the future.

Subject headings: gamma rays: general — radiation mechanisms: non-thermal

¹Department of Physics, Honghe University, 661199 Mengzi, China

²Key Laboratory for the Structure and Evolution of Celestial Objects, Chinese Academy of Sciences, 650011 Kunming, China

³Yunnan Observatories, Chinese Academy of Sciences, 650011 Kunming, Yunnan Province, China

⁴Center for Astronomical Mega-Science, Chinese Academy of Sciences, 20A Datun Road, Chaoyang District, 100012 Beijing, China

⁵University of Chinese Academy of Sciences, 100049 Beijing, China

1. Introduction

In addition to the classical long/short dichotomy, gamma-ray bursts (GRBs) have two special subclasses: X-ray flashes (XRFs) and X-ray riches (XRRs). XRFs are the GRBs characterized by the faint signals in the gamma-ray energy band. XRRs, which belong to an intermediate class between XRFs and classical GRBs (C-GRBs), have stronger X-ray emission compared to their gamma-ray emission (e.g, Barraud et al. 2003; Kippen et al. 2003; Amati et al. 2004; Sakamoto et al. 2005, 2008; D’Alessio et al. 2006). The physical origin of XRFs and XRRs are still under debate.

XRF 050406 was proposed as a GRB with prolonged central engine activity (Romano et al. 2006). This long-term activity was also observed in XRF 011030 (Galli & Piro 2006). GRB jet structure affects on the observed GRB energy release, and the off-axis effect may induce the observed XRFs/XRRs (e.g., Yamazaki et al. 2002; Barraud et al. 2005; Granot et al. 2005; Lamb et al. 2005; Xu et al. 2005; Donaghy 2006; Salafia et al. 2016). Observations have provided some further evidence for the off-axis jet injection (e.g., Bulter et al. 2005; Schady et al. 2006; de Ugarte Postigo 2007; Guidorzi et al. 2009). A dynamic transition with a different GRB jet opening angle may also be important to link C-GRBs and XRFs (Mizuta et al. 2006). Alternatively, thermal emission has been thought to be a possible component in the strong X-ray emission of GRBs. Ramirez-Ruiz (2005) proposed a photospheric model that can be used to interpret the dominated X-ray emission of XRFs. Pe’er et al. (2006) calculated the details of the photospheric component of the XRF prompt emission spectrum. XRFs can also be the indicators of the orphan GRB afterglows (Urata et al. 2015). These clues naturally lead to one suggestion that XRFs are low-luminosity GRBs (e.g., Virgili et al. 2009). Moreover, it has been found that supernova (SN) explosions can be associated with XRFs (e.g., XRF 020903, Bersier et al. 2006).

XRF 050215B was the first XRF observed by *Swift* (Levan et al. 2006), and *Swift* observational statistics can be well applied to study the physical origins of XRFs and XRRs (Gendre et al. 2007). Sakamoto et al. (2008) built one dataset provided by the *Swift* Burst Alert telescope (BAT) observation from 2004 December to 2006 September. From that sample, they obtained 10 XRFs and 97 XRRs among a total of 158 GRBs. They studied the prompt emission properties and the X-ray afterglow emission characteristics for XRFs, XRRs, and C-GRBs. Some distinct differences between XRFs and C-GRBs in the prompt emission and the X-ray afterglow emission have been illustrated. This exploration encourages us to comprehensively investigate the physical properties of XRFs/XRRs, the relation between XRFs/XRRs and C-GRBs, and the GRB central engine from the statistical point of view. Thus, a large GRB sample is necessary.

We utilize the latest third *Swift*-BAT3 catalog (Lien et al. 2016), which contains 1104

GRBs detected from 2004 December 17 to 2016 December 2, to systematically investigate the statistical properties of XRFs and XRRs. For each GRB, the catalog provides trigger time, coordinates, redshift, GRB duration time T_{90} , spectral models for spectral fitting, spectral photon index, observed peak energy E_{peak} , and fluence in difference energy bands. From this catalog, we classify the possible XRFs/XRRs and build a sample to comprehensively analyze the differences of XRFs/XRRs and C-GRBs. We identify 81 XRFs, 540 XRRs, and 394 C-GRBs included in the sample and statistically analyze their observational characteristics. We examine the possible associations between XRFs/XRRs and SNe. The host galaxy properties of XRFs are also presented. Some observational biases and selection effects are mentioned.

This paper is organized as follows. We classify XRFs, XRRs, and C-GRBs in Section 2. In Section 3, we present the different properties of XRFs, XRRs, and C-GRBs, respectively. A discussion is provided in Section 4, and conclusions are listed in Section 5. We adopt the cosmological parameters as $H_0 = 70 \text{ km s}^{-1} \text{ Mpc}^{-1}$, $\Omega_\Lambda = 0.7$, and $\Omega_M = 0.3$. The quoted errors are at the 90% confidence level unless stated otherwise.

2. Sample Selection

We classify XRFs, XRRs, and C-GRBs using the criteria provided by Sakamoto et al. (2008). The definitions of XRF, XRR, and C-GRB based on the fluence ratio of $S(25 - 50 \text{ keV})$ and $S(50 - 100 \text{ keV})$ are:

$$\begin{aligned} S(25 - 50 \text{ keV})/S(50 - 100 \text{ keV}) &\leq 0.72 && \text{(C - GRB)}, \\ 0.72 < S(25 - 50 \text{ keV})/S(50 - 100 \text{ keV}) &\leq 1.32 && \text{(XRR)}, \\ S(25 - 50 \text{ keV})/S(50 - 100 \text{ keV}) &> 1.32 && \text{(XRF)}. \end{aligned} \tag{1}$$

We obtain 81 XRFs, 540 XRRs, and 394 C-GRBs in the *Swift*-BAT3 catalog by the selection condition of Equation (1). We summarize the selection results in Table 1. We further consider three additional conditions. First, in order to compare the prompt emission and the X-ray afterglow emission of each XRF/XRR, we exclude 89 sources that have no *Swift* X-ray Telescope (XRT) data. Thus, we do not classify these sources as XRFs, XRRs, or C-GRBs. We also specify that 13 sources in our sample have no GRB duration T_{90} numbers. Thus, we cannot classify them as long-duration GRBs (L-GRBs, defined by $T_{90} \geq 2 \text{ s}$) or short-duration GRBs (S-GRBs, defined by $T_{90} \leq 2 \text{ s}$). Second, we also select GRBs that have the photon index $\alpha_{PL} < -2.0$ with a power-law fitting in the BAT3 dataset and identify them as XRFs. Third, we note the sources having values of E_{peak}^{obs} , which can be found in the BAT3 dataset. We also check whether these selected sources have E_{peak}^{obs} values in other datasets. Finally, we list XRFs and XRRs in Table 2.

The distributions with the fluence ratio of $S(25-50 \text{ keV})/S(50-100 \text{ keV})$ for the total 1015 GRBs in the BAT3 catalog are shown in Figure 1. XRFs, XRRs, and C-GRBs in the sample have the fractions of $(8.0 \pm 0.9)\%$, $(53.2 \pm 2.2)\%$, and $(38.8 \pm 1.9)\%$, respectively. The smaller sample given by Sakamoto et al. (2008) contains 158 GRBs. There are 10 XRFs, 97 XRRs, and 51 C-GRBs. XRFs, XRRs, and C-GRBs in their sample have the fractions of $(6.3 \pm 2.0)\%$, $(61.4 \pm 6.2)\%$, and $(32.3 \pm 4.5)\%$, respectively. It seems that our classified results are roughly consistent with those of Sakamoto et al. (2008). Here, we pay attention to four special cases: (1) GRB 050219B was identified as XRR by Sakamoto et al. (2008), while it is classified as C-GRB in our work. (2) GRB 050815 was identified as XRR by Sakamoto et al. (2008), while it is classified as XRF in our work. (3) There are 10 GRBs (GRB 050824, GRB 060512, GRB 060923B, GRB 060926, GRB070714A, GRB070721A, GRB080218B, GRB080515, GRB080520, and GRB081007) that have no fluences of $S(25-50 \text{ keV})$ and/or $S(50-100 \text{ keV})$ in BAT3 catalog, and we find the fluences of $S(25-50 \text{ keV})$ and/or $S(50-100 \text{ keV})$ from the *Swift*-BAT2 catalog (Sakamoto et al. 2011). (4) There are 11 XRFs (XRF 050406, XRF 050416A, XRF 050819, XRF 060428B, XRF 060805A, XRF 061218, XRF 070126, XRF 080218B, XRF 080315, XRF 080822B, and XRF 160525A) show a fluence ratio of $S(25-50 \text{ keV})/S(50-100 \text{ keV})$ larger than 3.0¹.

We plot the fluence ratio $S(25-50 \text{ keV})/S(50-100 \text{ keV})$ versus the BAT-observed GRB duration T_{90} in Figure 2. We calculate the fractions of L-GRBs and S-GRBs for XRFs, XRRs, and C-GRBs in our sample, respectively. Our findings are as follows: (1) For XRFs, there are 70 L-GRBs, 3 S-GRBs, and 8 duration-unclear sources, and the fractions are $(86.4 \pm 10.3)\%$, $(3.7 \pm 2.1)\%$, and $(9.9 \pm 3.5)\%$, respectively. (2) For XRRs, there are 509 L-GRBs, 27 S-GRBs, and 4 duration-unclear sources, and the fractions are $(94.3 \pm 4.2)\%$, $(5.0 \pm 1.0)\%$, and $(0.7 \pm 0.4)\%$, respectively. (3) For C-GRBs, there are 328 L-GRBs, 65 S-GRBs, and 1 duration-unclear source, and the fractions are $(83.2 \pm 4.6)\%$, $(16.5 \pm 2.0)\%$, and $(0.3 \pm 0.3)\%$, respectively. We note that XRFs and XRRs have less S-GRB proportion compared with C-GRBs². In the meantime, we also report the fraction of XRFs, XRRs, and C-GRBs for L-GRB and S-GRB classes. Three S-GRBs as XRFs have the fraction of $(3.2 \pm 1.8)\%$. Twenty-seven S-GRBs as XRRs have the fraction of $(28.4 \pm 5.5)\%$. Sixty-five S-GRBs as C-GRBs have the fraction of $(68.4 \pm 8.5)\%$. Seventy L-GRBs as XRFs have

¹XRF 080315 has the largest fluence ratio of 53.8 ± 143.0 but with large error. This source has no X-ray afterglow from *Swift*-XRT detection. Due to the lack of X-ray nondetection and the marginal BAT detection (Page & Gehrels 2008), we include this source in Table 1, 2 and 3, but we exclude it in all Figures of this paper. We also do not find any other notable issues for this burst.

²There are only three XRFs (XRF 090417A, XRF 110112A, and XRF 140622A) that are S-GRBs. GRB 110112A has no host galaxy evidence (Fong et al. 2013; Tunnicliffe et al. 2014). We do not find any other notable information for the short-duration XRFs.

the fraction of $(7.7 \pm 0.9)\%$. Five hundred and nine L-GRBs as XRRs have the fraction of $(56.1 \pm 2.5)\%$. Three hundred and twenty-eight L-GRBs as C-GRBs have the fraction of $(36.2 \pm 2.0)\%$.

3. Statistical Analysis

3.1. The Prompt Emission Properties

We collect E_{peak}^{obs} values of GRBs from the literature (e.g., Amati et al. 2008, 2009; Sakamoto et al. 2008, 2011; Grupe et al. 2013; D’Avanzo et al. 2014; Liang et al. 2015; Lien et al. 2016; Zaninoni et al. 2016), and we obtain the E_{peak}^{obs} values for 77 XRFs, 460 XRRs, and 265 C-GRBs. The fluence ratio $S(25-50 \text{ keV})/S(50-100 \text{ keV})$ versus E_{peak}^{obs} is shown in Figure 3. We clearly see the different occupied regions of XRFs, XRRs, and C-GRBs in the Figure. It was shown in the fluence ratio- E_{peak}^{obs} plot provided by Sakamoto et al. (2008) a gap of $S(25-50 \text{ keV})/S(50-100 \text{ keV})$ fluence ratio from 0.8 to 1.2, and Sakamoto et al. (2008) suggested that this gap is the result of selection effects. However, we do not find this gap in Figure 3, because we take a large sample from the BAT3 catalog. We further show the different E_{peak}^{obs} distributions for XRFs, XRRs, and C-GRBs in Figure 4. In order to quantitatively distinguish the different E_{peak}^{obs} properties to XRFs, XRRs, and C-GRBs, we use a nonparametric two-sample Kolmogorov-Smirnov (K-S) test to examine the different E_{peak}^{obs} distributions for the XRF/XRR samples, the XRR/C-GRB samples, and the XRF/C-GRB samples, respectively. Because the K-S probability numbers are very small (the P -values are far less than 0.0001), we confirm that the E_{peak}^{obs} distributions among XRFs, XRRs, and C-GRBs have significant differences.

The E_{peak}^{obs} distribution of XRFs ranges from 0.9 keV to 80.0 keV, with a mean value of 24.3 ± 1.6 keV. The E_{peak}^{obs} distribution of XRRs ranges from 1.2 keV to 1780.0 keV, with a mean value of 105.6 ± 5.3 keV. The E_{peak}^{obs} distribution of C-GRBs ranges from 64.6 keV to 2602.8 keV, with a mean value of 257.7 ± 14.1 keV. It is clear that XRFs and XRRs have smaller E_{peak}^{obs} values compared with C-GRBs. Our results are consistent with those of Sakamoto et al. (2005, 2008). We confirm that XRFs and XRRs release their prompt energies mostly in the X-ray band.

We also investigate the correlation between peak energy E_{peak}^{obs} and the fluence $S(15-150 \text{ keV})$ for all GRBs in our sample. The data are plotted in Figure 5. In principle, the effect of the data errors should be taken into account when we perform the correlation fitting. In this paper, we adopt the maximum likelihood method that has been well applied for the $E_{peak,z}-E_{\gamma,iso}$ correlation fitting given by Amati et al. (2008). We use the maximum

likelihood method and obtain the correlation fitting as $\log(E_{peak}^{obs})(\text{keV})=(2.96 \pm 0.13) + (0.16 \pm 0.02) \log[S(15 - 150)]\text{keV}$ with the extrinsic scatter $\sigma = 0.39 \pm 0.01$. We also plot the correlation of $\log(E_{peak}^{obs})(\text{keV})=(5.46 \pm 0.25) + (0.62 \pm 0.14) \log[S(15 - 150)\text{keV}]$ that was given by Sakamoto et al. (2008). We see that our fitting result is different from that of Sakamoto et al. (2008). In order to clarify the difference of this correlation among XRFs, XRRs, and C-GRBs, we separate C-GRBs as one group and put XRRs and XRFs as the other group. We obtain the fitting for C-GRBs as $\log(E_{peak}^{obs})(\text{keV})=(3.01 \pm 0.13) + (0.12 \pm 0.02) \log[S(15 - 150)]\text{keV}$ with the extrinsic scatter $\sigma = 0.26 \pm 0.01$, and the fitting for XRRs and C-GRBs as $\log(E_{peak}^{obs})(\text{keV})=(2.67 \pm 0.16) + (0.13 \pm 0.03) \log[S(15 - 150)]\text{keV}$ with the extrinsic scatter $\sigma = 0.36 \pm 0.01$. Therefore, although the difference between XRFs and XRRs/C-GRBs is clear, it seems no significant difference between XRFs/XRRs and C-GRBs because XRRs and C-GRBs has large overlap region seen in Fig. 5.

3.2. The Observed Properties with Redshift

The redshift distributions of the XRFs, XRRs, and C-GRBs are shown in Figure 6. Using the K-S test to the redshift distributions for the XRFs and XRRs samples, the XRRs and C-GRBs samples, and the XRFs and C-GRBs samples, we find that K-S test probabilities are $P = 0.13$, $P = 0.36$, and $P = 0.13$, respectively. The K-S test results confirm that there are not significant differences among XRFs, XRRs, and C-GRBs for the redshift distribution.

We also plot the BAT-observed duration T_{90} and the fluence $S(15-150 \text{ keV})$ as a function of redshift in Figure 7 and Figure 8, respectively. We do not find significant differences of T_{90} and $S(15-150 \text{ keV})$ distributions among XRFs, XRRs, and C-GRBs, and we do not see significant redshift evolutions of T_{90} and $S(15-150 \text{ keV})$ for XRFs, XRRs, and C-GRBs.

3.3. The Correlations among $E_{X,iso}$, $E_{\gamma,iso}$, and $E_{peak,z}$

There is a universal correlation among the isotropic prompt energy $E_{\gamma,iso}$ emitted in the rest frame $1 - 10^4 \text{ keV}$ energy band, the rest frame energy peak of the prompt emission energy spectrum $E_{peak,z}$ in which $E_{peak,z}=(1+z)E_{peak}^{obs}$, and the X-ray energy emitted in the rest frame $0.3 - 10 \text{ keV}$ energy band $E_{X,iso}$ for GRBs (e.g., Bernardini et al. 2012; Margutti et al. 2013; D’Avanzo et al. 2014; Zaninoni et al. 2016). In order to check whether XRFs, XRRs, and C-GRBs in our sample follow this correlation, respectively, we collect the $E_{\gamma,iso}$ and $E_{X,iso}$ data of the GRBs in our sample from Amati et al. (2008), Margutti et al. (2013), and Liang et al. (2015). First, the relation between $E_{X,iso}$ and

$E_{\gamma,iso}$ is shown in Figure 9. We perform the maximum likelihood method and obtain the fitting of $(E_{X,iso}) = (13.31 \pm 2.73) + (0.73 \pm 0.05)\log(E_{\gamma,iso})$ with the extrinsic scatter of $\sigma = 0.57 \pm 0.04$. The $E_{X,iso}-E_{\gamma,iso}$ relation is consistent with that derived by Margutti et al. (2013). Second, we also investigate the correlation between $E_{peak,z}$ and $E_{\gamma,iso}$. The result is shown in Figure 10. The correlation fitted by the maximum likelihood method is $\log(E_{peak,z})(\text{keV})=(2.17 \pm 0.04) + (0.46 \pm 0.03) \log[E_{\gamma,iso}/(10^{52} \text{erg})]$ with the extrinsic scatter of $\sigma = 0.26 \pm 0.02$. Our result is consistent with the correlation reported by Amati (2006). Third, in Figure 11, we present the relation between $E_{X,iso}$ and $E_{peak,z}$ by the maximum likelihood method with the fitting of $\log(E_{X,iso}) = (49.69 \pm 0.27) + (0.75 \pm 0.11)\log(E_{peak,z})$, and the extrinsic scatter is $\sigma = 0.73 \pm 0.04$. Our result is consistent with that of Margutti et al. (2013). Finally, the $E_{X,iso}-E_{\gamma,iso}-E_{peak,z}$ relation is shown in Figure 12. The result with the fitting of $\log(E_{X,iso}) = (4.78 \pm 2.79) + (0.92 \pm 0.06)(\log E_{\gamma,iso} - 0.60\log(E_{peak}))$ and the extrinsic scatter of $\sigma = 0.44 \pm 0.04$ produced by the maximum likelihood method is consistent with that of Margutti et al. (2013) as well.

We also examine the difference between XRFs/XRRs and C-GRBs from the above correlations. We separate XRFs/XRRs and C-GRBs as two groups. From Figure 9, we obtain $(E_{X,iso}) = (9.85 \pm 2.77) + (0.79 \pm 0.05)\log(E_{\gamma,iso})$ with the extrinsic scatter of $\sigma = 0.68 \pm 0.07$ for C-GRBs and $(E_{X,iso}) = (13.45 \pm 2.53) + (0.73 \pm 0.05)\log(E_{\gamma,iso})$ with the extrinsic scatter of $\sigma = 0.39 \pm 0.04$ for XRRs/XRFs. Thus, we do not find significant difference in this correlation. we analyze the data in Figure 10 that the relation of $\log(E_{peak,z})(\text{keV})=(2.83 \pm 0.06) + (0.11 \pm 0.05) \log[E_{\gamma,iso}/(10^{52} \text{erg})]$ with the extrinsic scatter of $\sigma = 0.31 \pm 0.04$ is for C-GRBs and the relation of $\log(E_{peak,z})(\text{keV})=(2.11 \pm 0.03) + (0.41 \pm 0.04) \log[E_{\gamma,iso}/(10^{52} \text{erg})]$ with the extrinsic scatter of $\sigma = 0.23 \pm 0.03$ is for XRRs/XRFs. Thus, we clearly see the difference between XRRs/XRFs and C-GRBs in this correlation. From Figure 11, We obtain the relation of $\log(E_{X,iso}) = (48.07 \pm 1.03) + (1.24 \pm 0.35)\log(E_{peak,z})$ with the extrinsic scatter of $\sigma = 0.86 \pm 0.09$ for C-GRBs and the relation of $\log(E_{X,iso}) = (49.46 \pm 0.28) + (0.90 \pm 0.12)\log(E_{peak,z})$ with the extrinsic scatter of $\sigma = 0.62 \pm 0.05$ for XRRs/XRFs. Thus, it seems that XRRs/XRFs and C-GRBs have no significant difference in this correlation. Finally, from Figure 12, we obtain the relation of $\log(E_{X,iso}) = (5.67 \pm 3.36) + (0.90 \pm 0.07)(\log E_{\gamma,iso} - 0.6\log(E_{peak}))$ with the extrinsic scatter of $\sigma = 0.54 \pm 0.08$ for C-GRBs and the relation of $\log(E_{X,iso}) = (4.10 \pm 2.88) + (0.93 \pm 0.06)(\log E_{\gamma,iso} - 0.60\log(E_{peak}))$ with the extrinsic scatter of $\sigma = 0.36 \pm 0.05$. Therefore, we do not find any significant difference between XRRs/XRFs and C-GRBs in this correlation.

In order to investigate the γ -ray isotropic-equivalent luminosity ($L_{\gamma,iso}$) distributions for XRFs, XRRs, and C-GRBs, we collect the $L_{\gamma,iso}$ values of the GRBs in our sample from D’Avanzo et al. (2014), Liang et al. (2015), and Cano et al. (2017). We obtained 55 sources with $L_{\gamma,iso}$ values, including 5 XRFs, 26 XRRs, and 24 C-GRBs. The $L_{\gamma,iso}$

distributions are shown in Figure 13. Our results are as follows: the $L_{\gamma,iso}$ values have the range from 2.60×10^{46} to 6.89×10^{50} erg s⁻¹ for XRFs; the $L_{\gamma,iso}$ values are from 1.03×10^{49} to 3.51×10^{52} erg s⁻¹ for XRRs; and the $L_{\gamma,iso}$ values are from 1.20×10^{50} to 1.78×10^{53} erg s⁻¹ for C-GRBs. We find that XRFs and XRRs have lower $L_{\gamma,iso}$ values than C-GRBs. This indicates that XRF sources are low-luminosity GRBs.

3.4. The X-Ray Lightcurve Shapes

In order to investigate the X-ray afterglow properties of XRFs, XRRs, and C-GRBs, we simply examine the types of X-ray afterglow light curves for XRFs, XRRs, and C-GRBs from *Swift*-XRT GRB lightcurve repository³. The type definitions of X-ray afterglow light curve given by Margutti et al. (2013) are as follows: type 0 (simple power law), type I (broken power law), type II (broken power law plus power-law decay), and Type III (double broken power laws). We further check the X-ray lightcurve types of XRFs, XRRs, and C-GRBs in our sample. Our results are as follows: (1) There are 33 XRFs having the XRT light curves. For these XRFs, the proportions of Type 0, Type I, Type II, and Type III are $(14.7 \pm 6.6)\%$, $(44.1 \pm 11.4)\%$, $(32.4 \pm 9.8)\%$, and $(8.8 \pm 5.1)\%$, respectively. (2) There are 198 XRRs having the XRT light curves. For these XRRs, the proportions of Type 0, Type I, Type II, and Type III are $(17.4 \pm 2.9)\%$, $(30.8 \pm 3.9)\%$, $(45.3 \pm 4.7)\%$, and $(6.5 \pm 1.8)\%$, respectively. (3) There are 135 C-GRBs having the XRT light curves. For these C-GRBs, the proportions of Type 0, Type I, Type II, and Type III are $(25.2 \pm 4.3)\%$, $(44.4 \pm 5.7)\%$, $(27.4 \pm 4.5)\%$, and $(3.0 \pm 1.5)\%$, respectively. The statistical results are summarized in Table 3. According to these results, we find that there are not significant differences of the XRT lightcurve type among XRFs, XRRs, and C-GRBs.

3.5. Investigation of the Association of XRF/XRR with Supernova

If we propose that XRFs and XRRs are low-luminosity GRBs, it is reasonable to consider the possible association between XRFs/XRRs and SNe (Soderberg et al. 2005; Woosley & Bloom 2006)⁴. An example is XRF 060218 that is associated with SN 2006aj (Pian et al. 2006). We take the statistical results from Hjorth & Bloom (2012), and Cano (2013), and

³http://www.swift.ac.uk/xrt_curves/

⁴Although we focus on low-luminosity GRBs and XRFs in this paper, we note that high-luminosity GRBs may also have SN association. For example, bright GRB 130427A is associated with SN 2013cq (Maselli et al. 2014; Melandri et al. 2014; Vestrand et al. 2014).

Cano et al. (2017). Twenty-three GRBs in our sample are associated with the SN explosion. These GRBs include 6 XRFs (XRF 050416A, XRF 050824, XRF 060218/SN 2006aj, XRF 070419A, XRF 081007/SN 2008hw, and XRF 100316D/SN 2010bh), 14 XRRs (XRR 050525A/SN 2005nc, XRR 060729, XRR 060904B, XRR 090618, XRR 091127/SN 2009nz, XRR 101219B/SN 2010ma, XRR 101225A, XRR 111228A, XRR 120422A/SN 2012bz, XRR 120714B/SN 2012eb, XRR 120729A, XRR 130215A/SN 2103ez, XRR 130831A/SN 2013fu, and XRR 150818A), and 3 C-GRBs (GRB 080319B, GRB 111209A/SN 2011kl, and GRB 130427A/SN 2013cq). Our statistical results are shown in Table 4. It seems that XRFs and XRRs are more favorable to link with SN events than C-GRBs.

3.6. Host Galaxy Properties

The host galaxies of XRFs were investigated in the work of Bloom et al. (2003). Here, we investigate the host galaxy properties for the XRFs, XRRs, and C-GRBs in the BAT3 catalog. We pay attention to several parameters of GRB host galaxies from the GRB Host Studies (GHostS) database⁵. The physical quantities of GRB host galaxy are stellar mass (M^*), metallicity (Z), and star formation rate (SFR). The distributions of M^* for XRFs, XRRs, and C-GRBs are shown in Figure 14. This Figure includes 6 XRFs, 17 XRRs, and 28 C-GRBs. We cannot find the significant differences among XRFs, XRRs, and C-GRBs, as we estimate the K-S test probabilities between XRFs and XRRs ($P = 0.67$), XRRs and C-GRBs ($P = 0.30$), and XRFs and C-GRBs ($P = 0.28$). The distributions of metallicity Z for XRFs, XRRs, and C-GRBs are shown in Figure 15. We obtain metallicity values of 5 XRFs, 6 XRRs, and 13 C-GRBs. It is hard to distinguish the differences among XRFs, XRRs, and C-GRBs. The K-S test probabilities between XRFs and XRRs, between XRRs and C-GRBs, between XRFs and C-GRBs are $P = 0.97$, $P = 0.44$, and $P = 0.90$, respectively. The distributions of SFR are shown in Figure 16. 4 XRFs, 11 XRRs, and 22 C-GRBs are included. The K-S test probabilities are $P = 0.27$ (between XRFs and XRRs), $P = 0.09$ (between XRRs and C-GRBs), and $P = 0.03$ (between XRFs and C-GRBs). Therefore, it seems that there is an SFR difference between XRFs and C-GRBs. Here, we also note that only four XRFs have SFR values. This limitation prevents us for the further investigation.

GRB host galaxies are usually considered to be low-mass, low-metallicity, and star-forming galaxies (Christensen et al. 2004; Fynbo et al. 2009; Savaglio et al. 2009). However, we see that some GRBs are hosted in massive and/or high-metallicity galaxies (e.g.,

⁵see the webpage <http://www.grbhosts.org/>. We note that GRB 120422 is classified as XRF in GhostS, but it is identified as XRR in this paper.

Hashimoto et al. 2015). Mao (2010) proposed a possible redshift evolution of GRB host galaxies from the theoretical point of view. From the observational point of view, one survey of *Swift*-GRB host galaxy has recently been performed (Perley et al. 2016). We hope that more GRB host properties of XRFs, XRRs, and C-GRBs can be explored for the further statistical analysis in the future.

3.7. Observational Biases and Selection Effects

We should mention some selection effects and observational biases that may affect on our statistical results. First, the GRB prompt emission spectrum is usually fitted by the Band function (Band et al. 1993). However, the detection energy range of *Swift*-BAT is 15 – 350 keV, such that the spectral fitting is performed in the narrow energy range. The E_{peak}^{obs} determination is from the cutoff power-law spectral model. Thus, the E_{peak}^{obs} values in this sample might be different from those obtained from other space telescope detections with a wide energy range. Because GRB detections in a large energy range with a low energy threshold are required to accurately measure the E_{peak}^{obs} numbers, some future sensitive telescopes, such as the Space Variable Objects Monitor (SVOM) and the Einstein Probe (EP), are expected (Yuan et al. 2017). Second, GRB redshift values are determined by the spectral observations in the optical band. Thus, we cannot ignore the fact that many XRFs/XRRs have no redshift determinations. Hence, the XRF/XRR quantities related to the redshift cannot be determined. One incomplete sample may have bias on the redshift distribution (e.g., Fiore et al. 2007). Third, the observations for GRB host galaxies are also complicated. The detection of the high-redshift GRB host galaxies is one challenge. For example, Basa et al. (2012) performed the host galaxy search for three GRBs with $z > 5$ using the *Hubble Space Telescope*, and they did not find any evidence of high-redshift GRB hosts. Although Mao et al. (2010) presented the possible redshift evolution of GRB host properties, the GRB redshift distribution with the cosmic star formation has some biased effects (e.g., Dainotti et al. 2015).

4. Summary

We present a comprehensively statistical analysis to study the XRF/XRR properties in the *Swift*-BAT3 catalog. We have obtained 81 XRFs and 540 XRRs in our sample. We have analyzed the properties of γ -ray prompt emission, X-ray emission, X-ray light curve type, association with SNe, and host galaxy properties for XRFs, XRRs, and C-GRBs. We list the major findings as follows: (1) Most XRFs/XRRs have low values of E_{peak}^{obs} . We

confirm that XRFs/XRRs mainly release their energy in the X-ray band, and they are low-luminosity GRBs. (2) Most XRFs/XRRs are long-duration GRBs. (3) XRFs, XRRs, and C-GRBs follow the same $E_{X,iso}-E_{\gamma,iso}-E_{peak,z}$ correlations. (4) We do not find any differences of redshift distributions among XRFs, XRRs, and C-GRBs in our sample. (5) XRFs seem to favor the association with SN explosions. (6) We find marginal but interesting evidence that different SFRs are shown between XRRs/XRFs and C-GRBs.

Although we see some differences between XRFs/XRRs and C-GRBs in some correlation studies and statistic results, we notice that the properties of XRFs, XRRs, and C-GRBs do not show a sharp difference. We confirm that XRFs and XRRs are belong to GRBs. However, the physical origin of XRF/XRR is still unclear. The jet off-axis effect is traditionally applied to explain the observational phenomena of XRFs/XRRs. The constraints of the jet beaming and the opening angle were already proposed (Rhoads 1999; Frail et al. 2001). However, it is not the case that each GRB with the jet off-axis is XRF/XRR. For example, GRB 080710 with the observational evidence of the jet off-axis (Krühler et al. 2009) is classified as C-GRB in this paper. On the other hand, the direct measurements to identify the jet off-axis evidence cannot be performed for each GRB. The jet beaming angle statistics related to the study of XRF/XRR is expected (Gao & Dai 2010). It is suggested that the GRB thermal component in the X-ray band can be one possible reason to explain XRF/XRR energy release. As an example, GRB 090618, identified as XRR in this paper, had a detection of thermal X-ray emission by *Swift* X-ray telescope, and this XRR is associated with SN explosion (Cano et al. 2011; Page et al. 2011). Starling et al. (2012) presented 11 *Swift*-detected GRBs with optical SN explosions, and the thermal X-ray signatures were clearly identified. However, compared to the XRFs/XRRs listed in this paper, the observed GRBs with the thermal emission that have optical SN explosion evidence are still very rare. From some recent theoretical modeling analysis, thermal emission may regulate the GRB spectral peak energy (Beloborodov 2013). Photospheric models can reproduce the GRB thermal emission in the γ -ray band (Vurm et al. 2013). We expect further observational cases of the GRB thermal emissions, although most of XRR and XRF spectra are still nonthermal. Finally, the GRB detectors with wide energy range and low energy threshold are expected especially for the study of XRFs and XRRs in the future.

The work is financially supported by the Open Project Program of the Key Laboratory for the Structure and Evolution of Celestial Objects, Chinese Academy of Sciences (grant No. OP201501), the Scientific Research Foundation of the Education Department of Yunnan Province (grant No. 2014Y463), and the National Natural Science Foundation of China (11404103). J. M. is supported by the National Natural Science Foundation of China (11673062 and 11661161010), the Hundred Talent Program, the Major Program of the Chi-

nese Academy of Sciences (KJZD-EW-M06), and the Oversea Talent Program of Yunnan Province. J.-M. B. is partly supported by the National Natural Science Foundation of China (11433004) and the Ministry of Science and Technology of China (2016YFA0400700).

REFERENCES

- Amati, L., Frontera, F., in't Zand, J. J. M., et al. 2004, *A&A*, 426, 415
- Amati, L. 2006, *MNRAS*, 372, 233
- Amati, L., Guidorzi, C., Frontera, F., et al. 2008, *MNRAS*, 391, 577
- Amati, L., Frontera, F., Guidorzi, C. 2009, *A&A*, 508, 173
- Band, D., Matteson, J., Ford, L., et al. 1993, *ApJ*, 413, 281
- Barraud, C., Olive, J.-F., Lestrade, J. R., et al. 2003, *A&A*, 400, 1021B
- Barraud, C., Daigne, F., Mochkovitch, R., Atteia, J. L. 2005, *A&A*, 440, 809
- Basa S., Cuby, J. G., Savaglio, S., et al. 2012, *A&A*, 542, A103
- Beloborodov, A. M. 2013, *ApJ*, 764, 157
- Bernardini, M. G., Margutti, R., Zaninoni, E., & Chincarini, G. 2012, *MNRAS*, 425, 1199
- Bersier, D., Fruchter, A. S., Strolger, L.-G., et al. 2006, *ApJ*, 643, 284
- Bloom, J. S., Fox, D., van Dokkum, P. G., Kulkarni, S. R., Berger, E., Djorgovski, S. G., & Frail, D. A. 2003, *ApJ*, 599, 957
- Bulter, N. A., Sakamoto, T., Suzuki, M., et al. 2005, *ApJ*, 621, 884
- Cano, Z., Bersier, D., Guidorzi, C., et al. 2011, *MNRAS*, 413, 669
- Cano, Z. 2013, *MNRAS*, 434, 1098
- Cano, Z., Wang, S. Q., Dai, Z. G. & Wu, X.-F. 2017, *Advances in Astronomy*, 8929054, review to the special issue on “GRB in Swift/Fermi Era and Beyond”, arXiv:1604.03549
- Christensen, L., Hjorth, J., & Gorosabel, J. 2004, *A&A*, 425, 913
- de Ugarte Postigo, A., Fatkhullin, T. A., Jóhannesson, G., et al. 2007, *A&A*, 462, L57

- Dainotti, M. G., Del Vecchio, R., Shigehiro, N., & Capozziello, S. 2015, *ApJ*, 800, 31
- D’Alessio, V., Piro, L., Rossi, E. M. 2006, *A&A*, 460, 653
- D’Avanzo, P., Salvaterra, R., Bernardini, M. G., et al. 2014, *MNRAS*, 442, 2342
- Donaghy, T. Q. 2006, *ApJ*, 645, 436
- Fiore, F., Guetta, D., Piranomonte, S., et al. 2007, *A&A*, 470, 515
- Fong, W., Berger, E., Chornock, R., et al. 2013, *ApJ*, 769, 56
- Frail, D. A., Kulkarni, S. R., Sari, R., et al. 2001, *ApJ*, 562, L55
- Fynbo, J. P. U., Jakobsson, P., Prochaska, J. X., et al. 2009, *ApJS*, 185, 526
- Galli, A., & Piro, L. 2006, *A&A*, 455, 413
- Gao, Y., & Dai, Z.-G. 2010, *RAA*, 10, 142
- Gendre, B., Galli, A., Piroi, L. 2007, *A&A*, 465, L13
- Granot, J., Ramirez-Ruiz, E., & Perna, R. 2005, *ApJ*, 630, 1003
- Guidorzi, C., Clemens, C., Kobayashi, S., et al. 2009, *A&A*, 499, 439
- Grupe, D., Nousek, J. A., Veres, P., et al. 2013, *ApJS*, 209, 20
- Hashimoto J., Perley, D. A., Ohta, K., et al. 2015, *ApJ*, 806, 250
- Hjorth, J. & Bloom, J. S. 2012, *The Gamma-Ray Burst-Supernova Connection*, pp.169-190. Cambridge Univ. Press, Cambridge
- Kippen, R. M., Woods, P. M., Heise, J., in’t Zand, J. J. M., Briggs, M. S., & Preece, R. D. 2003, *AIPC*, 662, 244
- Krühler, T., Greiner, J., Afonso, P., et al. 2009, *A&A*, 508, 593
- Lamb, D. Q., Donaghy, T. Q., & Graziani, C. 2005, *ApJ*, 620, 355
- Levan, A. J., Osborne, J. P., Tanvir, N. R. et al. 2006, *ApJ*, 648, 1132
- Liang, E. W., Lin, T. T., Lü J., Lu, R.-J., Zhang J., & Zhang, B. 2015, *ApJ*, 813, 116
- Lien, A., Sakamoto, T., Barthelmy, S. D., et al. 2016, *ApJ*, 829, 7
- Mao, J. 2010, *ApJ*, 717, 140

- Margutti, R., Zaninoni, E., Bernardini, M. G., et al. 2013, MNRAS, 428, 729
- Maselli, A., Melandri, A., Nava, L., et al. 2014, Science, 343, 48
- Melandri, A., Pian, E., D’Elia, V., et al. 2014, A&A, 567, A29
- Mizuta, A., Yamasaki, T., Nagataki, S., & Mineshige, S. 2006, ApJ, 651, 960
- Page, K. L., & Gehrels, N. 2008, GCN circ. 7638
- Page, K. L., Starling, R. L. C., Fitzpatrick, G., et al. 2011, MNRAS, 416, 2078
- Pe’er, A., Mészáros, P., Rees, M. J. et al., 2006, ApJ, 642, 995
- Perley, D. A., Krühler, T., Schulze, S., et al. 2016, ApJ, 817, 7
- Pian, E., Mazzali, P., Masetti, N., et al. 2006, Nature, 442, 1011
- Ramirez-Ruiz, E. 2005, MNRAS, 363, L61
- Rhoads, J. E. 1999, ApJ, 525, 737
- Romano, P., Moretti, A., Banat, P. L., et al. 2006, A&A, 450, 59
- Sakamoto, T., Lamb, D. Q., Kawai, N., et al. 2005, ApJ, 629, 311
- Sakamoto, T., Barbier, L., Barthelmy, S. D., et al. 2006, ApJ, 636, L73
- Sakamoto, T., Hullinger, D., Sato, G., et al. 2008, ApJ, 679, 570
- Sakamoto, T., Barthelmy, S. D., Baumgartner, W. H., et al. 2011, ApJS, 192, 1
- Salafia, O. S., Ghisellini, G., Pescalli, A., Ghirlanda, G., & Nappo, F. 2016, MNRAS, 461, 3607
- Savaglio, S., Glazebrook, K., & Le Borgne, D. 2009, ApJ, 691, 182
- Schady, P., Mason, K. O., Osborne, M. J., et al. 2006, ApJ, 643, 276
- Starling, R. L. C., Page, K. L., Pe’er, A., et al. 2012, MNRAS, 427, 2950
- Soderberg, A. M., Kulkarni, S. R., Fox, D. B., et al. 2005, ApJ, 627, 877
- Tunnicliffe, R. L., Levan, A. J., Tanvir, N. R., et al. 2014, MNRAS, 437, 1495
- Urata, Y., Huang, K., Yamazaki, R., & Sakamoto, T. 2015, ApJ, 806, 222

- Vestrand, W. T., Wren, J. A., Panaitescu, A., et al. 2014, *Science*, 343, 38
- Virgili, F., Liang, E.-W., & Zhang, B. 2009, *MNRAS*, 392, 91
- Vurm, I., Lyubarsky, Y., & Piran, T. 2013, *ApJ*, 764, 143
- Woosley, S. E., & Bloom, J. S. 2006, *ARA&A*, 44, 507
- Xu, L., Wu, X. F., & Dai, Z. G. 2005, *ApJ*, 634, 1155
- Yamazaki, R., Ioka, K., & Nakamura, T. 2002, *ApJ*, 571, L31
- Yuan, W., Amati, L., Cannizzo, J. K. et al. 2017, *Space Science Reviews*, 202, 235
- Zaninoni, E., Bernardini, M. G., Margutti, R., et al. 2016, *MNRAS*, 455, 1375

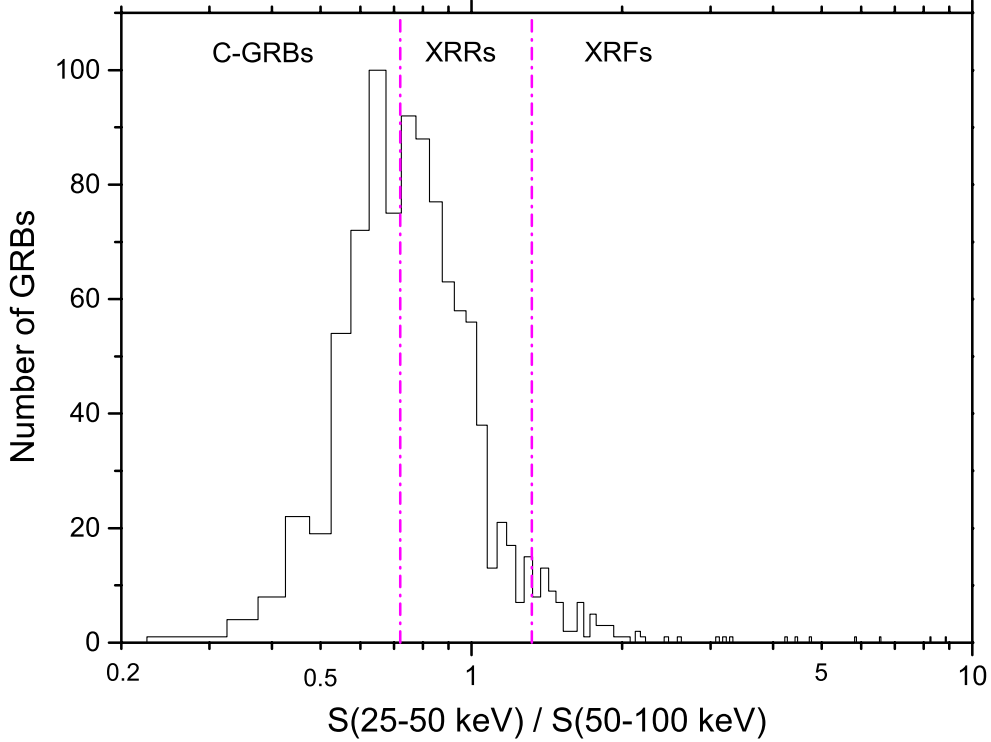


Fig. 1.— Distributions of the fluence ratio $S(25-50 \text{ keV})/S(50-100 \text{ keV})$ of GRBs in *Swift*-BAT3 sample. The dashed lines show the distribution borders between C-GRBs and XRRs, and between XRRs and XRFs, respectively. Here, we list the sources with the fluence ratio larger than 3.0: XRF 050819 (the ratio is 3.08 ± 0.99), XRF 050406 (the ratio is 3.15 ± 1.22), XRF 060805A (the ratio is 3.29 ± 2.20), XRF 080218B (the ratio is 4.24 ± 3.08), XRF 060428B (the ratio is 4.44 ± 1.80), XRF 080822B (the ratio is 4.74 ± 2.86), XRF 050416A (the ratio is 5.83 ± 2.39), XRF 160525A (the ratio is 6.50 ± 5.47), XRF 061218 (the ratio is 8.25 ± 10.66), and XRF 070126 (the ratio is 8.82 ± 9.46).

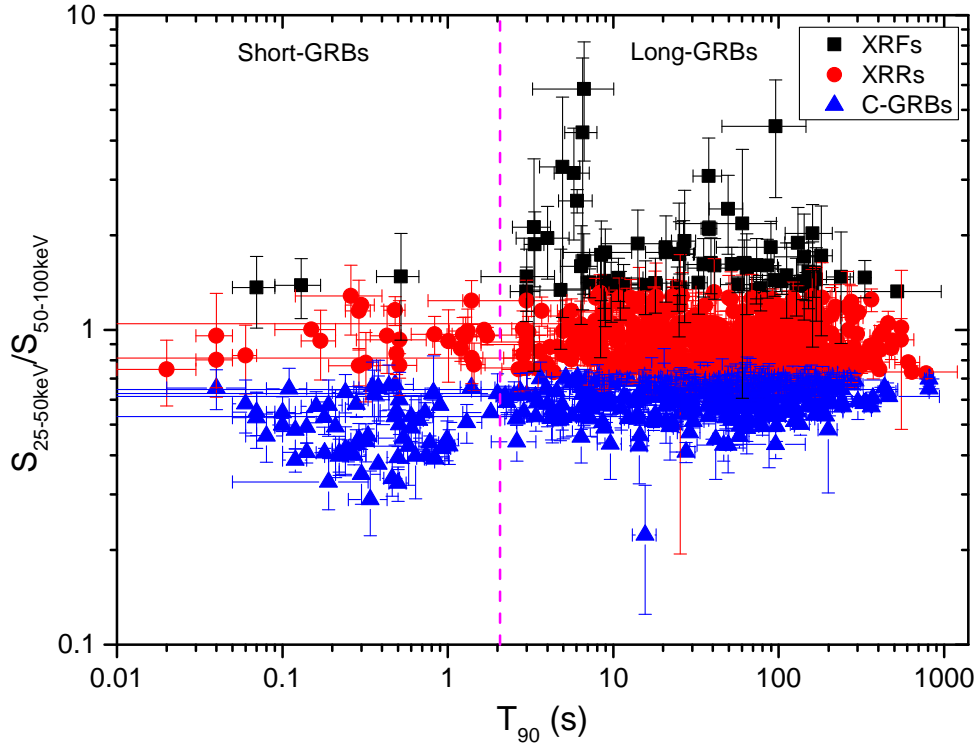


Fig. 2.— The fluence ratio of $S(25-50 \text{ keV})/S(50-100 \text{ keV})$ vs. the duration T_{90} of GRBs in the *Swift*-BAT3 sample. XRFs, XRRs, and C-GRBs are marked as black squares, red dots, and blue triangles, respectively. The dashed line shows the distribution border between long GRBs and short GRBs.

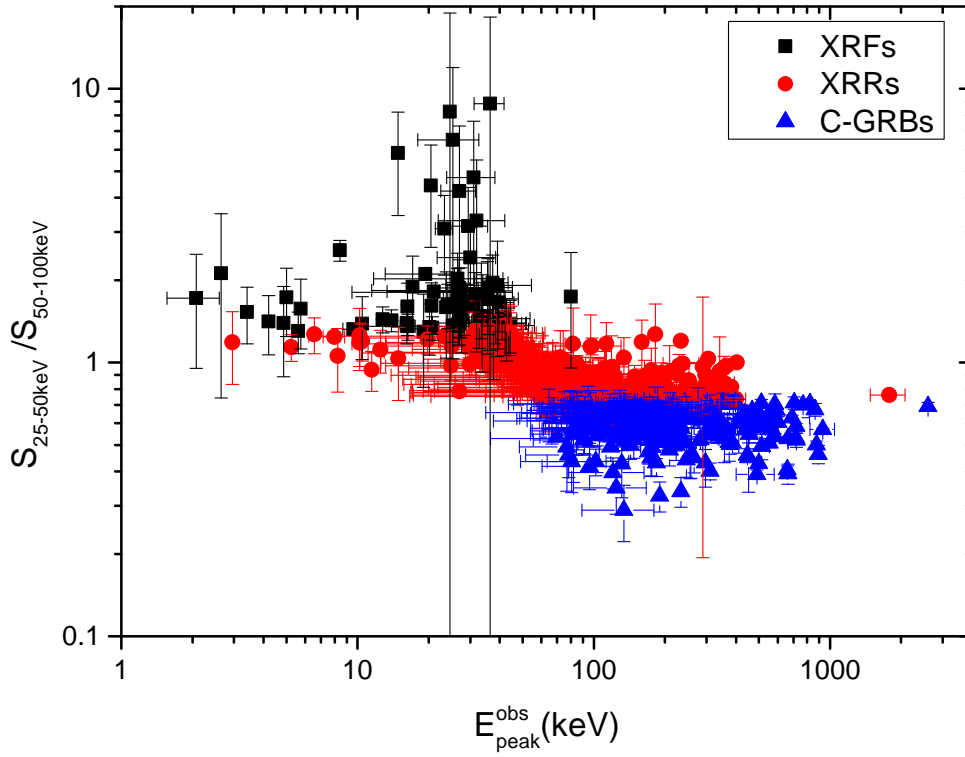


Fig. 3.— Fluence ratio of $S(25-50 \text{ keV})/S(50-100 \text{ keV})$ versus the peak energy E_{peak}^{obs} for XRFs, XRRs, and C-GRBs. XRFs, XRRs, and C-GRBs are marked as black squares, red dots, and blue triangles, respectively. XRF 061218 and XRF 070126 have large fluence ratio error bars, and they are not included in Figure 2 because they have no T_{90} values.

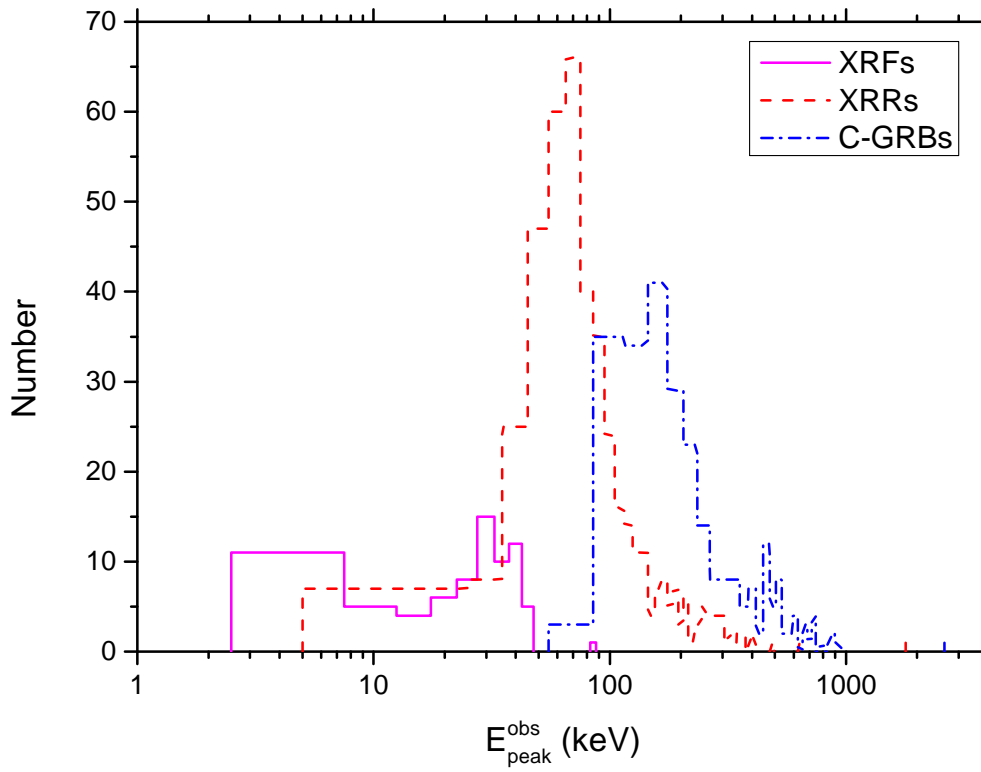


Fig. 4.— E_{peak}^{obs} distribution for XRFs, XRRs, and C-GRBs. XRFs, XRRs, and C-GRBs are marked as the pink solid line, the red dashed line, and the blue dash-dotted line, respectively.

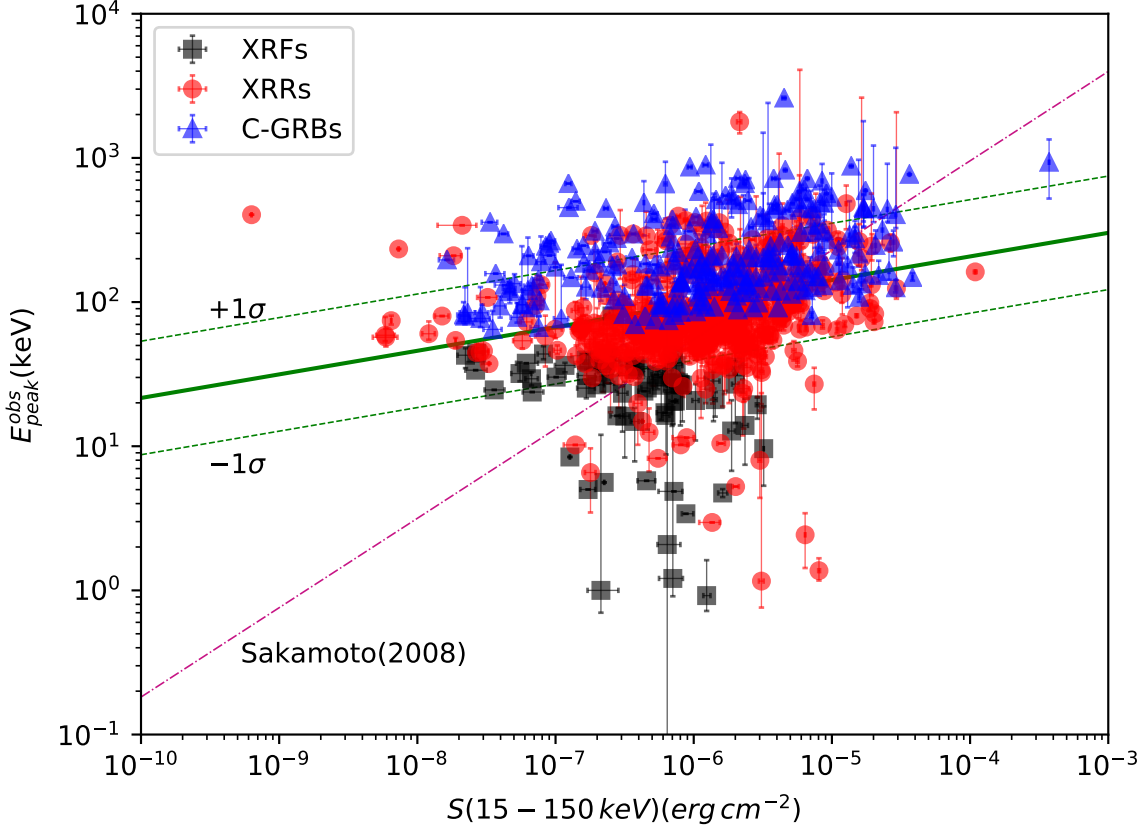


Fig. 5.— Relationship of the 15-150 keV fluence and the E_{peak}^{obs} for XRFs, XRRs, and C-GRBs. The green solid line is the best fit to the data with the function of $\log(E_{peak}^{obs})(\text{keV}) = (2.96 \pm 0.13) + (0.16 \pm 0.02) \log[S(15 - 150)]\text{keV}$, and the green dashed lines are marked for the 1σ regions. The extrinsic scatter $\sigma = 0.39 \pm 0.01$. The pink dashed-dotted line is the best fit to the data without taking into account the errors reported by Sakamoto et al. (2008), and the function is $\log(E_{peak}^{obs})(\text{keV}) = (5.46 \pm 0.25) + (0.62 \pm 0.14) \log[S(15 - 150)\text{keV}]$. The XRFs, XRRs, and C-GRBs are marked as black squares, red dots, and blue triangles, respectively.

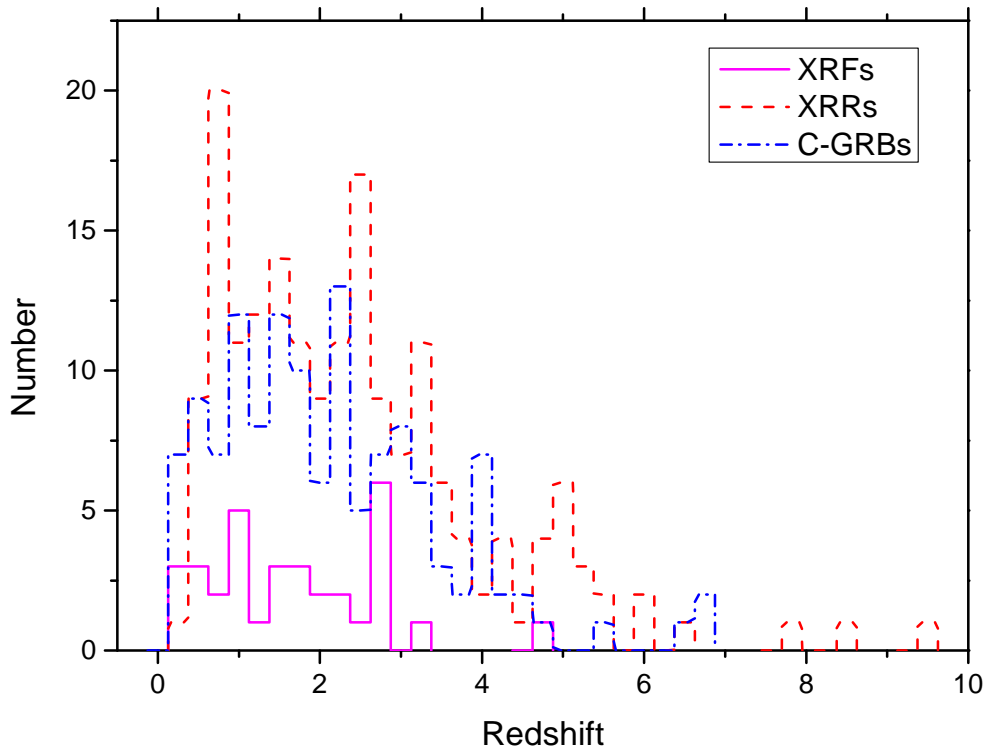


Fig. 6.— Redshift distribution of GRBs in the *Swift*-BAT3 sample. XRFs, XRRs, and C-GRBs are marked as the pink solid line, the red dashed line, and the blue dashed-dotted line, respectively.

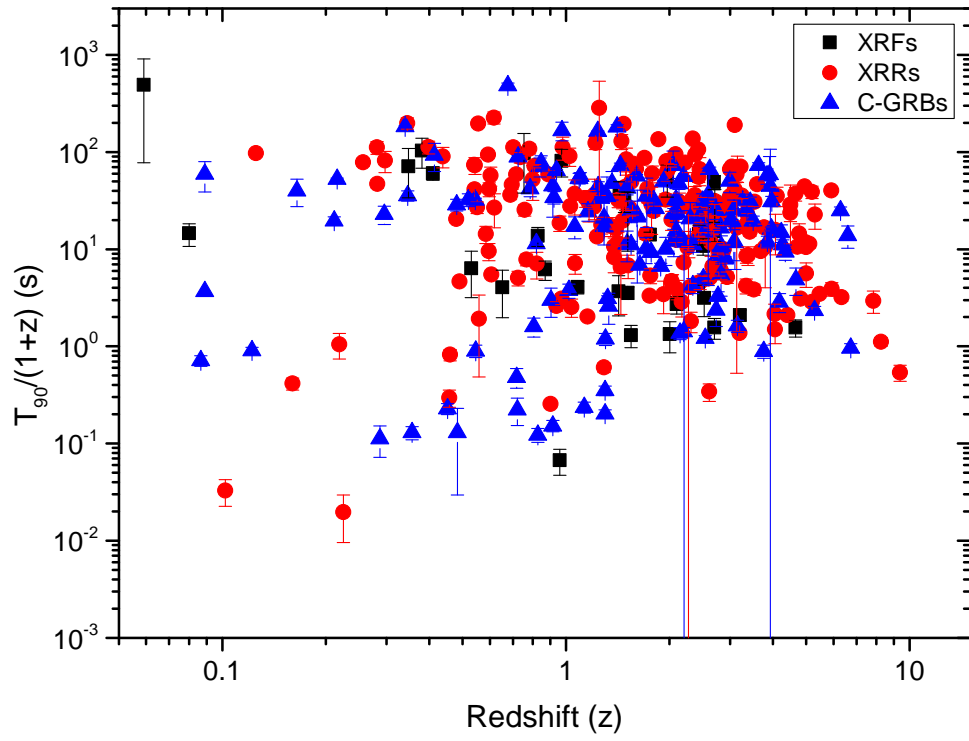


Fig. 7.— GRB duration T_{90} vs. redshift. XRFs, XRRs, and C-GRBs are marked as black squares, red dots, and blue triangles, respectively.

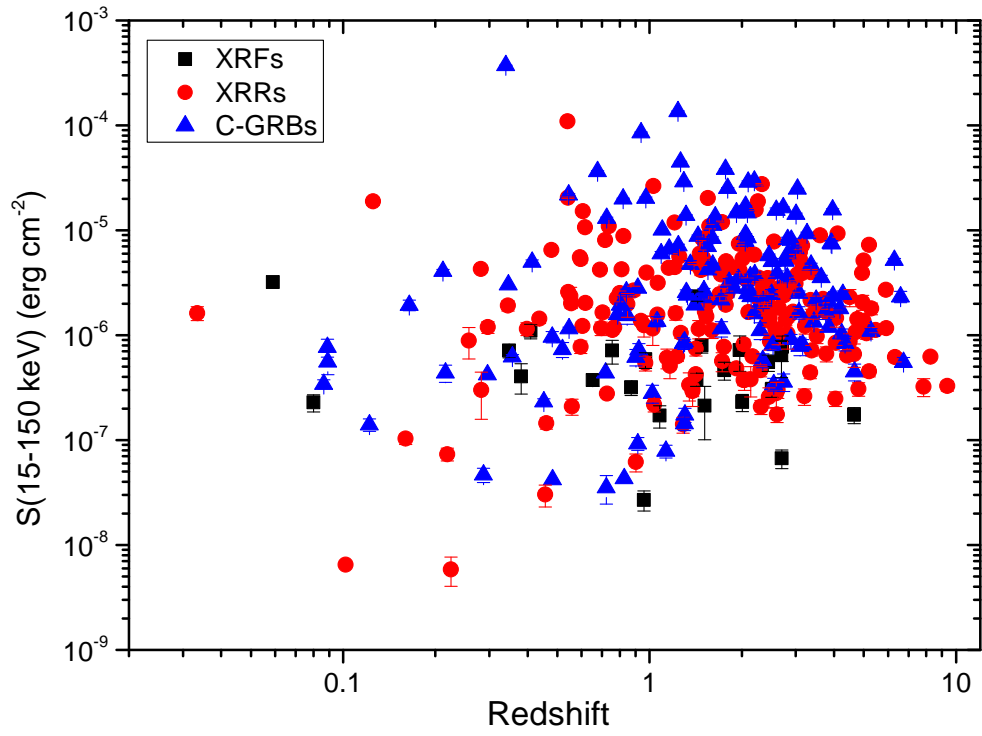


Fig. 8.— GRB fluence in the 15-150 keV band vs. redshift. XRFs, XRRs, and C-GRBs are marked as black squares, red dots, and blue triangles, respectively.

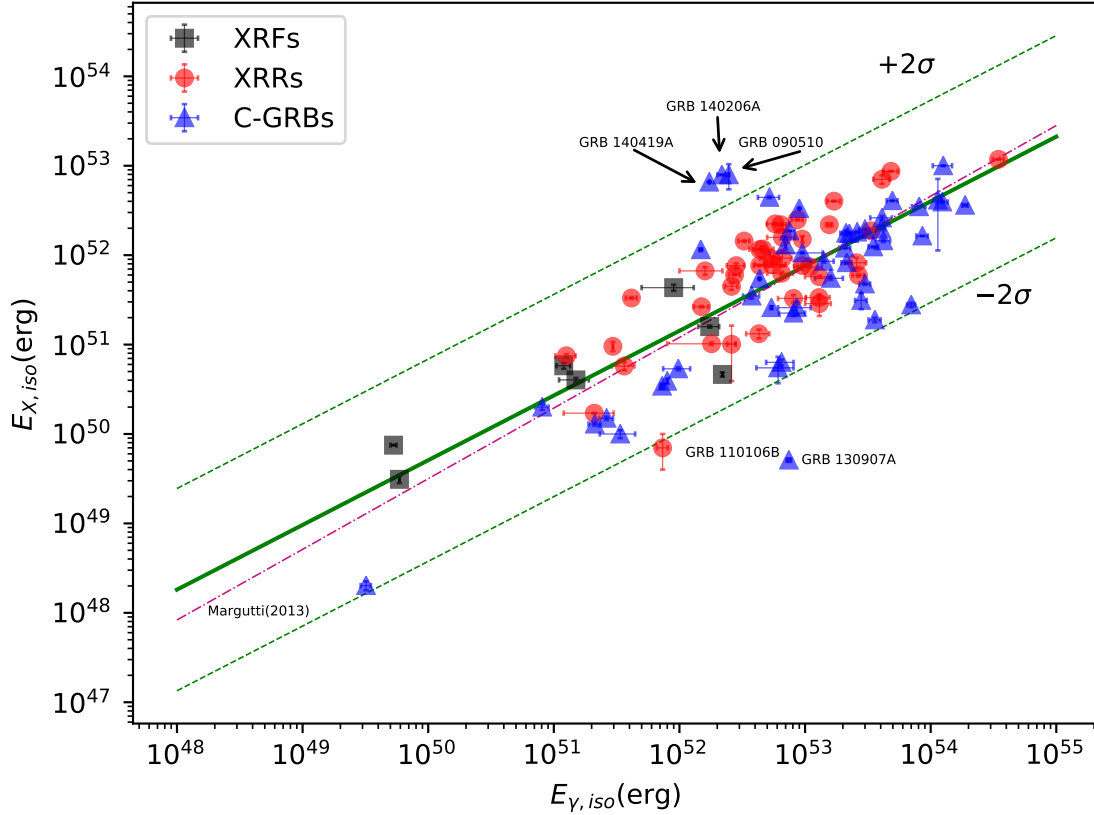


Fig. 9.— Correlation between $E_{X,iso}$ and $E_{\gamma,iso}$ in the *Swift*-BAT3 sample. The green solid line is the best fit with the function of $(E_{X,iso}) = (13.31 \pm 2.73) + (0.73 \pm 0.05)\log(E_{\gamma,iso})$, and the extrinsic scatter is $\sigma = 0.57 \pm 0.04$. The green dashed lines are marked for the 2σ regions. The pink dashed-dotted line is the best-fitting function of $\log(E_{X,iso}) = (10.0 \pm 20.6) + (0.79 \pm 0.01)\log(E_{\gamma,iso})$ reported by Margutti et al.(2013). XRFs, XRRs, and C-GRBs are marked as black squares, red dots, and blue triangles, respectively. The GRBs labeled as outliers in the figure are L-GRBs, and the exception is short GRB 090510.

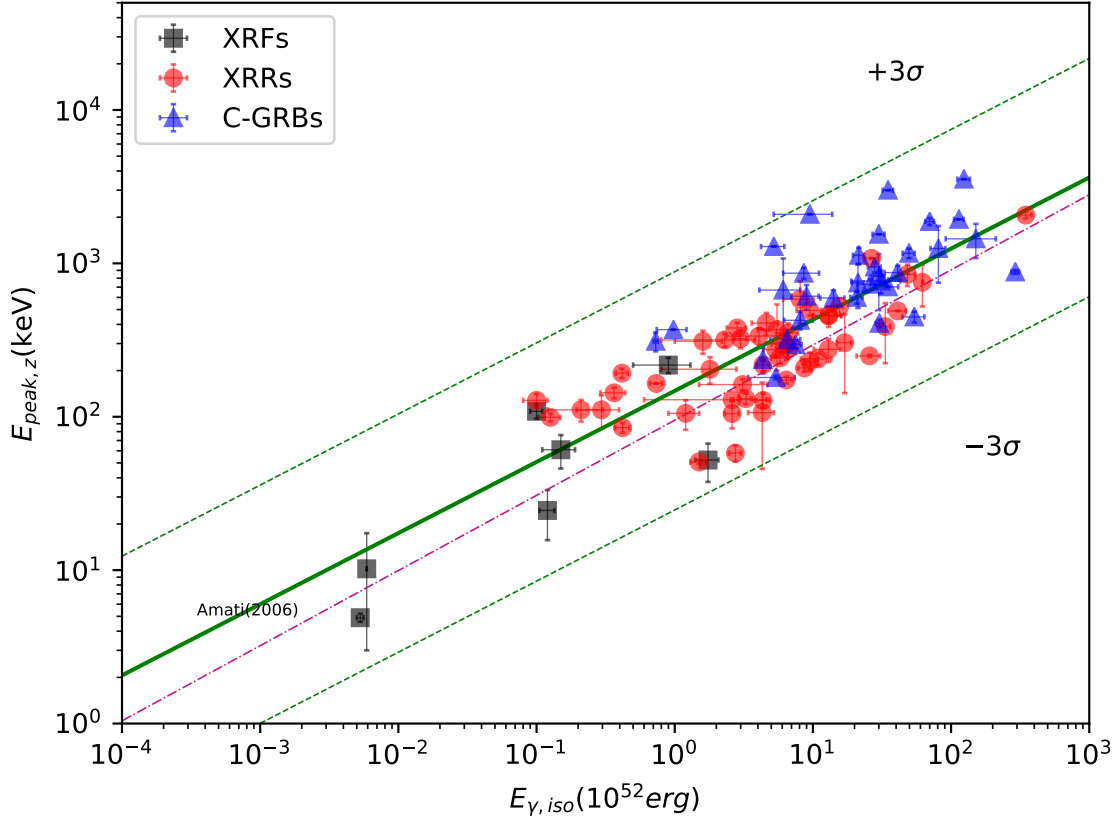


Fig. 10.— Correlation between GRB peak energy $E_{peak,z}$ in the rest frame and GRB isotropic-equivalent energy $E_{\gamma, iso}$. The green solid line is the best fit with the function of $\log(E_{peak,z})(\text{keV}) = (2.17 \pm 0.04) + (0.46 \pm 0.03) \log[E_{\gamma, iso}/(10^{52} \text{ erg})]$, and the extrinsic scatter is $\sigma = 0.26 \pm 0.02$. and the green dashed lines are marked for the 3σ regions. The pink dashed-dotted line is the best fit with the function of $E_{peak,z} = 95 \text{ keV} (E_{\gamma, iso}/10^{52} \text{ erg})^{0.49}$ reported by Amati (2006). XRFs, XRRs, and C-GRBs are marked as black squares, red dots, and blue triangles, respectively.

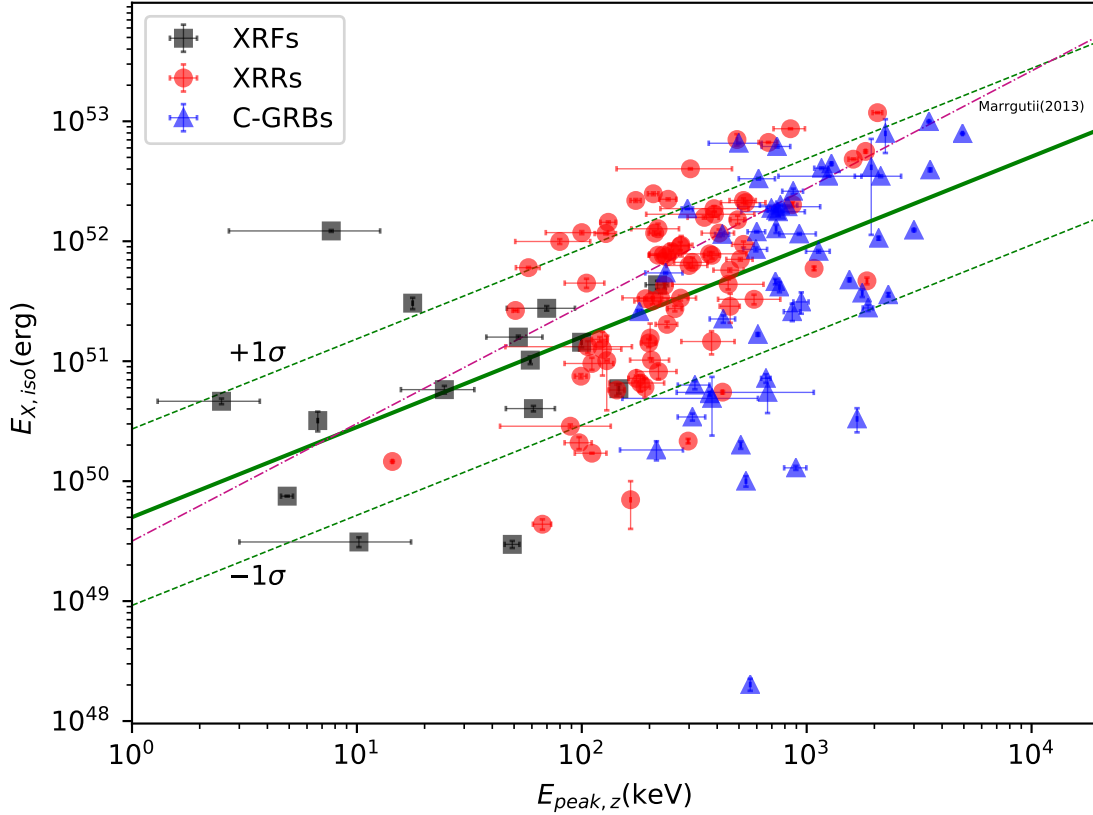


Fig. 11.— Correlation between GRB X-ray energy $E_{X,iso}$ and GRB peak energy $E_{peak,z}$. The green solid line is the best fit with the function of $\log(E_{X,iso}) = (49.69 \pm 0.27) + (0.75 \pm 0.11)\log(E_{peak,z})$, and the extrinsic scatter is $\sigma = 0.73 \pm 0.04$. The green dashed lines are marked for the 1σ regions. The pink dashed line is the best fit using the function of $\log(E_{X,iso}) = (49.50 \pm 0.15) + (0.98 \pm 0.02)\log(E_{peak,z})$ reported by Margutti et al. (2013). XRFs, XRRs, and C-GRBs are marked as black squares, red dots, and blue triangles, respectively.

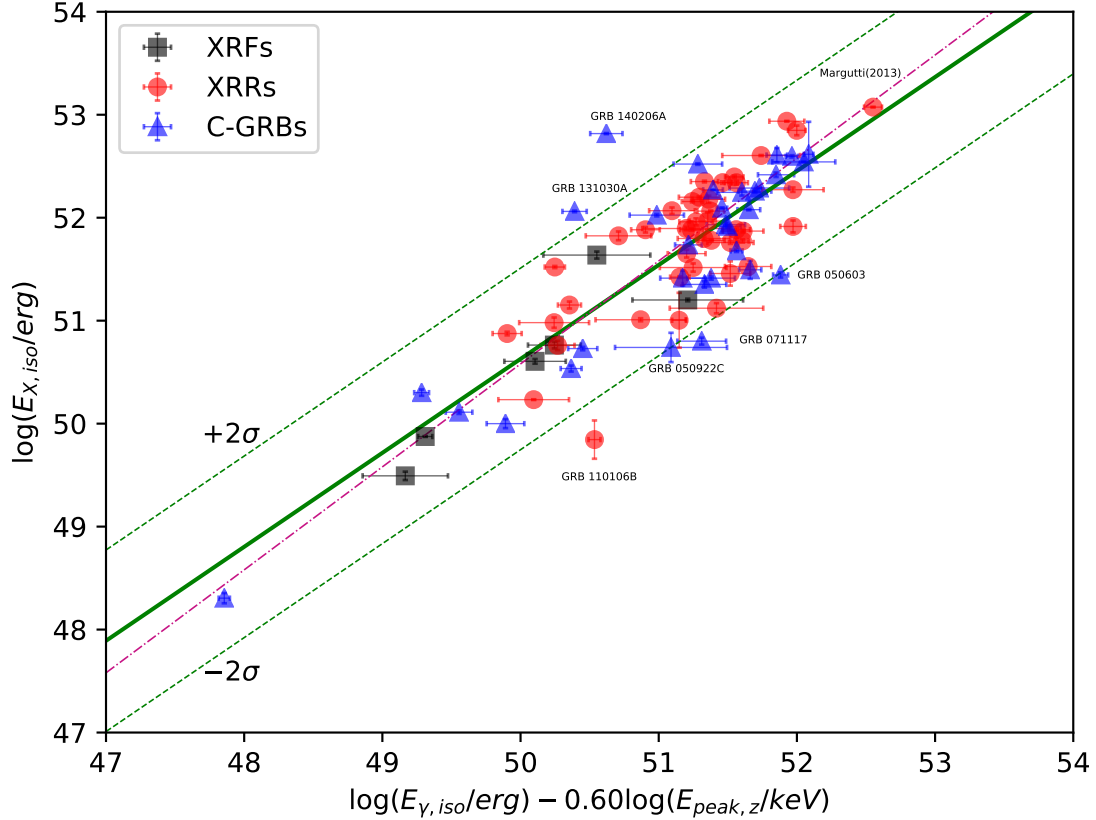


Fig. 12.— Correlation between $E_{X,iso}$ and $E_{\gamma,iso} - (E_{peak,z})$. The green solid line is the best fit with the function of $\log(E_{X,iso}) = (4.78 \pm 2.79) + (0.92 \pm 0.06)(\log E_{\gamma,iso} - 0.6\log(E_{peak}))$ with the extrinsic scatter of $\sigma = 0.44 \pm 0.04$. The green dashed lines are marked for the 2σ regions. The pink dashed-dotted line is the best fit using the function of $\log(E_{X,iso}) = (0.58 \pm 0.25) + (1.00 \pm 0.06)(\log(E_{\gamma,iso})) - (0.60 \pm 0.10)\log(E_{peak})$ reported by Margutti et al.(2013). XRFs, XRRs, and C-GRBs are marked as black squares, red dots, and blue triangles, respectively. All the GRBs labeled at outliers in the figure are L-GRBs.

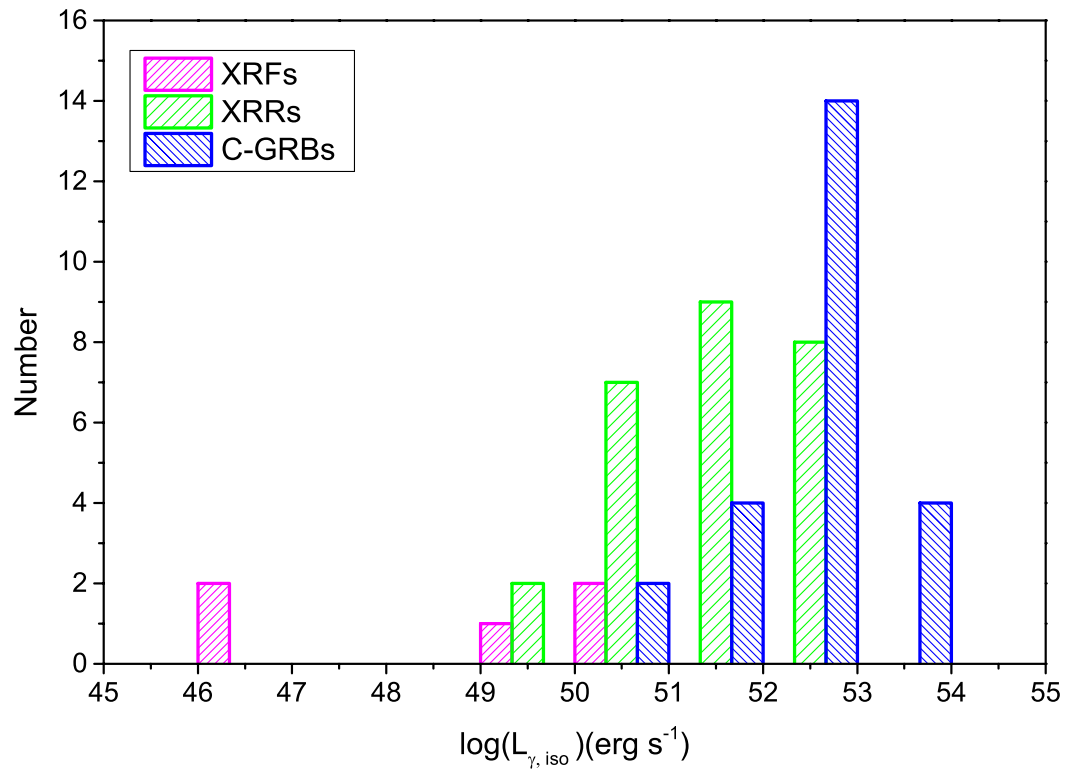


Fig. 13.— GRB isotropic luminosity $L_{\gamma, iso}$ distribution for XRF, XRR, and C-GRB classes. XRFs, XRRs, and C-GRBs are marked as pink, green, and blue, respectively.

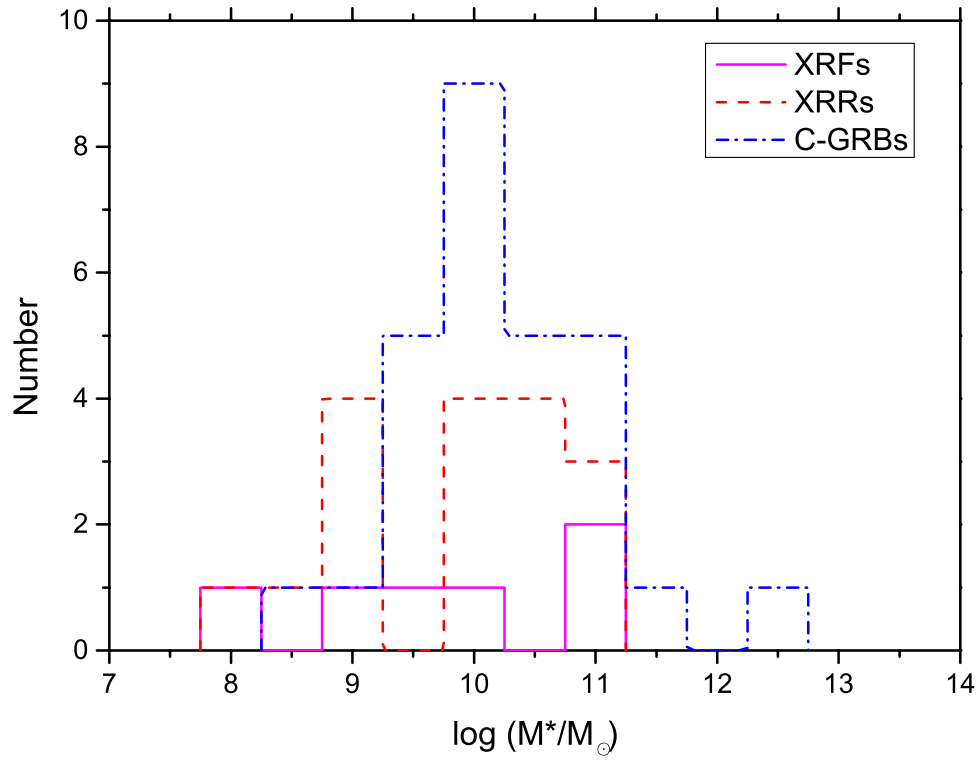


Fig. 14.— Distribution of stellar mass (M^*) in GRB host galaxy for XRFs, XRRs, and C-GRBs. XRFs, XRRs, and C-GRBs are marked as the pink solid line, the red dashed line, and the blue dashed-dotted line, respectively.

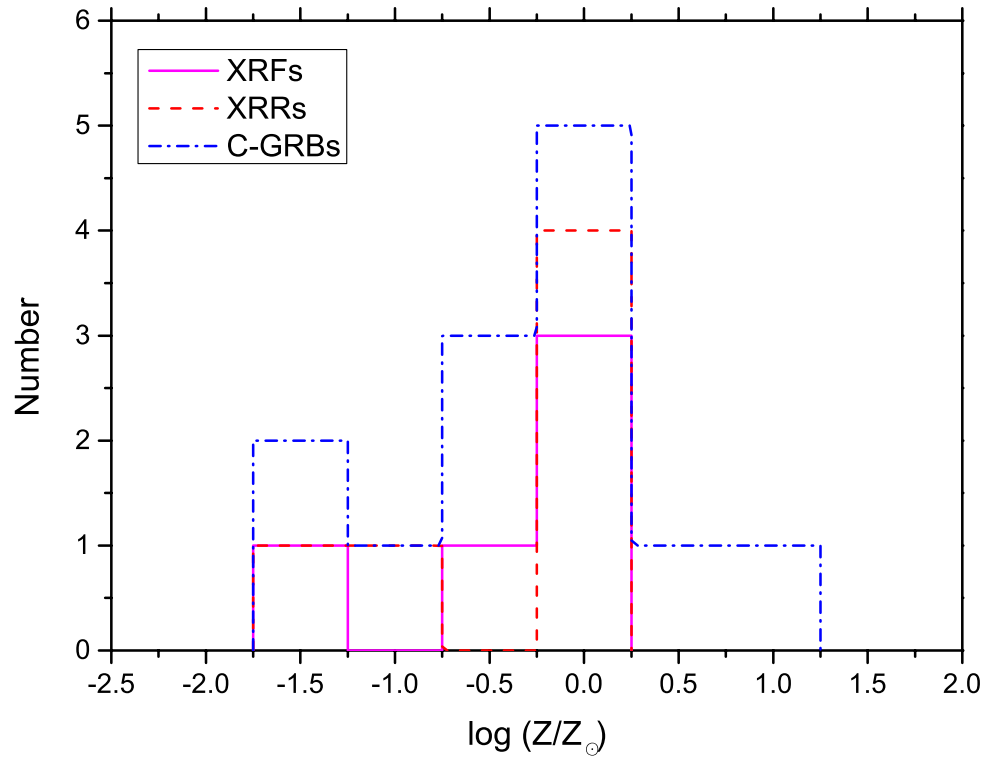


Fig. 15.— Distribution of metallicity (Z) in GRB host galaxy for the XRFs, XRRs, and C-GRBs. XRFs, XRRs, and C-GRBs are marked as the pink solid line, the red dashed line, and the blue dashed-dotted line, respectively.

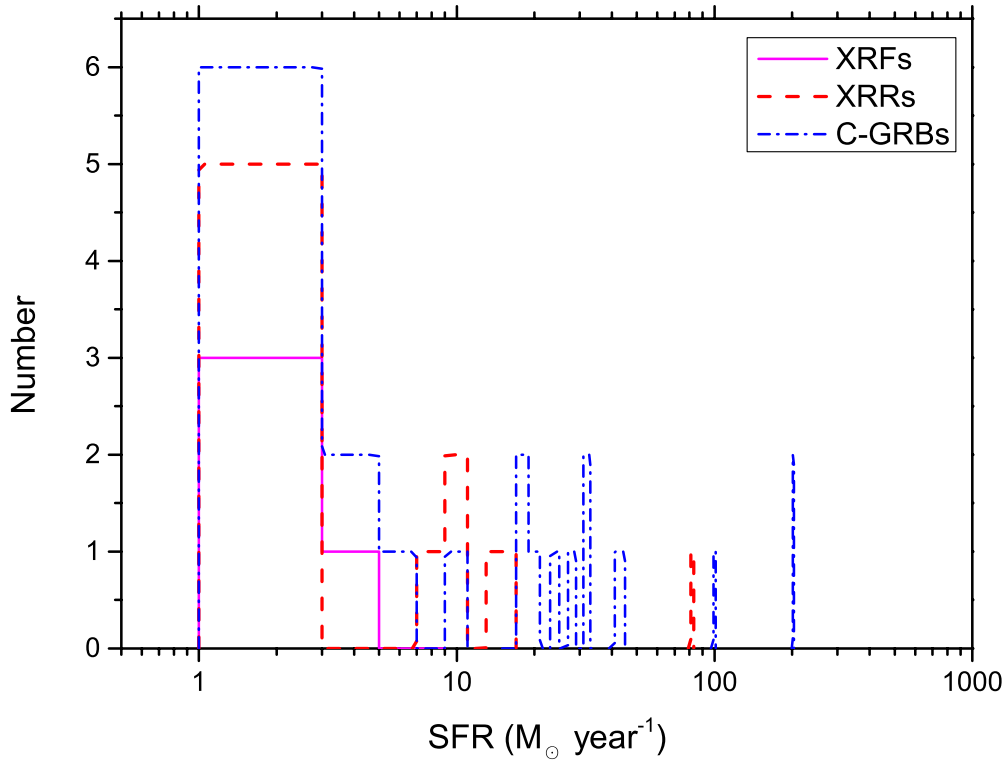


Fig. 16.— Distribution of star formation rate (SFR) in GRB host galaxy for XRFs, XRRs, and C-GRBs. XRFs, XRRs, and C-GRBs are marked as the pink solid line, the red dashed line, and the blue dashed-dotted line, respectively.

Table 1. Statistical Results of XRF, XRR, and C-GRB in the *Swift*-BAT3 GRB catalog

Class	Total Number [fraction]	L-GRB Number [fraction]	S-GRB Number [fraction]	Unknown ^b [fraction]
XRF	81 [(7.3 ± 0.8)%]	70 [(86.4 ± 10.3)%]	3 [(3.7 ± 2.1)%]	8 [(9.9 ± 3.5)%]
XRR	540 [(48.9 ± 2.1)%]	509 [(94.3 ± 4.2)%]	27 [(5.0 ± 1.0)%]	4 [(0.7 ± 0.4)%]
C-GRB	394 [(35.7 ± 1.8)%]	328 [(83.2 ± 4.6)%]	65 [(16.5 ± 2.0)%]	1 [(0.3 ± 0.3)%]
Unknown ^a	89 [(8.1 ± 0.9)%]	-	-	-

Note. — “a” indicates that these sources have no *Swift*-XRT observations, and we do not clarify them as XRFs, XRRs, or C-GRBs; “b” indicates that these sources have no T_{90} numbers, and we cannot judge whether they belong to long-duration GRB or short-duration GRB subclass.

Table 2. XRF and XRR samples

GRB Name	z	T_{90} (s)	α_{PL}	α_{CPL}	$S(15-150 \text{ keV})$ ($10^{-8} \text{ erg cm}^{-2}$)	SR	E_{peak}^{obs} (keV)	Ref
XRF 050215B	2.52	11.04	-2.25±0.12	-1.95	22.5	1.30±0.23	5.6	Lie16
XRF 050406	2.7	5.78	-2.40±0.17	$0.42^{+1.50}_{-0.89}$	6.7±0.7	3.15±1.22	$29.4^{+3.1}_{-3.0}$	Lie16
XRF 050416A	0.6528	6.67	-3.17±0.14	$-0.82^{+1.08}_{-0.77}$	37.4±2.4	5.83±2.39	$14.8^{+7.0}_{-3.6}$	Lie16
XRF 050714B	2.438	49.36	-2.40±0.17	$-0.01^{+1.04}_{-0.72}$	55.0±4.9	2.42±0.68	$30.1^{+3.1}_{-5.2}$	Lie16
XRF 050815	-	2.99	-1.82±0.12	$0.40^{+0.86}_{-0.67}$	8.2±0.8	1.32±0.26	$43.6^{+5.8}_{-3.5}$	Lie16
XRF 050819	2.5043	37.72	-2.64±0.14	$-0.49^{+1.04}_{-0.65}$	30.5±2.4	3.08±0.99	$23.3^{+3.0}_{-10.7}$	Lie16
XRF 050822	1.434	104.29	-2.33±0.07	$-1.81^{+0.36}_{-0.10}$	234.8±11.5	1.43±0.13	$13.9^{+7.4}_{-6.5}$	Lie16
XRF 050824	0.8278	25.01	-2.79±0.18	-1.00	25.6±2.5	1.74±0.79	80.0	Lie16
XRF 051109B	0.08	15.70	-1.98±0.12	$-0.36^{+0.75}_{-0.56}$	22.8±2.1	1.39±0.27	$39.4^{+5.9}_{-4.1}$	Lie16
XRF 060218	0.03342	-	-2.18±0.10	$-1.65^{+0.48}_{-0.18}$	162.2±12.1	1.37±0.18	4.7±0.3	Ama08
XRF 060219	-	62.04	-2.53±0.16	$-0.97^{+0.98}_{-0.52}$	43.6±4.1	1.63±0.30	24.1	Lie16
XRF 060428B	0.348	96.00	-2.78±0.12	$-0.41^{+1.21}_{-0.79}$	71.2±5.1	4.44±1.80	20.4	Lie16
XRF 060512	2.1	8.40	-2.36±0.15	$-1.58^{+1.08}_{-0.21}$	-	1.30±0.48	19.0	Lie16
XRF 060516	-	128.00	-2.04±0.12	$-0.80^{+0.80}_{-0.79}$	74.6±7.4	1.40±0.29	$36.3^{+6.8}_{-8.8}$	Lie16
XRF 060805A	-	4.93	-2.11±0.19	$0.49^{+3.69}_{-1.13}$	5.5±0.9	3.29±2.20	$31.9^{+6.3}_{-3.7}$	Lie16
XRF 060923B	1.51	8.95	-2.47±0.12	$-1.81^{+0.65}_{-0.09}$	-	1.38±0.36	10.5	Lie16
XRF 060923C	-	73.73	-2.24±0.11	$-1.13^{+0.84}_{-0.44}$	138.8±13.0	1.60±0.35	$28.3^{+4.6}_{-13.4}$	Lie16
XRF 060926	3.2086	8.82	-2.50±0.11	-1.93	-	1.41±0.34	4.2	Lie16
XRF 061027	-	-	-1.88±0.23	0.14±1.02	24.0±5.5	1.46±0.25	41.0	Lie16
XRF 061210	0.4095	85.23	-1.55±0.14	$-1.56^{+0.14}_{-0.13}$	109.8±8.8	1.60±0.34	-	-
XRF 061218	-	-	-2.61±0.29	$0.87^{+3.95}_{-1.42}$	3.6±0.6	8.25±10.66	24.6	Lie16
XRF 070126	-	-	-1.88±0.25	2.39±0.50	11.7±1.9	8.82±9.46	$36.4^{+1.5}_{-3.8}$	Lie16
XRF 070330	-	6.64	-1.88±0.25	$0.67^{+1.04}_{-0.66}$	16.7±1.4	1.66±0.36	$39.6^{+3.8}_{-2.5}$	Lie16
XRF 070419A	0.9705	160.0	-2.37±0.12	$-0.84^{+0.78}_{-0.53}$	58.2±4.9	2.02±0.48	$26.5^{+3.6}_{-11.2}$	Lie16
XRF 070714A	-	3.00	-2.56±0.10	-1.97±0.46	-	1.48±0.33	1.8±0.7	Lie16
XRF 070721A	-	3.35	-2.35±0.18	$1.35^{+3.80}_{-1.27}$	-	1.87±0.50	$26.9^{+2.8}_{-2.7}$	Lie16
XRF 071008	-	17.98	-2.14±0.13	$-1.11^{+0.70}_{-0.52}$	22.5±2.2	1.41±0.28	32.7	Lie16
XRF 071031	2.6918	180.64	-2.35±0.13	$-1.99^{+0.14}_{-0.01}$	64.3±12.5	1.72±0.76	$2.1^{+187.8}_{-107.5}$	Lie16
XRF 071101	-	4.82	-2.00±0.22	$-0.82^{+1.48}_{-0.66}$	6.1±1.1	1.34±0.47	37.7	Lie16
XRF 071227	0.381	142.48	-2.01±0.18	$-0.23^{+1.69}_{-0.87}$	40.4±6.4	1.71±0.63	35.5±5.3	Lie16
XRF 080218B	-	6.53	-2.53±0.14	$1.30^{+2.43}_{-1.07}$	-	4.24±3.08	$27.0^{+1.8}_{-2.7}$	Lie16
XRF 080315	-	-	-2.18±0.27	1.58	10.1±1.5	53.78±143.02	30.1	Lie16
XRF 080319D	-	26.94	-1.79±0.17	$0.49^{+2.47}_{-1.15}$	23.5±4.3	1.92±0.86	39.1±4.1	Lie16
XRF 080330	1.5119	60.36	-2.65±0.25	$-1.98^{+0.56}_{-0.01}$	21.3±5.6	2.18±1.57	$1.0^{+11.0}_{-0.3}$	Lie16
XRF 080515	-	20.86	-2.19±0.08	$-0.39^{+0.59}_{-0.48}$	-	1.76±0.54	$33.5^{+2.3}_{-3.1}$	Lie16
XRF 080520	1.5457	3.32	-3.08±0.26	-1.90	-	2.12±1.38	2.6	Lie16
XRF 080822B	-	-	-2.41±0.26	$2.00^{+2.83}_{-1.35}$	16.8±2.4	4.74±2.86	$31.0^{+3.4}_{-3.8}$	Lie16
XRF 081007	0.5295	9.73	-2.43±0.10	$-1.52^{+0.55}_{-0.33}$	-	1.35±0.29	39.9±9.8	Ama09
XRF 090111	-	25.26	-2.28±0.08	$-1.79^{+0.38}_{-0.22}$	63.0±3.6	1.36±0.15	$16.4^{+8.1}_{-7.6}$	Lie16
XRF 090205	4.6497	8.81	-2.01±0.11	$-0.39^{+0.74}_{-0.56}$	17.4±1.5	1.43±0.36	$38.4^{+5.0}_{-3.8}$	Lie16
XRF 090308A	-	25.10	-2.34±0.17	$-1.09^{+0.94}_{-0.76}$	19.9±2.3	1.74±0.46	26.7	Lie16
XRF 090417A	-	0.07	-2.81±0.16	0.39±0.76	2.2±0.3	1.36±0.35	$42.86^{+5.1}_{-8.0}$	Lie16
XRF 090726	2.71	56.68	-2.29±0.10	$-1.30^{+0.50}_{-0.41}$	78.7±4.4	1.39±0.08	26.9	Lie16
XRF 090807A	-	146.35	-2.22±0.07	$-1.48^{+0.37}_{-0.27}$	199.8±10.9	1.38±0.14	$27.0^{+4.4}_{-12.5}$	Lie16
XRF 100212A	-	163.76	-2.24±0.10	$-2.22^{+0.09}_{-0.23}$	102.0±7.9	1.52±0.25	-	-

Table 2—Continued

GRB Name	z	T_{90} (s)	α_{PL}	α_{CPL}	$S(15-150 \text{ keV})$ ($10^{-8} \text{ erg cm}^{-2}$)	SR	E_{peak}^{obs} (keV)	Ref
XRF 100316D	0.0591	521.88	-2.36±0.08	-1.88 ^{+0.37} _{-0.06}	321.0	1.33	9.6 ^{+9.3} _{-4.3}	Lie16
XRF 100324A	-	6.40	-2.28±0.22	-1.40 ^{+1.34} _{-0.34}	6.8±1.2	1.59±0.55	23.8	Lie16
XRF 100425A	1.755	38.97	-2.44±0.16	-0.88 ^{+1.23} _{-0.67}	46.1±4.5	1.63±0.33	25.4 ^{+4.7} _{-12.3}	Lie16
XRF 110112A	-	0.52	-2.12±0.23	-0.89 ^{+1.67} _{-0.61}	2.6±0.5	1.48±0.55	33.7	Lie16
XRF 110312A	-	35.14	-2.33±0.13	-1.53 ^{+0.73} _{-0.38}	73.6	1.61±0.34	20.6	Lie16
XRF 110319A	-	20.68	-2.55±0.04	1.38±0.22	143.2±3.6	1.82±0.10	21.0 ^{+2.7} _{-5.0}	Lie16
XRF 111018A	-	32.71	-2.18±0.14	-2.16 ^{+1.28} _{-0.03}	36.3±4.0	1.41±0.29	-	-
XRF 111029A	-	7.20	-2.11±0.07	-0.77 ^{+0.39} _{-0.33}	37.3±1.9	1.42±0.15	36.1 ^{+2.7} _{-3.0}	Lie16
XRF 111129A	1.0796	8.48	-2.53±0.19	-1.91	17.2±2.1	1.73±0.49	5.0	Lie16
XRF 120116A	-	38.04	-2.69±0.04	-1.31 ^{+0.22} _{-0.20}	288.3±6.4	2.11±0.11	19.4 ^{+2.4} _{-3.9}	Lie16
XRF 120724A	1.48	77.92	-2.43±0.13	-0.75 ^{+0.84} _{-0.33}	80.1±6.2	1.36±0.21	26.7 ^{+3.7} _{-12.8}	Lie16
XRF 121108A	-	89.55	-2.29±0.10	-1.01 ^{+0.64} _{-0.48}	82.8±6.4	1.83±0.38	26.5 ^{+3.4} _{-11.7}	Lie16
XRF 121212A	-	6.06	-2.50±0.19	-1.88	12.7	2.57±0.22	8.4	Lie16
XRF 121229A	2.707	111.46	-2.27±0.19	-1.32 ^{+1.19} _{-0.38}	77.5±10.6	1.49±0.40	27.6	Lie16
XRF 130608A	-	151.85	-2.62±0.20	-1.93	87.8±8.4	1.53±0.36	3.4	Lie16
XRF 130612A	2.006	4.00	-1.99±0.12	0.84 ^{+1.11} _{-0.75}	23.0±2.1	1.96±0.51	37.3 ^{+3.4} _{-2.6}	Lie16
XRF 130615A	-	332.56	-2.09±0.08	-0.72 ^{+0.52} _{-0.41}	199.7±12.8	1.46±0.20	35.5 ^{+3.3} _{-3.6}	Lie16
XRF 131002B	-	52.00	-2.23±0.08	-0.89 ^{+0.46} _{-0.38}	68.9±3.9	1.62±0.22	31.0 ^{+2.7} _{-5.1}	Lie16
XRF 131018A	-	73.22	-2.24±0.07	-1.71 ^{+0.33} _{-0.14}	102.5±5.4	1.34±0.13	20.8 ^{+6.2} _{-9.8}	Lie16
XRF 131120A	-	130.43	-2.87±0.24	-0.79	61.9±7.5	1.89±0.56	17.1	Lie16
XRF 131127A	-	94.97	-2.35±0.08	-1.82 ^{+0.35} _{-0.09}	187.6±10.1	1.44±0.16	12.8 ^{+8.1} _{-6.0}	Lie16
XRF 140622A	0.959	0.13	-3.08±0.15	1.23 ^{+1.17} _{-0.65}	2.7±0.3	1.39±0.30	44.2 ^{+3.4} _{-3.9}	Lie16
XRF 140730A	-	40.90	-2.39±0.15	-1.68 ^{+0.81} _{-0.16}	27.8±3.0	1.60±0.35	16.2	Lie16
XRF 141026A	-	139.48	-2.33±0.09	-1.99	123.9±7.3	1.43±0.18	0.9 ^{+0.7} _{-0.2}	Lie16
XRF 150120B	-	24.34	-2.24±0.13	-2.22	50.1±4.7	1.36±0.22	-	-
XRF 150201A	-	26.59	-2.35±0.13	-0.98 ^{+0.84} _{-0.45}	69.7±6.3	1.80±0.42	27.3 ^{+4.4} _{-13.5}	Lie16
XRF 150720A	-	238.54	-2.48±0.19	-1.98 ^{+0.83} _{-0.01}	70.6±13.4	1.47±0.57	1.2 ^{+13.0} _{-0.4}	Lie16
XRF 150821A	0.755	168.94	-1.93±0.17	0.61 ^{+1.49} _{-0.93}	71.3±9.2	1.45±0.38	42.1 ^{+7.1} _{-4.5}	Lie16
XRF 150901A	-	64.00	-2.59±0.25	-1.87	45.6±6.6	1.57±0.45	5.8	Lie16
XRF 150915A	1.968	160.00	-2.47±0.21	-1.92	71.9±13.4	1.39±0.51	4.9	Lie16
XRF 151023A	-	10.76	-2.25±0.12	-1.36 ^{+0.64} _{-0.39}	24.3±2.0	1.46±0.23	27.3	Lie16
XRF 151029A	1.423	8.95	-2.18±0.10	-0.28 ^{+0.65} _{-0.51}	38.0±2.8	1.76±0.33	34.0 ^{+3.0} _{-3.4}	Lie16
XRF 160117B	0.87	11.54	-2.29±0.11	-1.78 ^{+0.55} _{-0.11}	31.7±2.5	1.40±0.22	16.1 ^{+11.8} _{-7.8}	Lie16
XRF 160501A	-	-	-2.28±0.12	-0.64 ^{+0.79} _{-0.61}	53.8±4.5	1.77±0.36	31.3	Lie16
XRF 160525A	-	-	-2.62±0.27	0.93 ^{+3.11} _{-1.29}	16.7±2.4	6.50±5.47	25.3 ^{+3.5} _{-3.8}	Lie16
XRF 160827A	-	14.05	-2.14±0.15	0.24 ^{+1.29} _{-0.87}	33.0±3.5	1.88±0.52	35.6 ^{+4.2} _{-5.5}	Lie16
XRR 041219B	-	9.86	-2.03±0.16	-2.17 ^{+0.51} _{-0.17}	26.2	1.05±0.26	72.2	Lie16
XRR 041220	-	5.58	-1.67±0.06	-1.53 ^{+0.25} _{-0.13}	36.1±1.6	0.80±0.05	155.3±43.7	Lie16
XRR 041224	-	177.56	-1.73±0.03	-0.98±0.13	855.1±17.2	0.84±0.03	68.9 ^{+5.8} _{-3.4}	Lie16
XRR 041228	-	56.30	-1.59±0.04	-1.59 ^{+0.07} _{-0.04}	357.4±10.6	0.75±0.04	-	-
XRR 050223	0.584	22.68	-1.82±0.08	-1.46±0.33	62.7±3.8	0.92±0.08	68.1	Lie16
XRR 050315	1.95	95.40	-2.09±0.04	-1.77 ^{+0.18} _{-0.09}	307.9±8.4	1.09±0.05	33.9 ^{+6.6} _{-14.3}	Lie16
XRR 050318	1.4436	16.12	-1.89±0.05	-1.03±0.20	104.4±3.7	1.04±0.06	49.2 ^{+4.7} _{-3.0}	Lie16
XRR 050319	3.2425	151.58	-1.93±0.09	-1.62 ^{+0.37} _{-0.28}	129.0±8.6	1.00±0.10	51.4±24.6	Lie16
XRR 050410	-	64.00	-1.62±0.04	-0.81±0.18	434.9±12.4	0.78±0.03	75.6 ^{+10.5} _{-5.1}	Lie16

Table 2—Continued

GRB Name	z	T_{90} (s)	α_{PL}	α_{CPL}	$S(15-150 \text{ keV})$ ($10^{-8} \text{ erg cm}^{-2}$)	SR	E_{peak}^{obs} (keV)	Ref
XRR 050418	-	81.76	-1.67±0.03	-1.28±0.12	510.2±10.0	0.79±0.02	98.2 ^{+38.5} _{-10.1}	Lie16
XRR 050421	-	8.41	-1.67±0.22	-0.43 ^{+1.53} _{-0.85}	8.4±1.4	0.90±0.25	58.1±22.4	Lie16
XRR 050502B	5.2	17.72	-1.58±0.07	-1.15 ^{+0.31} _{-0.24}	45.1±2.5	0.78±0.06	89.8±15.0	Lie16
XRR 050507	-	15.00	-1.60±0.10	0.53 ^{+0.69} _{-0.53}	27.3±2.3	0.90±0.25	55.5 ^{+6.8} _{-4.1}	Lie16
XRR 050509A	-	10.51	-2.09±0.08	-2.09±0.08	33.5	1.23±0.11	-	-
XRR 050509B	0.2249	0.02	-1.28±0.20	2.19 ^{+3.37} _{-1.36}	0.6±0.1	0.75±0.18	58.9 ^{+20.0} _{-5.3}	Lie16
XRR 050525A	0.606	8.84	-1.78	-1.03±0.05	1513.1±10.0	0.79±0.01	80.4 ^{+1.7} _{-1.5}	Lie16
XRR 050607	-	48.00	-1.92±0.09	-1.80 ^{+0.42} _{-0.24}	60.3±3.9	0.96±0.10	73.4 ±36.7	Lie16
XRR 050701	-	21.70	-1.68±0.04	-1.57 ^{+0.17} _{-0.09}	134.7±3.9	0.81±0.03	186.2	Lie16
XRR 050713A	-	124.67	-1.53±0.04	-1.41 ^{+0.14} _{-0.08}	508.2±11.7	0.72±0.03	252.6	Lie16
XRR 050715	-	187.00	-1.66±0.07	-1.66 ^{+0.14} _{-0.29}	178.3±8.0	0.78	-	-
XRR 050721	-	104.70	-1.86±0.09	-1.09 ^{+0.48} _{-0.39}	373.8±24.9	0.97±0.10	54.4 ^{+258.2} _{-6.6}	Lie16
XRR 050724	0.257	98.68	-1.93±0.10	-2.02 ^{+0.29} _{-0.14}	89.0±14.8	0.94±0.15	11.5	Lie16
XRR 050801	1.38	19.57	-2.00±0.12	-2.03 ^{+0.56} _{-0.05}	31.1±2.5	0.99±0.13	36.1	Lie16
XRR 050814	5.3	142.85	-1.75±0.08	-0.99 ^{+0.40} _{-0.34}	179.2±11.4	0.90±0.09	61.8 ^{+55.2} _{-6.9}	Lie16
XRR 050906	-	-	-1.66±0.26	2.75 ^{+3.62} _{-1.32}	0.6±0.1	0.78±0.16	57.0 ^{+8.3} _{-7.9}	Lie16
XRR 050908	3.3467	18.28	-1.83±0.08	-0.94 ^{+0.41} _{-0.34}	44.2±2.9	1.02±0.11	50.5 ^{+15.7} _{-4.8}	Lie16
XRR 050911	-	16.24	-1.82±0.14	-1.79 ^{+0.57} _{-0.48}	31.9±3.2	0.88±0.13	-	-
XRR 050915B	-	43.10	-1.89±0.03	-1.37±0.13	340.4±7.1	0.95±0.03	59.4 ^{+7.3} _{-3.6}	Lie16
XRR 050916	-	85.18	-1.79±0.11	-0.93 ^{+0.75} _{-0.49}	104.6±9.7	0.97±0.13	54.7±7.1	Lie16
XRR 050922B	4.5	157.02	-2.11±0.13	-1.82 ^{+0.56} _{-0.31}	229.7±21.2	1.14±0.18	25.0±11.8	Lie16
XRR 051001	2.4296	190.26	-2.02±0.07	-1.63±0.26	168.8±8.6	1.08±0.09	39.9±15.7	Lie16
XRR 051012	-	12.80	-2.11±0.10	-1.31 ^{+0.55} _{-0.43}	25.0±1.9	1.27±0.18	34.2 ^{+7.7} _{-17.0}	Lie16
XRR 051016A	-	21.00	-1.74±0.12	-1.47 ^{+0.58} _{-0.35}	82.7±7.0	0.85±0.12	95.6	Lie16
XRR 051021B	-	46.51	-1.54±0.07	-0.48 ^{+0.36} _{-0.31}	81.9±4.5	0.78±0.06	68.7 ^{+15.9} _{-5.9}	Lie16
XRR 051113	-	93.30	-1.69±0.07	-1.49 ^{+0.37} _{-0.13}	255.1±11.5	0.81±0.06	130.0±31.5	Lie16
XRR 051117A	-	140.63	-1.82±0.03	-1.53±0.13	429.9±9.5	0.89±0.03	80.4 ^{+112.5} _{-9.2}	Lie16
XRR 051117B	-	9.02	-1.54±0.15	-0.54 ^{+0.74} _{-0.56}	16.4±1.9	0.77±0.13	70.8±10.6	Lie16
XRR 051213	-	71.06	-1.60±0.10	-0.74 ^{+0.50} _{-0.40}	73.6±5.8	0.83±0.10	66.6 ^{+103.7} _{-8.4}	Lie16
XRR 060108	2.03	14.22	-2.0±0.08	-2.01 ^{+0.31} _{-0.05}	37.2±2.0	1.00±0.09	30.4	Lie16
XRR 060109	-	115.59	-1.89±0.12	-1.31 ^{+0.55} _{-0.43}	62.1±5.8	1.02±0.15	50.2±20.2	Lie16
XRR 060110	-	21.34	-1.63±0.04	-1.59 ^{+0.12} _{-0.06}	150.0±3.3	0.78±0.03	-	-
XRR 060111A	-	13.21	-1.62±0.03	-0.88±0.14	119.7±2.9	0.80±0.03	73.9 ^{+8.5} _{-4.6}	Lie16
XRR 060115	3.5328	139.09	-1.70±0.06	-1.01±0.24	171.1±7.5	0.87±0.05	66.1 ^{+21.2} _{-6.1}	Lie16
XRR 060124	2.3	13.42	-1.81±0.09	-1.74 ^{+0.39} _{-0.32}	46.1±3.0	0.89±0.09	148.5	Lie16
XRR 060202	0.783	192.88	-1.77±0.06	-1.77 ^{+0.11} _{-0.06}	224.7±8.4	0.85±0.02	-	-
XRR 060203	-	69.52	-1.60±0.11	-1.47 ^{+0.55} _{-0.18}	90.5±6.9	0.76±0.09	198.8	Lie16
XRR 060206	4.0559	7.55	-1.66±0.04	-1.12±0.15	84.2±2.2	0.81±0.03	80.7 ^{+19.4} _{-7.0}	Lie16
XRR 060211A	-	126.46	-1.75±0.06	-0.94±0.23	157.6±7.0	0.92±0.06	58.7 ^{+11.1} _{-4.6}	Lie16
XRR 060211B	-	27.73	-1.53±0.10	-1.19 ^{+0.42} _{-0.25}	43.2±3.3	0.74±0.08	117.0	Lie16
XRR 060223A	4.41	11.32	-1.69±0.06	-1.05±0.23	63.9±2.7	0.85±0.05	69.9 ^{+30.2} _{-7.0}	Lie16
XRR 060223B	-	10.36	-1.47±0.03	-1.44±0.05	84.3±4.3	1.02±0.16	-	-
XRR 060306	1.559	60.94	-1.76±0.05	-1.25±0.19	205.4±7.0	0.88±0.04	69.4 ^{+34.5} _{-6.8}	Lie16
XRR 060312	-	44.66	-1.82±0.04	-1.35±0.16	183.7±5.0	0.92±0.04	64.7 ^{+19.1} _{-5.4}	Lie16
XRR 060322	-	229.47	-1.56±0.04	-1.07±0.15	521.5±13.3	0.75±0.03	96.8 ^{+34.3} _{-10.0}	Lie16

Table 2—Continued

GRB Name	z	T_{90} (s)	α_{PL}	α_{CPL}	$S(15-150 \text{ keV})$ ($10^{-8} \text{ erg cm}^{-2}$)	SR	E_{peak}^{obs} (keV)	Ref
XRR 060323	-	23.87	-1.54±0.08	-1.43 ^{+0.28} _{-0.42}	63.2±3.6	0.73±0.06	265.8	Lie16
XRR 060413	-	141.12	-1.66±0.04	-1.53±0.11	351.5±8.3	0.79±0.03	179.3±45.0	Lie16
XRR 060418	1.49	109.08	-1.68±0.03	-1.55±0.08	831.1±14.6	0.80±0.02	182.8±56.3	Lie16
XRR 060421	-	12.00	-1.52±0.04	-1.19±0.14	122.5±3.1	0.72±0.03	126.3 ^{+174.4} _{-18.6}	Lie16
XRR 060424	-	37.68	-1.70±0.09	-1.19 ^{+0.41} _{-0.31}	65.6±4.6	0.85±0.09	73.4±11.6	Lie16
XRR 060427	-	62.00	-1.88±0.14	-1.89±0.30	47.1±5.1	0.96±0.15	-	-
XRR 060428A	-	39.48	-2.02±0.05	-1.71±0.19	135.7±4.7	1.05±0.06	42.0±20.9	Lie16
XRR 060507	-	183.31	-1.81±0.04	-1.45±0.17	398.5±13.4	0.96±0.05	72.4 ^{+108.1} _{-8.2}	Lie16
XRR 060510B	4.941	262.94	-1.77±0.04	-1.59±0.12	391.3±9.8	0.86±0.03	113.8±21.9	Lie16
XRR 060522	5.11	69.12	-1.54±0.07	-0.70 ^{+0.42} _{-0.34}	104.3±6.5	0.78±0.07	73.3 ^{+55.4} _{-8.4}	Lie16
XRR 060526	3.2213	298.04	-1.96±0.11	-1.97±0.51	122.4±10.0	0.97±0.11	24.9±5.0	Ama08
XRR 060604	2.1357	96.00	-2.05±0.21	-2.12 ^{+0.87} _{-0.07}	37.9±6.1	1.03	74.5	Lie16
XRR 060605	3.773	79.84	-1.52±0.10	-0.88 ^{+0.48} _{-0.38}	66.3±5.4	0.77±0.08	79.5±12.6	Lie16
XRR 060607B	-	31.58	-1.62±0.06	-1.52 ^{+0.22} _{-0.10}	103.5±7.8	0.97±0.10	229.6	Lie16
XRR 060614	0.1254	109.10	-2.04±0.02	-2.23 ^{+0.01} _{-0.11}	1882.9±69.7	1.15±0.08	98.5 ^{+29.9} _{-1.8}	Lie16
XRR 060707	3.424	66.64	-1.67±0.06	-0.42 ^{+0.34} _{-0.29}	157.7±7.5	0.85±0.06	61.9 ^{+7.5} _{-4.1}	Lie16
XRR 060708	1.92	10.03	-1.64±0.06	-1.22±0.22	48.0± 2.1	0.80±0.05	88.9±12.9	Lie16
XRR 060714	2.7108	116.06	-1.89±0.05	-1.54±0.19	276.9±10.3	0.97±0.05	56.9±6.7	Lie16
XRR 060717	-	3.00	-1.66±0.18	-0.41 ^{+1.38} _{-0.85}	5.8±0.9	0.96±0.24	53.9±6.2	Lie16
XRR 060719	1.532	66.92	-1.89±0.05	-1.67±0.18	150.1±5.3	0.95±0.05	68.6±11.2	Lie16
XRR 060728	-	-	-1.44±0.22	-0.17 ^{+1.35} _{-0.73}	19.6±3.7	0.79±0.59	64.6±12.8	Lie16
XRR 060729	0.5428	113.04	-1.69±0.06	-1.60±0.25	258.5±12.3	0.81±0.06	201.2±68.9	Lie16
XRR 060804	-	18.19	-1.78±0.13	-0.16 ^{+1.68} _{-0.93}	43.7±6.4	1.27±0.36	43.6±4.7	Lie16
XRR 060807	-	54.05	-1.54 ±0.10	-1.40 ^{+0.44} _{-0.17}	85.3±6.2	0.73±0.08	208.7	Lie16
XRR 060825	-	7.98	-1.69±0.03	-1.07±0.14	95.5±2.3	0.84±0.03	71.4 ^{+10.4} _{-4.9}	Lie16
XRR 060904A	2.55	80.06	-1.54±0.02	-1.51 ^{+0.06} _{-0.02}	782.8±8.1	0.73 ±0.01	163.0±31.0	GCN5518
XRR 060904B	0.7029	189.98	-1.66±0.07	-1.23 ^{+0.32} _{-0.24}	164.3±8.8	0.82±0.06	84.1±13.3	Lie16
XRR 060906	3.6856	44.59	-1.98±0.05	-1.55±0.20	220.4±7.9	1.03 ±0.06	47.8 ^{+21.4} _{-9.5}	Lie16
XRR 060912A	0.937	5.03	-1.73±0.04	-1.73±0.04	136.4±3.0	0.83±0.02	-	-
XRR 060919	-	9.00	-1.83±0.09	-0.84 ^{+0.52} _{-0.42}	49.9±3.5	0.98±0.11	53.3 ^{+24.4} _{-5.4}	Lie16
XRR 060923A	2.47	58.49	-1.78±0.11	-0.28 ^{+0.75} _{-0.54}	87.3±7.7	1.02±0.15	50.8 ^{+11.5} _{-4.6}	Lie16
XRR 060927	5.4636	22.42	-1.61±0.04	-0.81±0.17	112.0±3.4	0.81±0.03	70.7 ^{+9.7} _{-4.8}	Lie16
XRR 060929	-	552.96	-1.91±0.21	-1.92±0.34	73.8±20.2	1.02±1.05	-	-
XRR 061002	-	17.63	-1.72±0.10	-1.72±0.10	69.6±4.3	0.82±0.10	-	-
XRR 061004	-	6.26	-1.77±0.04	-1.40±0.18	54.8±1.8	0.88±0.04	74.2 ^{+244.8} _{-9.0}	Lie16
XRR 061006	0.4377	129.79	-1.74±0.08	-1.74±0.08	143.2±6.9	0.83±0.07	-	-
XRR 061019	-	180.38	-1.98±0.18	-1.58 ^{+0.76} _{-0.29}	226.9±28.6	1.05±0.24	44.6	Lie16
XRR 061110A	0.7578	44.51	-1.64±0.06	-1.56 ^{+0.22} _{-0.10}	111.6±4.6	0.79±0.05	240.3	Lie16
XRR 061202	-	94.19	-1.55±0.03	-1.44 ^{+0.13} _{-0.07}	342.1±7.5	0.73±0.02	276.7	Lie16
XRR 061222B	3.355	37.25	-1.96±0.06	-1.31±0.25	215.4±10.1	1.05±0.24	47.3 ^{+10.3} _{-5.7}	Lie16
XRR 070103	2.6208	18.41	-1.89±0.10	-1.22 ^{+0.53} _{-0.41}	30.3±2.7	1.06±0.15	46.6±20.8	Lie16
XRR 070110	2.3521	88.43	-1.57±0.06	-1.57±0.06	164.7±5.4	0.74±0.03	110.4±50.7	Lia15
XRR 070129	2.3384	459.75	-1.99±0.07	-1.63 ^{+0.35} _{-0.26}	288.0±16.7	1.05±0.10	43.5±13.2	Lie16
XRR 070208	1.165	64.00	-1.97±0.18	-1.65 ^{+0.70} _{-0.26}	50.8±6.2	1.00±0.23	51.3±25.0	Lie16
XRR 070219	-	18.00	-1.81±0.11	-1.81 ^{+0.32} _{-0.16}	28.1±2.6	0.86±0.06	-	-

Table 2—Continued

GRB Name	z	T_{90} (s)	α_{PL}	α_{CPL}	$S(15-150 \text{ keV})$ ($10^{-8} \text{ erg cm}^{-2}$)	SR	E_{peak}^{obs} (keV)	Ref
XRR 070223	-	128.00	-1.89±0.06	-1.48±0.23	169.7±8.3	0.98±0.07	54.4±7.2	Lie16
XRR 070306	1.49594	209.24	-1.63±0.04	-1.60 ^{+0.12} _{-0.06}	545.6±13.5	0.77	-	-
XRR 070411	2.9538	115.69	-1.66±0.05	-1.66±0.05	272.4±7.5	0.79±0.03	-	-
XRR 070412	-	33.88	-1.41±0.10	-0.34 ^{+0.54} _{-0.44}	42.4±3.8	0.75±0.09	69.9 ^{+51.7} _{-8.3}	Lie16
XRR 070419B	1.9588	238.01	-1.65±0.03	-1.62 ^{+0.08} _{-0.04}	744.5±10.1	0.79±0.02	27.0 ^{+8.0} _{-9.0}	Lia15
XRR 070429A	-	168.00	-2.10±0.13	-2.18 ^{+0.20} _{-0.28}	78.1±15.9	1.17±0.41	81.8	Lie16
XRR 070429B	0.9023	0.49	-1.65±0.11	-1.10 ^{+0.62} _{-0.36}	6.2±0.6	0.84±0.12	72.9±13.0	Lie16
XRR 070506	2.309	5.99	-1.73±0.09	-0.77 ^{+0.46} _{-0.38}	20.7±1.6	0.95±0.11	55.1 ^{+24.6} _{-5.6}	Lie16
XRR 070509	-	7.83	-2.21±0.11	-1.95 ^{+0.61} _{-0.01}	17.9±1.6	1.27±0.19	6.6±3.1	Lie16
XRR 070517	-	7.82	-1.91±0.12	-1.18 ^{+0.67} _{-0.46}	20.1±2.0	1.07±0.18	46.4	Lie16
XRR 070518	-	5.50	-2.01±0.11	-1.84 ^{+0.54} _{-0.28}	16.4±1.4	1.04±0.16	37.5	Lie16
XRR 070520A	-	48.00	-1.69±0.15	-0.29 ^{+0.82} _{-0.61}	35.7±4.0	0.86±0.15	60.3 ^{+34.3} _{-7.5}	Lie16
XRR 070521	2.0865	38.63	-1.33±0.02	-1.11±0.07	331.2±10.7	0.99±0.04	237.7 ^{+166.0} _{-36.4}	Lie16
XRR 070611	2.0394	13.18	-1.66±0.12	-0.75 ^{+0.83} _{-0.51}	37.2±3.7	0.87±0.13	62.9±6.5	Lie16
XRR 070612A	0.617	365.28	-1.64±0.05	-1.44±0.12	1065.9±33.4	0.79±0.04	137.7	Lie16
XRR 070612B	-	18.00	-1.56±0.06	-1.08±0.23	177.0±7.3	0.74±0.05	100.8 ^{+411.8} _{-14.4}	Lie16
XRR 070616	-	406.88	-1.59±0.02	-1.47±0.07	1949.4±15.0	0.75±0.01	245.0±50.6	Lie16
XRR 070621	-	33.26	-1.53±0.03	-1.48±0.08	440.0±7.8	0.72±0.02	-	-
XRR 070704	-	384.94	-1.65±0.04	-1.57 ^{+0.13} _{-0.07}	589.2±14.0	0.78±0.03	264.3±79.6	Lie16
XRR 070724A	0.4571	0.43	-1.86±0.16	-0.68 ^{+0.91} _{-0.65}	3.0±0.4	0.96±0.23	45.9±8.6	Lie16
XRR 070731	-	2.86	-1.58±0.11	-0.55 ^{+0.63} _{-0.51}	15.3±1.4	0.83±0.11	64.3 ^{+85.5} _{-7.9}	Lie16
XRR 070802	2.4541	15.80	-1.75±0.13	-1.04 ^{+0.75} _{-0.28}	25.9±2.8	0.93±0.15	58.3	Lie16
XRR 070805	-	26.43	-1.73±0.09	-1.73±0.09	55.1±2.9	0.93±0.09	-	-
XRR 070809	0.2187	1.28	-1.66±0.11	-1.43 ^{+0.54} _{-0.22}	7.3±0.5	0.95±0.14	111.1±43.2	Lie16
XRR 070810A	2.17	9.04	-2.05±0.06	-1.37±0.28	62.9±3.0	1.15±0.09	39.0 ^{+5.7} _{-10.9}	Lie16
XRR 070911	-	161.72	-1.71±0.02	-1.67 ^{+0.07} _{-0.03}	1267.7±12.7	0.82±0.01	481.7±161.8	Lie16
XRR 070913	-	2.68	-1.41±0.12	0.72 ^{+1.07} _{-0.70}	14.8±1.5	0.75±0.11	62.3 ^{+15.3} _{-5.8}	Lie16
XRR 070917	-	8.72	-1.50±0.03	-1.41±0.06	123.9±5.9	0.97±0.04	364.5	Lie16
XRR 070920A	-	55.76	-1.60±0.10	-1.16 ^{+0.48} _{-0.21}	49.2±4.2	0.80±0.10	85.9±20.4	Lie16
XRR 070920B	-	22.26	-1.87±0.05	-0.39±0.27	69.5±2.8	1.18±0.14	44.7 ^{+2.6} _{-1.9}	Lie16
XRR 071001	-	57.43	-1.67±0.08	-1.36 ^{+0.18} _{-0.25}	76.0±4.6	0.83±0.07	92.2±18.3	Lie16
XRR 071013	-	75.58	-1.61±0.25	-1.64 ^{+0.17} _{-0.75}	25.0±5.9	0.93±0.33	-	-
XRR 071018	-	273.57	-1.56±0.12	-1.57±0.12	106.0±8.3	0.73±0.07	-	-
XRR 071021	2.452	228.72	-1.66±0.10	-1.65 ^{+0.16} _{-0.44}	137.2±7.9	0.78±0.08	-	-
XRR 071025	5.2	241.30	-1.71±0.03	-1.65±0.06	727.5±12.9	0.82±0.02	295.0	Lie16
XRR 071028A	-	26.86	-1.79±0.12	-0.74 ^{+0.78} _{-0.56}	26.6±2.9	1.05±0.19	49.0±6.2	Lie16
XRR 071118	-	105.60	-1.53±0.14	-1.14 ^{+0.66} _{-0.33}	63.3±7.4	0.75±0.12	99.7	Lie16
XRR 071122	1.14	71.43	-1.62±0.15	-1.42 ^{+0.61} _{-0.25}	60.7±6.4	0.78±0.13	138.9	Lie16
XRR 071129	-	408.08	-1.86±0.07	-1.47±0.24	351.6±18.5	0.96±0.07	59.3±7.2	Lie16
XRR 080121	-	0.32	-1.61±0.23	-1.32 ^{+0.89} _{-0.54}	3.2±0.5	0.79±0.20	107.7	Lie16
XRR 080123	0.495	114.91	-2.07±0.25	-1.98	55.2±8.5	1.06±0.28	8.2	Lie16
XRR 080205	-	106.30	-1.96±0.06	-1.83±0.20	200.4±7.2	0.99±0.07	58.8±24.2	Lie16
XRR 080207	2.0858	292.46	-1.56±0.03	-1.25±0.12	623.1±12.1	0.74±0.04	124.6 ^{+90.2} _{-16.5}	Lie16
XRR 080210	2.6419	42.26	-1.72±0.05	-1.71±0.06	182.4±5.7	0.82	-	-
XRR 080212	-	126.31	-1.51±0.06	-0.23±0.28	301.4±12.9	0.74±0.04	69.9 ^{+8.6} _{-4.5}	Lie16

Table 2—Continued

GRB Name	z	T_{90} (s)	α_{PL}	α_{CPL}	$S(15-150 \text{ keV})$ ($10^{-8} \text{ erg cm}^{-2}$)	SR	E_{peak}^{obs} (keV)	Ref
XRR 080229A	-	64.00	-1.81±0.03	-1.81±0.03	912.9±16.2	0.88±0.03	-	-
XRR 080307	-	124.00	-1.70±0.10	-1.70 ^{+0.27} _{-0.10}	94.4±4.5	0.80±0.05	-	-
XRR 080310	2.42743	363.21	-2.22±0.07	-1.65 ^{+0.38} _{-0.38}	225.7±9.9	1.25±0.10	23.3 ^{+5.7} _{-11.4}	Lie16
XRR 080319A	-	43.62	-1.54±0.06	-1.32 ^{+0.24} _{-0.14}	440.9±16.2	0.73±0.05	167.7	Lie16
XRR 080320	-	13.82	-1.62±0.11	-1.51 ^{+0.45} _{-0.16}	28.0±2.3	0.78±0.09	189.7	Lie16
XRR 080325	1.78	166.74	-1.56±0.08	-1.56 ^{+0.17} _{-0.08}	503.8±22.4	0.75±0.04	-	-
XRR 080409	-	22.66	-2.04±0.09	-0.69 ^{+0.56} _{-0.45}	56.1±3.9	1.28±0.17	40.3±4.5	Lie16
XRR 080411	1.0301	56.33	-1.68±0.01	-1.66±0.02	2645.4±16.1	0.80±0.01	258.1±34.5	Ama08
XRR 080413A	2.433	46.36	-1.53±0.03	-1.43 ^{+0.11} _{-0.07}	349.0±5.9	0.72±0.02	170.1±52.4	Ama08
XRR 080426	-	1.73	-1.91±0.06	-1.75±0.20	36.9±1.5	0.96±0.06	69.8±25.5	Lie16
XRR 080430	0.767	13.87	-1.73±0.04	-1.73±0.08	118.7±2.4	0.83	-	-
XRR 080503	-	176.00	-1.87±0.06	-1.68±0.21	199.2±8.7	0.94±0.06	73.2±28.7	Lie16
XRR 080506	-	152.20	-1.75±0.09	-1.76±0.09	130.5±8.0	0.84±0.05	-	-
XRR 080516	3.2	5.76	-1.82±0.13	-1.56 ^{+0.59} _{-0.35}	26.1±2.4	0.91±0.13	76.6±38.2	Lie16
XRR 080603B	2.6892	59.12	-1.73±0.03	-1.21±0.13	246.4±5.3	0.85±0.03	74.9 ^{+12.9} _{-5.4}	Lie16
XRR 080604	1.4171	77.61	-1.68±0.09	-1.19 ^{+0.42} _{-0.35}	74.4±5.5	0.86±0.09	72.3±11.2	Lie16
XRR 080701	-	17.82	-2.12±0.08	-1.65 ^{+0.35} _{-0.19}	70.0±4.2	1.20±0.12	29.8	Lie16
XRR 080703	-	3.52	-1.45±0.11	-0.42 ^{+0.70} _{-0.50}	19.0±1.9	0.75±0.10	71.5 ^{+214.8} _{-10.2}	Lie16
XRR 080707	1.2322	30.16	-1.70±0.08	-1.70±0.09	62.9±3.5	0.81	-	-
XRR 080723A	-	17.34	-1.72±0.10	-1.43 ^{+0.50} _{-0.24}	33.1±2.8	0.86±0.10	85.5±20.1	Lie16
XRR 080802	-	179.50	-1.67±0.09	-0.98±0.45	123.4±9.6	0.88±0.10	63.3±8.4	Lie16
XRR 080903	-	66.34	-1.66±0.05	-0.93±0.22	118.8±3.7	0.95±0.07	68.0 ^{+17.5} _{-5.7}	Lie16
XRR 080905B	2.3739	120.94	-1.65±0.07	-1.58 ^{+0.28} _{-0.38}	179.7±8.6	0.79±0.06	256.1	Lie16
XRR 080915A	-	26.29	-1.58±0.15	-1.29 ^{+1.20} _{-0.30}	28.0±3.9	0.78±0.10	103.1	Lie16
XRR 080916A	0.6887	61.35	-1.55±0.02	-1.19±0.09	421.8±6.3	0.73±0.02	121.0 ^{+35.2} _{-12.3}	Lie16
XRR 080928	1.6919	233.66	-1.73±0.06	-1.73 ^{+0.12} _{-0.24}	246.0±6.3	0.82±0.03	-	-
XRR 081008	1.9683	187.82	-1.62±0.04	-1.35±0.14	414.7±10.2	0.78±0.03	118.2 ^{+953.0} _{-18.6}	Lie16
XRR 081017	-	-	-1.63±0.12	-1.51 ^{+0.42} _{-0.18}	142.4±11.3	0.77±0.09	201.7	Lie16
XRR 081022	-	157.58	-1.62±0.06	-1.31 ^{+0.25} _{-0.18}	251.2±10.4	0.78±0.05	108.3±20.1	Lie16
XRR 081028A	3.038	284.42	-1.77±0.04	-1.40±0.16	379.6±11.4	0.88±0.04	75.2 ^{+71.3} _{-8.6}	Lie16
XRR 081102	-	50.32	-1.66±0.06	-1.47 ^{+0.26} _{-0.15}	222.3±10.5	0.81±0.05	129.7±32.7	Lie16
XRR 081104	-	64.00	-1.94±0.07	-1.52±0.27	202.9±10.2	1.00±0.08	51.2±18.4	Lie16
XRR 081109A	0.9787	221.49	-1.61±0.04	-1.45 ^{+0.17} _{-0.13}	394.2±11.7	0.77±0.03	169.7±42.3	Lie16
XRR 081118	2.58	53.40	-2.11±0.08	-1.73 ^{+0.33} _{-0.19}	113.3±6.3	1.15±0.11	29.7 ^{+19.9} _{-14.0}	Lie16
XRR 081127	-	17.30	-2.04±0.15	-2.11 ^{+0.36} _{-0.15}	38.4	0.94±0.32	60.6	Lie16
XRR 081128	-	102.32	-1.88±0.04	-0.94±0.20	233.6±7.9	1.03±0.05	49.9 ^{+4.0} _{-2.7}	Lie16
XRR 081203B	-	161.60	-1.69±0.07	-1.69±0.07	184.4±15.1	1.00±0.13	-	-
XRR 081221	2.26	33.91	-1.75±0.01	-1.30±0.06	1888.0±15.1	0.82±0.01	90.4 ^{+6.0} _{-3.8}	Lie16
XRR 081230	2.03	60.69	-1.91±0.08	-1.49 ^{+0.34} _{-0.29}	82.1±4.8	1.00±0.09	52.2±20.0	Lie16
XRR 090107A	-	12.08	-1.64±0.14	0.29 ^{+1.23} _{-0.71}	18.9±2.4	1.10±0.26	48.8 ^{+14.9} _{-5.2}	Lie16
XRR 090113	1.7493	9.10	-1.53±0.05	-1.46±0.12	77.3±2.4	0.73±0.03	394.6	Lie16
XRR 090123	-	137.34	-1.59±0.06	-1.57±0.17	292.6±11.4	0.75±0.04	-	-
XRR 090313	3.3736	83.04	-1.90±0.14	-1.90 ^{+0.46} _{-0.20}	146.6±14.9	0.93±0.13	-	-
XRR 090401A	-	117.00	-1.63±0.02	-1.52±0.07	1108.0±15.5	0.77±0.02	242.7±58.9	Lie16
XRR 090404	2.87	82.02	-2.26±0.04	-1.94 ^{+0.16} _{-0.08}	301.5±7.2	1.24±0.05	8.0 ^{+9.7} _{-3.6}	Lie16

Table 2—Continued

GRB Name	z	T_{90} (s)	α_{PL}	α_{CPL}	$S(15-150 \text{ keV})$ ($10^{-8} \text{ erg cm}^{-2}$)	SR	E_{peak}^{obs} (keV)	Ref
XRR 090407	1.4485	315.47	-1.65±0.14	-1.59 ^{+0.45} _{-0.66}	115.1±11.3	0.78	310.0	Lie16
XRR 090417B	0.345	266.94	-1.81±0.07	-2.30 ^{+0.27} _{-0.07}	190.8±10.7	1.17±0.23	112.9	Lie16
XRR 090418B	-	38.00	-1.68±0.02	-1.55±0.06	1640.9±14.2	0.80±0.01	200.9 ^{+2417.5} _{-34.6}	Lie16
XRR 090422	-	8.48	-1.68±0.14	-1.71 ^{+0.20} _{-0.13}	15.9±2.0	1.00±0.20	-	-
XRR 090423	8.26	10.30	-1.81±0.05	-0.76±0.22	62.4±2.3	0.98±0.05	53.2 ^{+4.7} _{-2.9}	Lie16
XRR 090426	2.609	1.24	-1.84±0.11	-1.11 ^{+0.50} _{-0.40}	17.6±1.4	0.97±0.13	55.1±8.1	Lie16
XRR 090429B	9.38	5.58	-1.89±0.06	-0.54±0.34	32.9±1.7	1.15±0.11	45.3 ^{+4.2} _{-2.7}	Lie16
XRR 090509	-	336.38	-1.70±0.10	-1.33±0.40	320.5±23.0	0.83±0.09	88.5±29.3	Lie16
XRR 090516A	4.109	181.01	-1.67±0.06	-1.67 ^{+0.14} _{-0.25}	928.2±33.6	0.80±0.03	315.0±15.0	Gru13
XRR 090529A	2.625	70.44	-1.99±0.08	-0.87 ^{+0.47} _{-0.39}	93.4±6.0	1.19±0.13	42.1 ^{+5.7} _{-4.2}	Lie16
XRR 090530	1.266	40.46	-1.56±0.08	-1.08±0.27	104.8±6.0	0.76±0.06	92.1±15.3	Lie16
XRR 090531A	-	42.80	-1.58±0.05	-0.94±0.20	154.0±5.8	0.78±0.04	78.6 ^{+26.7} _{-7.8}	Lie16
XRR 090618	0.54	113.34	-1.58±0.01	-1.49±0.04	10890.3±60.5	0.74±0.01	162.0±3.0	Gru13
XRR 090621A	-	219.24	-1.67±0.05	-1.30±0.19	282.9±10.0	0.82±0.04	90.5 ^{+450.6} _{-12.6}	Lie16
XRR 090708	-	8.71	-1.86±0.11	-1.17 ^{+0.48} _{-0.39}	47.3±3.8	0.99±0.13	53.0±8.8	Lie16
XRR 090715B	3	266.40	-1.58±0.03	-1.58 ^{+0.10} _{-0.03}	567.2±11.8	0.75±0.02	134.0±30.0	Gru13
XRR 090728	-	64.00	-1.92±0.13	-1.56 ^{+0.52} _{-0.32}	106.2±9.2	0.98±0.17	55.8±27.9	Lie16
XRR 090813	-	7.14	-1.70±0.06	-1.67±0.21	132.7±4.9	0.81±0.04	-	-
XRR 090814A	0.696	78.06	-1.84±0.10	-1.02±0.39	116.4±8.6	0.99± 0.12	52.4 ^{+47.5} _{-6.3}	Lie16
XRR 090823	-	25.60	-2.26±0.15	-2.35 ^{+0.93} _{-0.15}	19.3±1.9	1.19±0.24	159.7	Lie16
XRR 090904A	-	129.53	-2.01±0.05	-1.67±0.17	289.7±9.8	1.05±0.05	42.4±20.4	Lie16
XRR 090904B	-	64.00	-1.56±0.04	-1.56 ^{+0.07} _{-0.04}	1276.6±26.9	0.75±0.02	-	-
XRR 090912	-	135.52	-1.68±0.05	-0.96±0.20	447.9±15.5	0.84±0.04	69.1 ^{+14.3} _{-5.5}	Lie16
XRR 090929B	-	357.36	-1.81±0.04	-1.64 ^{+0.17} _{-0.12}	570.3±16.8	0.89±0.04	98.1±21.1	Lie16
XRR 091020	1.71	38.92	-1.53±0.03	-1.45 ^{+0.13} _{-0.07}	377.9±7.9	0.72±0.02	187.0±25.0	Gru13
XRR 091026	-	174.00	-1.70±0.07	-1.61±0.26	200.9±10.6	0.82±0.06	183.9±82.1	Lie16
XRR 091029	2.752	39.18	-1.88±0.03	-1.46±0.13	240.5±5.3	0.95±0.03	61.3 ^{+12.5} _{-4.6}	Lie16
XRR 091104	-	107.14	-1.73±0.12	-1.12 ^{+0.62} _{-0.25}	71.1±7.1	0.91±0.13	62.3±18.7	Lie16
XRR 091127	0.49044	6.96	-2.02±0.04	-1.80±0.14	-	1.02±0.06	34.0±1.0	Gru13
XRR 091130B	-	101.76	-2.09±0.07	-1.52 ^{+0.32} _{-0.24}	137.3±7.5	1.19±0.11	34.1 ^{+6.6} _{-14.3}	Lie16
XRR 091208B	1.0633	14.80	-1.76±0.05	-1.58 ^{+0.21} _{-0.14}	316.0±11.1	0.85±0.05	116.1±25.5	Lie16
XRR 091221	-	62.90	-1.58±0.03	-1.55±0.04	565.7±8.2	0.75±0.02	-	-
XRR 100111A	-	14.00	-1.74±0.07	-1.71±0.28	67.4±3.1	0.84±0.06	341.0	Lie16
XRR 100203A	-	11.20	-1.59±0.18	-1.59 ^{+0.60} _{-0.18}	24.5±3.4	0.75	-	-
XRR 100205A	-	25.84	-1.58±0.12	-1.38 ^{+0.56} _{-0.22}	35.6±3.4	0.76±0.10	142.6	Lie16
XRR 100213B	0.604	91.86	-2.29±0.08	-2.28±0.07	122.0	1.25±0.10	-	-
XRR 100302A	4.813	17.95	-1.72±0.10	-1.43±0.32	30.7±2.2	0.85±0.09	90.2±19.9	Lie16
XRR 100316C	-	9.27	-1.57±0.13	-1.49 ^{+0.46} _{-0.17}	18.2±1.5	0.74±0.09	289.9	Lie16
XRR 100424A	2.465	104.00	-1.83±0.06	-1.69±0.22	147.5±7.0	0.91±0.06	95.3±36.9	Lie16
XRR 100427A	-	24.00	-1.71±0.14	-1.00 ^{+0.72} _{-0.46}	23.6±2.5	0.87±0.14	65.5±10.5	Lie16
XRR 100504A	-	97.00	-1.76±0.05	-1.68±0.18	232.2±7.9	0.86±0.04	179.8±57.0	Lie16
XRR 100513A	4.772	83.50	-1.59±0.07	-1.52±0.30	142.0±6.9	0.76±0.05	321.4	Lie16
XRR 100514A	-	23.02	-1.98±0.13	-0.91 ^{+0.68} _{-0.52}	36.4±3.5	1.17±0.20	42.5 ^{+20.5} _{-12.6}	Lie16
XRR 100522A	-	48.00	-1.90±0.05	-1.61±0.17	199.5±6.8	0.96±0.05	60.6±8.0	Lie16
XRR 100526A	-	97.60	-1.84±0.08	-1.84 ^{+0.22} _{-0.49}	231.3±14.6	0.93±0.07	-	-

Table 2—Continued

GRB Name	z	T_{90} (s)	α_{PL}	α_{CPL}	$S(15-150 \text{ keV})$ ($10^{-8} \text{ erg cm}^{-2}$)	SR	E_{peak}^{obs} (keV)	Ref
XRR 100614A	-	225.00	-1.86±0.07	-1.75±0.26	260.8±14.1	0.93±0.07	92.2±44.5	Lie16
XRR 100615A	1.398	38.82	-1.86±0.02	-1.65±0.09	482.1±6.4	0.91±0.02	85.5 ^{+54.0} _{-8.6}	Lie16
XRR 100619A	-	97.70	-1.78±0.03	-1.74 ^{+0.12} _{-0.05}	438.9±7.9	0.86±0.05	337.7±145.5	Lie16
XRR 100621A	0.542	63.55	-1.90±0.01	-1.81±0.05	2041.9±17.8	0.93±0.01	83.0±9.0	Gru13
XRR 100628A	0.102	0.04	-1.25±0.12	2.65 ^{+1.85} _{-0.91}	0.6	0.96±0.35	74.3 ^{+6.1} _{-4.5}	Lie16
XRR 100702A	-	0.51	-1.61±0.08	-1.06±0.31	13.9±0.8	0.77±0.07	87.5±12.7	Lie16
XRR 100704A	-	196.88	-1.70±0.03	-1.65 ^{+0.12} _{-0.04}	582.1±11.2	0.81±0.02	381.8	Lie16
XRR 100719A	-	36.00	-1.68±0.13	-1.68 ^{+0.33} _{-0.12}	53.2±4.3	0.80±0.10	-	-
XRR 100724A	1.288	1.39	-1.92±0.10	-0.51 ^{+0.64} _{-0.52}	14.1±1.2	1.24±0.20	42.5 ^{+7.6} _{-4.1}	Lie16
XRR 100725B	-	173.70	-1.82±0.03	-1.82±0.03	653.9±9.5	0.88±0.01	-	-
XRR 100727A	-	71.90	-1.81±0.06	-1.47±0.21	115.9±5.7	0.91±0.06	69.5±10.5	Lie16
XRR 100728A	1.567	193.38	-1.12±0.01	-1.06±0.01	1089.4±26.7	0.99±0.04	-	-
XRR 100728B	2.106	12.08	-1.54±0.07	-1.34 ^{+0.30} _{-0.16}	165.3±7.6	0.73±0.06	104.0±14.0	Gru13
XRR 100802A	-	487.34	-1.82±0.05	-1.40±0.20	331.7±13.0	0.92±0.05	64.6 ^{+186.9} _{-7.4}	Lie16
XRR 100805A	-	16.74	-1.76±0.12	-1.17 ^{+0.54} _{-0.47}	48.7±4.0	0.88±0.26	68.3±21.1	Lie16
XRR 100823A	-	17.74	-2.17±0.09	-1.82 ^{+0.42} _{-0.11}	39.4±2.7	1.22±0.14	19.8±9.6	Lie16
XRR 100902A	-	428.83	-1.99±0.07	-1.97 ^{+0.23} _{-0.18}	321.5±13.3	0.99±0.07	84.8	Lie16
XRR 100904A	-	31.25	-1.67±0.08	-1.57 ^{+0.31} _{-0.28}	125.8±7.1	0.80±0.07	199.0	Lie16
XRR 100906A	1.727	114.63	-1.72±0.02	-1.72±0.02	1192.0±14.3	0.83±0.02	142.0±60.0	Gru13
XRR 100928A	-	4.16	-1.80±0.14	-1.37 ^{+0.64} _{-0.45}	38.0±3.6	0.88±0.13	73.3	Lie16
XRR 101008A	-	103.50	-1.55±0.12	-1.55±0.12	116.0±10.2	0.73±0.10	-	-
XRR 101020A	-	172.34	-2.07±0.09	-1.61 ^{+0.44} _{-0.26}	243.1±16.0	1.14±0.12	35.2±13.7	Lie16
XRR 101024A	-	18.69	-1.83±0.04	-1.15±0.15	145.4±3.6	0.92±0.03	60.3 ^{+6.1} _{-3.5}	Lie16
XRR 101030A	-	98.67	-1.75±0.04	-1.75±0.04	299.4±7.7	0.84±0.03	-	-
XRR 101219B	0.55185	41.86	-1.77±0.13	-0.88 ^{+0.68} _{-0.50}	236.7±24.6	0.96±0.16	54.8±7.8	Lie16
XRR 101225A	0.847	-	-1.83±0.15	-1.45 ^{+0.67} _{-0.38}	198.4±25.3	0.97±0.20	57.0±24.9	Lie16
XRR 110106A	-	3.00	-1.57±0.14	-1.24 ^{+0.63} _{-0.58}	23.3±2.3	0.76±0.12	110.9	Lie16
XRR 110106B	0.618	43.42	-1.82±0.06	-1.67±0.23	202.0±8.9	0.90±0.06	102.0	Lie16
XRR 110107A	-	77.00	-1.60±0.03	-1.50±0.06	556.1±8.6	0.76±0.02	280.1±82.9	Lie16
XRR 110205A	2.22	249.42	-1.67±0.02	-1.59±0.06	1571.7±21.3	0.80±0.02	263.3±84.1	Lie16
XRR 110208A	-	15.98	-1.94±0.13	-1.02 ^{+0.68} _{-0.51}	21.1±2.1	1.13±0.20	43.7	Lie16
XRR 110210A	-	192.89	-1.77±0.15	-1.73 ^{+0.62} _{-0.52}	87.5±9.5	0.86±0.14	253.1	Lie16
XRR 110212A	-	3.70	-1.94±0.08	-0.79 ^{+0.47} _{-0.38}	23.9±1.5	1.15±0.12	44.2 ^{+6.1} _{-3.7}	Lie16
XRR 110213A	1.4607	48.00	-1.83±0.06	-1.83 ^{+0.13} _{-0.38}	599.7±23.2	0.89±0.04	98.4±8.5	Gru13
XRR 110223A	-	7.00	-1.58±0.16	-0.67 ^{+0.38} _{-0.65}	15.2±2.1	0.84±0.17	65.2±10.7	Lie16
XRR 110223B	-	61.45	-1.65±0.10	-1.65±0.11	61.7±4.1	1.14±0.13	-	-
XRR 110305A	-	12.00	-1.59±0.10	-1.30 ^{+0.38} _{-0.19}	78.1±5.3	0.76±0.07	120.3	Lie16
XRR 110315A	-	87.68	-1.77±0.04	-1.66 ^{+0.16} _{-0.09}	404.2±10.3	0.85±0.03	155.6±40.7	Lie16
XRR 110318A	-	15.96	-1.58±0.03	-1.06±0.11	492.8±9.1	0.75±0.02	94.6 ^{+16.7} _{-7.4}	Lie16
XRR 110402A	-	56.21	-1.56±0.08	-1.29 ^{+0.38} _{-0.21}	319.0±18.0	0.74±0.07	132.7±32.3	Lie16
XRR 110407A	-	155.57	-1.73±0.06	-0.74±0.30	172.4±8.7	0.92±0.07	57.8 ^{+10.9} _{-4.4}	Lie16
XRR 110411A	-	79.40	-2.04±0.04	-1.50±0.15	329.5±8.1	1.08±0.04	41.9 ^{+3.5} _{-4.5}	Lie16
XRR 110412A	-	24.00	-1.54±0.07	-0.78±0.29	166.3±9.3	0.78±0.06	74.8 ^{+40.8} _{-8.5}	Lie16
XRR 110414A	-	153.12	-1.67±0.07	-1.66 ^{+0.23} _{-0.41}	350.0±15.8	0.79±0.07	-	-
XRR 110420A	-	13.87	-2.27±0.03	-1.99 ^{+0.08} _{-0.01}	640.0	1.20±0.04	2.4±1.0	Lie16

Table 2—Continued

GRB Name	z	T_{90} (s)	α_{PL}	α_{CPL}	$S(15-150 \text{ keV})$ ($10^{-8} \text{ erg cm}^{-2}$)	SR	E_{peak}^{obs} (keV)	Ref
XRR 110530A	-	55.73	-1.87±0.14	-1.88	41.4±5.0	0.89±0.13	-	-
XRR 110715A	0.8224	13.00	-1.63±0.01	-1.25±0.06	877.7	0.96	119.8 ^{+13.3} _{-7.5}	Lie16
XRR 110719A	-	41.23	-1.74±0.08	-1.40 ^{+0.34} _{-0.23}	184.8±10.9	0.86±0.08	81.3±11.2	Lie16
XRR 110726A	1.036	5.16	-1.86±0.09	-0.64 ^{+0.48} _{-0.39}	21.8±1.6	1.11±0.14	46.5 ^{+7.8} _{-4.1}	Lie16
XRR 110801A	1.858	385.26	-1.82±0.05	-1.61 ^{+0.20} _{-0.15}	445.2±16.0	0.90±0.05	83.5±14.7	Lie16
XRR 110808A	1.348	40.70	-2.11±0.18	-1.35 ^{+1.30} _{-0.53}	33.6±5.0	1.31±0.56	31.8	Lie16
XRR 110818A	3.36	102.84	-1.58±0.05	-1.47 ^{+0.11} _{-0.23}	396.1±13.4	0.75±0.11	247.5	Lie16
XRR 110820A	-	264.62	-1.99±0.14	-1.99 ^{+0.44} _{-0.51}	82.2±6.6	1.00±0.12	-	-
XRR 110921A	-	32.55	-1.64±0.08	-1.54 ^{+0.29} _{-0.55}	216.2±11.7	0.78±0.07	213.5	Lie16
XRR 111008A	4.9907	62.85	-1.82±0.04	-1.70±0.17	514.7±14.7	0.89±0.04	122.6±29.7	Lie16
XRR 111016A	-	549.00	-1.91±0.06	-1.91±0.12	390.6±14.7	0.93±0.16	-	-
XRR 111022A	-	22.82	-1.73±0.04	-0.93±0.18	191.7±5.9	0.88±0.09	63.7 ^{+8.2} _{-4.0}	Lie16
XRR 111022B	-	83.03	-1.65±0.10	-1.52 ^{+0.44} _{-0.17}	88.5±7.1	0.80±0.09	165.6	Lie16
XRR 111026A	-	3.58	-1.68±0.10	-1.09 ^{+0.52} _{-0.36}	15.7±1.3	0.86±0.10	69.4±11.2	Lie16
XRR 111109A	-	13.00	-1.86±0.13	-1.06 ^{+0.73} _{-0.53}	22.1±2.5	1.06±0.18	47.4±23.6	Lie16
XRR 111121A	-	113.33	-1.61±0.06	-1.61 ^{+0.19} _{-0.06}	215.1±7.4	0.76±0.05	1780.0±300.0	Gru13
XRR 111123A	3.1516	290.00	-1.66±0.03	-1.64 ^{+0.08} _{-0.04}	715.6±12.9	0.79±0.02	-	-
XRR 111201A	-	20.80	-1.67±0.15	-1.68±0.17	29.3	0.99±0.21	-	-
XRR 111204A	-	48.00	-1.83±0.15	-1.83 ^{+0.55} _{-0.62}	47.0±4.5	0.89±0.14	-	-
XRR 111208A	-	168.00	-1.55±0.15	-0.78 ^{+0.70} _{-0.48}	93.0±9.3	0.73±0.12	84.3±15.2	Lie16
XRR 111212A	-	56.30	-1.63±0.09	-0.88 ^{+0.50} _{-0.40}	130.6±9.4	0.82±0.09	71.1±9.4	Lie16
XRR 111215A	-	373.82	-1.60±0.10	-1.16 ^{+0.43} _{-0.22}	260.8±20.5	0.79±0.09	87.9±17.0	Lie16
XRR 111225A	0.297	105.73	-1.75±0.08	-1.30 ^{+0.36} _{-0.26}	119.3±7.5	0.89±0.08	68.2±9.6	Lie16
XRR 111228A	0.71627	101.24	-2.22±0.03	-1.99	805.9±12.0	1.16±0.03	33.8±4.1	Zan16
XRR 111229A	1.3805	25.37	-1.83±0.17	-1.80±0.68	29.4±4.2	0.96±0.07	289.8	Lie16
XRR 120102A	-	38.71	-1.59±0.03	-1.59±0.03	432.8±7.1	0.75±0.02	291.0±33.0	Gru13
XRR 120106A	-	63.50	-1.53±0.08	-1.32±0.18	97.1±6.0	0.73±0.07	154.3	Lie16
XRR 120118B	2.943	20.30	-2.07±0.05	-1.59±0.21	167.4±6.4	1.12±0.07	36.9 ^{+5.9} _{-13.9}	Lie16
XRR 120215A	-	7.92	-1.68±0.10	-1.26 ^{+0.48} _{-0.21}	24.5±2.0	0.84±0.10	78.6±12.9	Lie16
XRR 120219A	1.728	92.53	-1.54±0.11	0.39 ^{+0.19} _{-0.63}	56.5±5.9	0.96±0.16	53.5 ^{+12.3} _{-4.8}	Lie16
XRR 120308A	-	61.26	-1.72±0.06	-1.10±0.25	109.4±5.6	0.88±0.07	65.0 ^{+40.3} _{-7.1}	Lie16
XRR 120311B	-	29.69	-1.94±0.07	-1.24±0.30	104.7±5.3	0.98±0.09	44.9 ^{+13.6} _{-5.1}	Lie16
XRR 120312A	-	14.16	-1.71±0.12	-1.19 ^{+0.62} _{-0.36}	54.8±4.5	0.83±0.11	78.2±13.4	Lie16
XRR 120320A	-	24.98	-1.57±0.09	-0.31±0.42	55.3±4.1	0.82±0.09	63.3 ^{+17.9} _{-6.0}	Lie16
XRR 120326A	1.798	69.48	-1.99±0.04	-1.40±0.15	251.7±6.2	1.05±0.04	46.8 ^{+3.9} _{-3.3}	Lie16
XRR 120328A	-	29.93	-1.87±0.10	-0.88 ^{+0.58} _{-0.45}	42.5±3.6	1.09±0.15	46.6 ^{+30.3} _{-5.2}	Lie16
XRR 120401A	4.5	130.27	-1.71±0.11	-1.16 ^{+0.57} _{-0.37}	87.4±7.9	0.87±0.12	68.5±21.3	Lie16
XRR 120403A	-	1.40	-1.59±0.14	-0.42 ^{+0.76} _{-0.57}	10.0±1.1	0.81±0.14	64.9 ^{+123.4} _{-8.8}	Lie16
XRR 120403B	-	7.28	-1.79±0.16	-1.30 ^{+0.61} _{-0.39}	20.0±2.3	0.91±0.06	65.6±25.2	Lie16
XRR 120404A	2.876	38.72	-1.85±0.07	-1.81 ^{+0.25} _{-0.32}	157.1±6.5	0.91±0.06	226.3	Lie16
XRR 120422A	0.28253	60.35	-1.99±0.22	-2.24 ^{+1.22} _{-0.06}	30.1±7.2	1.14±0.35	97.0	Lie16
XRR 120514A	-	164.34	-1.57±0.05	-1.43 ^{+0.20} _{-0.12}	277.0±9.2	0.74±0.10	209.8	Lie16
XRR 120521C	5.93	27.07	-1.66±0.06	-1.36 ^{+0.23} _{-0.18}	116.8±4.8	0.81±0.05	103.0±18.8	Lie16
XRR 120701A	-	14.16	-0.97±0.05	-0.90 ^{+0.16} _{-0.12}	16.1	0.97±0.30	-	-
XRR 120703A	-	51.70	-1.59±0.04	-1.49 ^{+0.12} _{-0.07}	375.5±8.9	0.75±0.03	262.2	Lie16

Table 2—Continued

GRB Name	z	T_{90} (s)	α_{PL}	α_{CPL}	$S(15-150 \text{ keV})$ ($10^{-8} \text{ erg cm}^{-2}$)	SR	E_{peak}^{obs} (keV)	Ref
XRR 120711B	-	60.10	-1.71±0.15	-0.89 ^{+1.09} _{-0.60}	52.2±7.7	0.96±0.21	55.3±16.6	Lie16
XRR 120714A	-	20.00	-1.67±0.08	-1.13 ^{+0.36} _{-0.30}	85.1±5.5	0.83±0.08	75.1±11.1	Lie16
XRR 120714B	0.3984	157.31	-1.53±0.08	-0.69 ^{+0.41} _{-0.34}	114.9±8.0	0.79±0.19	71.2 ^{+50.9} _{-8.6}	Lie16
XRR 120722A	0.9586	36.32	-2.01±0.12	-2.29±0.33	123.7±13.8	0.92±0.33	118.7	Lie16
XRR 120728A	-	20.98	-1.77±0.06	-1.39±0.22	233.9±9.8	0.86±0.06	80.9±11.6	Lie16
XRR 120729A	0.8	93.93	-1.61±0.04	-1.61 ^{+0.14} _{-0.04}	251.1±6.5	0.76±0.03	175.9±17.6	Can17
XRR 120802A	3.796	50.29	-1.85±0.05	-1.22±0.22	164.2±6.2	0.95±0.05	57.3 ^{+15.0} _{-4.7}	Lie16
XRR 120807A	-	19.88	-1.83±0.15	-1.84 ^{+0.37} _{-0.15}	29.6±3.1	1.02±0.25	-	-
XRR 120811A	-	29.01	-1.96±0.07	-1.96±0.07	75.3±3.1	0.97±0.06	-	-
XRR 120811C	2.671	24.34	-1.99±0.03	-1.33±0.13	284.5±5.7	1.05±0.03	47.3 ^{+2.6} _{-2.4}	Lie16
XRR 120817A	-	28.21	-1.97±0.08	-1.82 ^{+0.34} _{-0.19}	69.5±3.1	1.00±0.08	53.2±25.0	Lie16
XRR 120819A	-	71.02	-1.48±0.11	-0.51 ^{+0.74} _{-0.52}	129.6±11.7	0.73±0.09	76.1±10.7	Lie16
XRR 120907A	0.97	6.08	-1.65±0.09	-0.80 ^{+0.56} _{-0.42}	54.1±4.3	0.87±0.10	63.0 ^{+196.8} _{-7.8}	Lie16
XRR 120911A	-	21.47	-1.72±0.08	-1.07 ^{+0.45} _{-0.35}	99.7±6.8	0.89±0.09	63.5±8.3	Lie16
XRR 120913A	-	36.04	-2.18±0.07	-2.17±0.11	83.6±4.5	1.19±0.10	26.0±4.0	Gru13
XRR 120913B	-	122.59	-1.63±0.02	-1.54±0.06	1101.9±13.9	0.77±0.02	271.2	Lie16
XRR 120918A	-	25.10	-1.60±0.05	-1.00±0.19	298.1±9.6	0.77±0.02	85.9 ^{+28.7} _{-8.4}	Lie16
XRR 120922A	3.1	168.22	-2.00±0.04	-1.58±0.16	530.8±14.5	1.04±0.04	46.1 ^{+7.5} _{-6.8}	Lie16
XRR 120923A	7.84	26.08	-1.80±0.12	0.30 ^{+0.99} _{-0.69}	32.2±3.1	1.28±0.24	44.5 ^{+6.9} _{-3.5}	Lie16
XRR 120927A	-	35.06	-1.63±0.04	-0.66±0.18	231.3±6.8	0.81±0.03	67.8 ^{+6.5} _{-3.8}	Lie16
XRR 121014A	-	80.00	-1.87±0.09	-1.87 ^{+0.11} _{-0.33}	107.2±6.6	0.91±0.05	-	-
XRR 121017A	-	4.61	-1.75±0.09	-1.29 ^{+0.41} _{-0.29}	62.7±4.2	0.88±0.09	69.9±9.8	Lie16
XRR 121027A	1.773	80.09	-1.81±0.05	-1.58 ^{+0.21} _{-0.17}	194.6±8.6	0.96±0.06	82.5±16.2	Lie16
XRR 121028A	-	2.88	-1.71±0.08	-1.40 ^{+0.36} _{-0.22}	32.7±1.9	0.84±0.07	91.8	Lie16
XRR 121102A	-	54.68	-1.86±0.04	-1.73±0.16	202.3±6.1	0.92±0.04	99.6±21.9	Lie16
XRR 121123A	-	326.09	-1.72±0.02	-0.99±0.10	1242.7±18.2	0.84±0.02	69.9 ^{+4.0} _{-2.7}	Lie16
XRR 121128A	2.2	23.43	-1.86±0.02	-1.32±0.09	583.0±7.6	0.91±0.02	64.9 ^{+4.2} _{-2.7}	Lie16
XRR 121201A	3.385	38.00	-1.87±0.08	-1.83±0.29	71.6±4.2	0.92±0.08	192.9±92.8	Lie16
XRR 121202A	-	19.54	-1.60±0.05	-0.90±0.23	106.4±4.4	0.79±0.05	76.0 ^{+27.4} _{-7.5}	Lie16
XRR 121211A	1.023	182.70	-2.26±0.13	-2.47 ^{+0.45} _{-0.14}	116.0±18.1	1.27±0.37	182.0	Lie16
XRR 121217A	3.1	778.09	-1.54±0.04	-1.50 ^{+0.14} _{-0.06}	616.4±15.8	0.73±0.03	183.9±56.1	Lia15
XRR 121226A	-	1.01	-1.50±0.14	-1.52±0.14	8.4±1.5	0.92±0.24	-	-
XRR 130102A	-	132.78	-1.55±0.11	-0.52 ^{+0.58} _{-0.46}	78.3±6.6	0.76±0.09	72.0 ^{+72.4} _{-8.6}	Lie16
XRR 130131A	-	51.52	-2.13±0.16	-1.51 ^{+0.80} _{-0.30}	28.7±3.4	1.25±0.28	30.8±12.3	Lie16
XRR 130206A	-	121.00	-1.59±0.08	-1.59 ^{+0.28} _{-0.08}	197.8±9.7	0.75±0.06	132.6 ^{+34.0} _{-34.0}	Gru13
XRR 130211A	-	30.75	-1.85±0.12	-1.69 ^{+0.49} _{-0.31}	64.2±5.7	0.92±0.13	84.7	Lie16
XRR 130215A	0.597	66.22	-1.61±0.07	-1.18±0.24	529.0±23.8	0.76±0.06	101.6±16.9	Lie16
XRR 130306A	-	272.38	-1.75±0.02	-1.56±0.10	2928.6±43.5	0.84±0.02	124.4 ^{+1950.3} _{-19.0}	Lie16
XRR 130313A	-	0.17	-1.51±0.17	-1.35±0.75	1.8±0.3	0.92±0.23	209.7	Lie16
XRR 130315A	-	230.51	-1.73±0.04	-1.34±0.17	438.7±12.9	0.84±0.04	83.6 ^{+95.5} _{-9.9}	Lie16
XRR 130327A	-	6.37	-2.17±0.16	-2.32 ^{+0.50} _{-0.14}	22.7	1.04±0.19	134.2	Lie16
XRR 130418A	1.218	274.92	-2.07±0.08	-1.29 ^{+0.50} _{-0.35}	162.3±11.5	1.23±0.15	36.1 ^{+8.0} _{-17.2}	Lie16
XRR 130427B	2.78	25.90	-1.63±0.08	-1.13 ^{+0.35} _{-0.28}	139.6±8.1	0.80±0.07	82.9±12.8	Lie16
XRR 130502A	-	7.57	-1.86±0.13	-1.74 ^{+0.55} _{-0.30}	42.6±3.8	0.92±0.12	99.1	Lie16
XRR 130504A	-	120.03	-1.61±0.09	-0.96 ^{+0.41} _{-0.34}	112.6±7.5	0.80±0.08	76.1±10.5	Lie16

Table 2—Continued

GRB Name	z	T_{90} (s)	α_{PL}	α_{CPL}	$S(15-150 \text{ keV})$ ($10^{-8} \text{ erg cm}^{-2}$)	SR	E_{peak}^{obs} (keV)	Ref
XRR 130505A	2.27	89.34	-1.71±0.07	-1.71±0.06	351.9±13.9	0.81±0.04	631.0±31.0	Gru13
XRR 130508A	-	42.91	-1.85±0.12	-1.19 ^{+0.82} _{-0.49}	56.0±6.7	1.04±0.20	48.5	Lie16
XRR 130514A	3.6	214.19	-1.76±0.03	-1.64±0.08	891.2±14.2	0.84±0.02	165.5±37.2	Lie16
XRR 130515A	-	0.30	-0.77±0.09	-0.33 ^{+0.45} _{-0.28}	0.7	1.20	233.6	Lie16
XRR 130528A	1.25	640.00	-1.55±0.05	-1.46 ^{+0.18} _{-0.09}	563.0±17.5	0.74±0.03	295.3	Lie16
XRR 130529A	-	87.59	-1.61±0.07	-1.20 ^{+0.31} _{-0.24}	120.2±7.1	0.80±0.07	88.9±15.4	Lie16
XRR 130603A	-	69.13	-1.84±0.06	-1.71 ^{+0.23} _{-0.12}	176.1±7.9	0.84±0.06	104.2	Lie16
XRR 130604A	1.06	76.28	-1.63±0.07	-1.63±0.07	157.1±6.7	0.77±0.05	-	-
XRR 130605A	-	10.18	-1.62±0.09	-0.93 ^{+0.42} _{-0.35}	217.5±14.2	0.80±0.08	75.2 ^{+461.7} _{-10.0}	Lie16
XRR 130606A	5.9134	276.66	-1.52±0.06	-1.29 ^{+0.24} _{-0.15}	269.7±12.1	0.73±0.05	150.3±36.2	Lie16
XRR 130609A	-	7.06	-1.88±0.06	-1.28±0.22	54.2±2.3	0.98±0.06	53.9 ^{+14.8} _{-5.0}	Lie16
XRR 130623A	-	17.62	-1.80±0.10	0.82 ^{+0.85} _{-0.62}	71.8±5.8	1.19±0.18	47.1 ^{+4.1} _{-3.0}	Lie16
XRR 130627A	-	18.05	-1.75±0.13	1.08 ^{+0.86} _{-0.67}	69.4±6.8	0.99±0.17	51.9 ^{+5.3} _{-4.0}	Lie16
XRR 130627B	-	48.00	-1.75±0.09	-0.90 ^{+0.48} _{-0.39}	75.8±5.7	0.94±0.11	56.9 ^{+55.9} _{-6.4}	Lie16
XRR 130701A	1.155	4.38	-1.58±0.02	-0.90±0.10	437.6±6.6	0.73±0.02	89.2 ^{+7.7} _{-4.7}	Lie16
XRR 130719A	-	146.97	-1.68 ±0.09	-1.67±0.09	210.4±11.7	0.80±0.07	-	-
XRR 130725A	-	101.52	-1.60 ± 0.15	-1.62 ^{+0.30} _{-0.15}	98.6±8.4	0.77±0.06	-	-
XRR 130727A	-	13.56	-1.65±0.02	-1.42±0.09	378.1±5.4	0.78±0.02	137.8 ^{+163.1} _{-19.7}	Lie16
XRR 130803A	-	43.57	-1.65±0.07	-1.17 ^{+0.35} _{-0.27}	136.2±6.7	0.79±0.06	88.6±13.4	Lie16
XRR 130807A	-	293.04	-1.64±0.07	-0.92 ^{+0.33} _{-0.29}	208.5±10.4	0.81±0.06	72.7 ^{+43.2} _{-7.7}	Lie16
XRR 130816A	-	29.98	-1.86±0.17	-1.52 ^{+0.91} _{-0.35}	39.2±11.2	0.96±0.19	59.1	Lie16
XRR 130816B	-	8.68	-1.83±0.09	-0.34 ^{+0.55} _{-0.44}	24.8±1.8	1.14±0.14	46.2 ^{+6.4} _{-3.4}	Lie16
XRR 130822A	-	0.04	-1.67±0.15	0.45 ^{+1.12} _{-0.78}	1.2±0.1	0.80±0.15	60.3 ^{+13.1} _{-5.5}	Lie16
XRR 130831A	0.4791	30.19	-1.93±0.02	-1.91 ^{+0.09} _{-0.11}	649.7±8.8	0.95±0.02	67.0±4.0	Gru13
XRR 130831B	-	37.58	-1.75±0.10	-0.24 ^{+0.76} _{-0.55}	130.9±11.0	0.98±0.13	53.0 ^{+13.0} _{-4.7}	Lie16
XRR 130919A	-	99.68	-1.51±0.07	-0.39 ^{+0.41} _{-0.34}	136.2±7.9	0.77±0.06	68.5 ^{+17.2} _{-6.0}	Lie16
XRR 130929A	-	12.24	-1.96±0.09	-0.97 ^{+0.48} _{-0.39}	64.7±4.6	1.13±0.14	43.8 ^{+9.0} _{-5.7}	Lie16
XRR 131001A	-	5.00	-1.85±0.06	-0.91±0.28	51.6±2.4	0.99±0.07	52.5 ^{+7.6} _{-3.8}	Lie16
XRR 131002A	-	56.53	-1.62±0.10	-0.54 ^{+0.51} _{-0.42}	51.1±4.2	0.86±0.11	61.9 ^{+29.3} _{-6.7}	Lie16
XRR 131024A	-	112.00	-1.84±0.09	-1.44 ^{+0.43} _{-0.35}	115.4±8.4	0.95±0.10	59.2±10.8	Lie16
XRR 131103A	0.5955	15.21	-1.79±0.09	-1.34 ^{+0.38} _{-0.27}	77.5±5.4	0.92±0.10	63.4±10.1	Lie16
XRR 131110A	-	76.80	-1.67±0.05	-1.39±0.16	336.8±11.1	0.80±0.04	109.0±19.3	Lie16
XRR 131117A	4.042	10.88	-1.81±0.09	0.17 ^{+0.80} _{-0.55}	24.8±2.0	1.26±0.20	44.4 ^{+5.2} _{-3.0}	Lie16
XRR 131128A	-	3.00	-1.81±0.09	-1.11±0.33	30.4±1.8	0.92±0.09	60.9 ^{+68.0} _{-7.2}	Lie16
XRR 131202A	-	30.20	-1.54±0.12	-1.44 ^{+0.50} _{-0.38}	60.4±4.9	0.73±0.09	275.7	Lie16
XRR 131224B	-	8.35	-2.08±0.09	-1.05 ^{+0.51} _{-0.41}	23.5±1.7	1.31±0.19	36.3 ^{+5.5} _{-8.6}	Lie16
XRR 140108A	-	95.23	-1.53±0.02	-1.51 ^{+0.08} _{-0.04}	714.4±8.8	0.72±0.01	-	-
XRR 140114A	3.0	139.95	-2.07±0.04	-1.80 ^{+0.19} _{-0.16}	310.4±9.5	1.08±0.05	32.5 ^{+8.1} _{-13.9}	Lie16
XRR 140118A	-	84.09	-1.87±0.07	-1.36 ^{+0.32} _{-0.27}	243.9±12.2	0.97±0.07	55.6±6.5	Lie16
XRR 140211A	-	109.53	-2.07±0.07	-1.68 ^{+0.32} _{-0.28}	180.3±9.5	1.12±0.10	34.2±14.3	Lie16
XRR 140213A	1.2076	59.93	-1.80±0.02	-1.62±0.08	1182.9±14.0	0.87±0.02	113.7 ^{+158.7} _{-14.9}	Lie16
XRR 140301A	1.416	27.80	-1.96±0.14	-2.03 ^{+0.38} _{-0.17}	42.5	1.03±0.31	14.9	Lie16
XRR 140311A	4.954	70.48	-1.70±0.12	-1.48 ^{+0.53} _{-0.22}	205.9±16.9	0.82±0.10	116.4	Lie16
XRR 140320A	-	0.51	-1.29±0.18	-1.15 ^{+0.59} _{-1.38}	2.1±0.6	0.93±0.31	340.8	Lie16
XRR 140331A	4.65	209.66	-1.96±0.15	-1.42 ^{+0.90} _{-0.47}	66.0±8.4	1.12±0.25	40.6	Lie16

Table 2—Continued

GRB Name	z	T_{90} (s)	α_{PL}	α_{CPL}	$S(15-150 \text{ keV})$ ($10^{-8} \text{ erg cm}^{-2}$)	SR	E_{peak}^{obs} (keV)	Ref
XRR 140412A	-	48.00	-2.03±0.09	-2.27 ^{+0.37} _{-0.07}	71.7±4.1	0.93±0.11	106.3	Lie16
XRR 140428A	-	17.42	-1.54±0.13	-0.40 ^{+0.70} _{-0.53}	30.7±3.3	0.82±0.13	64.4 ^{+98.1} _{-8.4}	Lie16
XRR 140430A	1.6	173.59	-2.01±0.11	-2.11 ^{+0.13} _{-0.23}	110.6±8.9	0.93±0.24	47.6	Lie16
XRR 140502A	-	15.12	-1.22±0.07	-1.23±0.06	23.1±2.3	1.01±0.18	-	-
XRR 140506A	0.889	111.10	-1.56±0.08	-1.45 ^{+0.29} _{-0.53}	265.8±13.5	0.74±0.06	271.0	Lie16
XRR 140509A	-	23.22	-1.59±0.10	-1.24 ^{+0.44} _{-0.19}	120.1±8.4	0.76±0.08	107.7±25.4	Lie16
XRR 140515A	6.33	23.42	-1.78±0.06	-0.98±0.28	61.9±3.2	0.95±0.07	56.4 ^{+15.6} _{-4.9}	Lie16
XRR 140516A	-	0.26	-1.89±0.16	0.49 ^{+1.37} _{-0.84}	2.7±0.3	1.28±0.32	44.6 ^{+8.0} _{-4.5}	Lie16
XRR 140518A	4.707	60.52	-1.89±0.06	-0.98±0.27	106.4±5.1	1.06±0.08	47.9 ^{+6.3} _{-3.6}	Lie16
XRR 140529A	-	8.14	-1.86±0.05	-1.31±0.21	216.4±7.8	0.94±0.05	60.0 ^{+20.1} _{-5.5}	Lie16
XRR 140607A	-	94.77	-1.74±0.11	-1.72 ^{+0.39} _{-0.50}	210.9±15.0	0.84±0.09	-	-
XRR 140610A	-	93.25	-1.57±0.03	-1.35±0.11	581.7±10.3	0.74±0.01	152.9 ^{+605.0} _{-25.5}	Lie16
XRR 140614B	-	49.87	-2.05±0.13	-0.95 ^{+0.75} _{-0.41}	53.0±5.1	1.26±0.23	38.8	Lie16
XRR 140619A	-	233.05	-1.56±0.02	-1.53 ^{+0.06} _{-0.02}	2121.4±19.8	0.74±0.01	-	-
XRR 140626A	-	16.16	-1.89±0.09	-0.62±0.40	35.3±2.4	1.13±0.13	45.7 ^{+6.4} _{-3.8}	Lie16
XRR 140628A	-	10.54	-1.56±0.04	-1.15±0.18	127.5±4.4	0.76±0.04	100.1 ^{+142.3} _{-13.9}	Lie16
XRR 140629A	2.275	38.27	-1.85±0.05	-1.33±0.21	219.8±8.3	0.94±0.05	60.9 ^{+27.8} _{-6.0}	Lie16
XRR 140703A	3.14	68.64	-1.70±0.07	-1.70±0.06	388.2±15.5	0.81±0.05	-	-
XRR 140706A	-	47.84	-1.75±0.05	-1.43±0.18	189.8±6.2	0.86±0.04	84.7±11.8	Lie16
XRR 140709A	-	105.19	-1.64±0.03	-1.28±0.12	542.2±10.5	0.78±0.02	103.8 ^{+48.6} _{-11.5}	Lie16
XRR 140710A	0.558	3.00	-2.04±0.11	-0.96 ^{+0.64} _{-0.50}	20.9±1.8	1.24±0.20	39.6	Lie16
XRR 140713A	-	6.02	-1.84±0.07	-1.82±0.23	36.5±1.8	0.90±0.07	296.9	Lie16
XRR 140716A-2	-	124.80	-1.69±0.09	-1.43 ^{+0.37} _{-0.21}	323.1±17.9	0.81±0.08	116.7±45.5	Lie16
XRR 140719A	-	48.00	-1.78±0.14	-0.86 ^{+0.77} _{-0.57}	41.6±4.7	0.97±0.17	53.8±6.1	Lie16
XRR 140719B	-	54.00	-1.72±0.09	-1.03 ^{+0.42} _{-0.35}	122.0±7.9	0.87±0.09	66.5 ^{+423.3} _{-8.3}	Lie16
XRR 140818B	-	31.55	-1.83±0.14	-1.76 ^{+0.59} _{-0.44}	64.6±5.8	0.89±0.13	163.9±81.9	Lie16
XRR 140824A	-	3.08	-1.99±0.10	-2.03 ^{+0.51} _{-0.04}	18.4±1.2	0.98±0.12	29.8	Lie16
XRR 140828A	-	19.15	-1.73±0.06	-0.80±0.29	136.9±6.7	0.90±0.07	59.8 ^{+12.2} _{-4.7}	Lie16
XRR 140907A	1.21	80.00	-1.65±0.04	-1.42±0.13	443.6±10.2	0.79±0.03	129.6±22.9	Lie16
XRR 140916A	-	68.98	-2.14±0.15	-1.13 ^{+0.89} _{-0.52}	139.8±14.1	1.26±0.24	37.0 ^{+12.9} _{-11.8}	Lie16
XRR 140919A	-	152.30	-1.68±0.06	-1.25 ^{+0.25} _{-0.22}	597.2±24.9	0.82±0.05	86.2±12.0	Lie16
XRR 141015A	-	11.00	-1.85±0.18	-1.63 ^{+1.05} _{-0.30}	15.4±2.3	0.95±0.24	66.9	Lie16
XRR 141017A	-	55.81	-1.56±0.03	-1.03±0.13	297.6±6.6	0.74±0.02	94.1 ^{+20.8} _{-8.2}	Lie16
XRR 141020A	-	14.90	-1.81±0.10	-1.32 ^{+0.48} _{-0.38}	41.4±3.4	0.96±0.11	59.8	Lie16
XRR 141109B	-	220.50	-2.18±0.17	-1.94	80.5±9.4	1.18±0.21	10.2	Lie16
XRR 141121A	1.47	481.00	-1.75±0.07	-1.43 ^{+0.32} _{-0.24}	417.3±23.3	0.88±0.07	79.0±15.5	Lie16
XRR 141130A	-	62.86	-1.56±0.04	-1.29 ^{+0.18} _{-0.15}	270.6±8.2	0.75±0.03	129.0±23.8	Lie16
XRR 141205A	-	1.66	-1.18±0.22	3.31±0.68	1.9	1.00	54.2 ^{+2.2} _{-5.7}	Lie16
XRR 141212A	-	0.29	-1.60±0.11	-1.15 ^{+0.47} _{-0.22}	7.2±0.6	0.77±0.10	94.9	Lie16
XRR 141221A	-	36.82	-1.74±0.04	-1.26±0.18	201.9±6.3	0.87±0.04	72.8 ^{+33.8} _{-7.2}	Lie16
XRR 150101A	-	0.06	-1.50±0.92	-1.00	1.5±0.2	0.83±0.20	80.0	Lie16
XRR 150103A	-	49.09	-1.61±0.09	0.03 ^{+0.56} _{-0.45}	82.5±6.4	0.94±0.12	54.2 ^{+8.6} _{-4.2}	Lie16
XRR 150110B	-	10.58	-1.89±0.07	-1.29 ^{+0.31} _{-0.27}	46.3±2.4	1.00±0.08	51.7 ^{+36.9} _{-5.7}	Lie16
XRR 150120A	0.46	1.20	-1.81±0.09	-1.81 ^{+0.30} _{-0.12}	14.5±0.9	0.87±0.08	-	-
XRR 150203A	-	24.44	-1.81±0.06	-1.61 ^{+0.22} _{-0.11}	91.7±3.6	0.89±0.05	89.6±16.1	Lie16

Table 2—Continued

GRB Name	z	T_{90} (s)	α_{PL}	α_{CPL}	$S(15-150 \text{ keV})$ ($10^{-8} \text{ erg cm}^{-2}$)	SR	E_{peak}^{obs} (keV)	Ref
XRR 150204A	-	14.00	-1.61±0.05	-1.55 ^{+0.18} _{-0.08}	87.8±3.0	0.76±0.04	367.6	Lie16
XRR 150213B	-	209.00	-1.74±0.07	-0.65±0.37	289.0±18.6	0.97±0.10	53.6 ^{+12.5} _{-4.6}	Lie16
XRR 150222A	-	15.84	-1.61±0.04	-1.28±0.14	211.9±5.4	0.77±0.03	110.4 ^{+150.4} _{-15.3}	Lie16
XRR 150301B	1.5169	17.14	-1.46±0.04	-1.35 ^{+0.13} _{-0.08}	167.5	1.03	305.9	Lie16
XRR 150302A	-	23.87	-1.69±0.16	-0.93 ^{+1.25} _{-0.64}	23.5±3.5	0.91±0.19	60.4±21.1	Lie16
XRR 150314A	1.758	14.78	-1.08±0.01	-1.00 ^{+0.05} _{-0.02}	417.6±59.1	1.01±0.07	-	-
XRR 150318A	-	87.44	-2.06±0.06	-1.53 ^{+0.24} _{-0.32}	231.0±11.3	1.15±0.09	36.3 ^{+7.0} _{-16.0}	Lie16
XRR 150323A	0.593	149.73	-1.74±0.04	-1.61 ^{+0.15} _{-0.09}	553.7±13.5	0.84±0.03	154.9±38.1	Lie16
XRR 150323C	-	159.66	-1.94±0.15	-0.04 ^{+1.12} _{-0.84}	115.4±13.1	1.28±0.27	43.2 ^{+11.4} _{-7.4}	Lie16
XRR 150402A	-	14.40	-2.28±0.24	-1.89	13.9±2.5	1.26±0.32	10.2	Lie16
XRR 150413A	3.139	243.60	-1.68±0.07	-1.48 ^{+0.27} _{-0.16}	421.4±19.3	0.81±0.06	128.4±31.1	Lie16
XRR 150428B	-	130.95	-1.81±0.05	-0.96±0.22	357.0±12.9	0.93±0.05	58.3 ^{+7.7} _{-3.9}	Lie16
XRR 150527A	-	108.80	-1.71±0.05	-1.41 ^{+0.21} _{-0.17}	310.7±11.4	0.84±0.04	58.6±1.6	Lie16
XRR 150530B	-	3.00	-1.68±0.10	-0.58 ^{+0.57} _{-0.45}	15.8±1.2	0.90±0.11	91.2 ^{+15.1} _{-22.3}	Lie16
XRR 150607A	-	25.99	-1.59±0.05	-0.98±0.19	229.7±7.9	0.77±0.04	84.2 ^{+28.5} _{-8.4}	Lie16
XRR 150615A	-	32.68	-1.80±0.10	-1.80 ^{+0.37} _{-0.10}	61.0±4.2	0.86±0.11	-	-
XRR 150616A	-	608.41	-1.66±0.03	-1.43±0.11	1930.8±34.1	0.79±0.02	131.7 ^{+434.1} _{-20.3}	Lie16
XRR 150626A	-	97.26	-2.03±0.09	-2.12 ^{+0.26} _{-0.05}	136.7±15.1	1.02±0.16	63.8	Lie16
XRR 150710A	-	0.15	-0.64±0.10	-0.40 ^{+0.49} _{-0.21}	0.1	1.00	403.7	Lie16
XRR 150711A	-	70.96	-1.77±0.04	-1.48±0.16	418.7±11.3	0.86±0.04	89.8±12.5	Lie16
XRR 150716A	-	42.57	-1.53±0.05	-1.01 ^{+0.21} _{-0.19}	141.1±4.9	0.74±0.04	94.5 ^{+57.2} _{-11.1}	Lie16
XRR 150722A	-	67.31	-1.84±0.13	-1.84 ^{+0.19} _{-0.56}	51.7±5.6	0.77±0.18	-	-
XRR 150724A	-	280.01	-1.99±0.07	-1.43±0.32	200.1±11.8	1.09±0.10	42.1±17.1	Lie16
XRR 150728A	-	0.83	-2.02±0.24	-2.08 ^{+0.55} _{-0.26}	3.3	0.97±0.13	37.4	Lie16
XRR 150801B	-	408.71	-1.80±0.07	-1.80 ^{+0.16} _{-0.07}	297.8±12.2	0.86	-	-
XRR 150811A	-	31.52	-2.13±0.13	-1.94 ^{+0.50} _{-0.03}	47.5±4.3	1.11±0.20	12.5±5.8	Lie16
XRR 150817A	-	38.00	-1.77±0.02	-1.61±0.09	586.3±7.9	0.85±0.02	123.2 ^{+3961.0} _{-18.9}	Lie16
XRR 150818A	0.282	143.06	-1.87±0.05	-1.88 ^{+0.13} _{-0.04}	428.5±14.9	0.92±0.03	99.8±10.1	Can17
XRR 150819A	-	51.66	-1.73±0.14	-1.17 ^{+0.75} _{-0.53}	44.2±5.0	0.90±0.15	64.1±12.3	Lie16
XRR 150831B	-	6.18	-1.90±0.10	-0.52 ^{+0.67} _{-0.49}	129.1±9.5	1.02±0.12	50.7 ^{+9.0} _{-4.6}	Lie16
XRR 150907B	-	62.02	-1.47±0.09	-0.16 ^{+0.58} _{-0.45}	111.5±8.5	0.76±0.08	67.6 ^{+23.1} _{-6.6}	Lie16
XRR 150911A	-	7.14	-1.93±0.03	-1.02±0.12	206.6±3.8	1.00±0.03	51.6 ^{+2.1} _{-1.7}	Lie16
XRR 150925A	-	122.13	-2.19±0.10	-2.18 ^{+0.73} _{-0.02}	129.7±9.4	1.26±0.17	-	-
XRR 151001B	-	131.52	-2.13±0.13	-1.96	157.0±10.0	1.20±0.18	10.5	Lie16
XRR 151004A	-	137.27	-1.95±0.11	-1.95 ^{+0.46} _{-0.36}	102.2±7.2	0.96±0.10	356.4	Lie16
XRR 151021A	2.33	110.06	-1.52±0.02	-1.52±0.02	2749.3±26.3	0.72	-	-
XRR 151022A	-	117.68	-1.89±0.14	-1.66 ^{+0.82} _{-0.38}	115.3±12.4	0.97±0.17	60.2	Lie16
XRR 151027A	0.81	129.58	-1.54±0.03	-1.55±0.03	422.6±17.1	1.00±0.05	-	-
XRR 151027B	4.063	80.00	-1.82±0.14	-1.66 ^{+0.49} _{-0.31}	145.7±13.2	0.89±0.13	104.5	Lie16
XRR 151118A	-	23.57	-1.71±0.10	-1.28 ^{+0.44} _{-0.20}	44.9±3.6	0.87±0.10	73.4±10.1	Lie16
XRR 151122A	-	36.80	-1.66±0.08	-1.60±0.35	45.3±2.3	0.79±0.06	288.2±135.5	Lie16
XRR 151205B	-	1.44	-1.60±0.16	-1.39 ^{+0.63} _{-0.26}	7.9±0.9	0.78±0.13	132.0	Lie16
XRR 151210A	-	86.96	-1.84±0.07	-1.05±0.33	136.0±8.5	1.01±0.10	50.8 ^{+23.3} _{-5.0}	Lie16
XRR 151215A	2.59	17.85	-1.99±0.16	-1.10 ^{+1.03} _{-0.54}	27.9±3.9	1.22±0.32	39.1	Lie16
XRR 151228B	-	48.00	-1.64±0.04	-1.10±0.15	232.3±6.2	0.80±0.03	82.0 ^{+21.5} _{-7.3}	Lie16

Table 2—Continued

GRB Name	z	T_{90} (s)	α_{PL}	α_{CPL}	$S(15-150 \text{ keV})$ ($10^{-8} \text{ erg cm}^{-2}$)	SR	E_{peak}^{obs} (keV)	Ref
XRR 160104A	-	16.56	-1.76±0.09	-1.02±0.36	37.7±2.9	0.93±0.11	58.0 ^{+140.6} _{-7.4}	Lie16
XRR 160117A	-	137.00	-2.15±0.06	-1.99	309.5±12.1	1.16±0.06	1.2±22.2	Lie16
XRR 160119A	-	120.14	-1.63±0.03	-1.63±0.03	697.5±10.2	0.78±0.02	-	-
XRR 160121A	-	10.50	-1.77±0.06	-1.05 ^{+0.31} _{-0.27}	57.5±2.9	0.92±0.07	59.6 ^{+22.4} _{-5.6}	Lie16
XRR 160123A	-	3.95	-1.51±0.08	-0.57 ^{+0.46} _{-0.37}	32.2±2.3	0.79±0.08	69.6 ^{+40.4} _{-8.0}	Lie16
XRR 160203A	3.52	17.44	-1.94±0.11	-1.78 ^{+0.47} _{-0.26}	97.7±7.3	0.98±0.10	58.5	Lie16
XRR 160225A	-	157.46	-1.57±0.12	-1.16 ^{+0.61} _{-0.31}	153.8±13.0	0.75±0.10	104.1±38.7	Lie16
XRR 160227A	2.38	316.35	-1.55±0.05	-0.75±0.23	312.2±12.7	0.77±0.04	75.5 ^{+18.9} _{-6.7}	Lie16
XRR 160314A	0.726	8.73	-1.53±0.11	-1.53±0.11	27.8	0.72±0.08	-	-
XRR 160321A	-	33.48	-1.89±0.10	-1.15±0.49	49.2±4.0	1.06±0.12	46.8±6.8	Lie16
XRR 160327A	4.99	33.74	-1.84±0.05	-1.84 ^{+0.18} _{-0.05}	137.0±3.8	0.89±0.05	-	-
XRR 160412A	-	32.18	-1.88±0.04	-1.72±0.16	190.6±5.7	0.94±0.04	80.3±14.5	Lie16
XRR 160417A	-	14.55	-1.93±0.12	-1.93±0.41	57.5±5.4	0.95±0.13	-	-
XRR 160425A	0.555	304.60	-2.18±0.09	-1.98±0.28	200.9±10.5	1.14±0.13	5.3	Lie16
XRR 160504A	-	53.96	-1.79±0.09	-1.79 ^{+0.17} _{-0.41}	58.2	0.86±0.10	-	-
XRR 160506A	-	260.53	-2.12±0.12	-1.99 ^{+0.21} _{-0.01}	136.3±22.3	1.18±0.35	3.0	Lie16
XRR 160519A	-	35.62	-1.97±0.13	-1.51 ^{+0.65} _{-0.32}	112.2±10.6	1.05±0.18	45.8	Lie16
XRR 160525B	-	0.29	-1.90±0.18	-0.60 ^{+1.10} _{-0.74}	2.8±0.4	1.15±0.29	45.0	Lie16
XRR 160611A	-	35.12	-1.68±0.06	-1.53±0.13	175.6±7.2	0.80±0.05	160.0	Lie16
XRR 160801A	-	2.85	-1.85±0.11	-1.00 ^{+0.57} _{-0.46}	16.2±1.4	1.01±0.14	51.3±7.1	Lie16
XRR 160804A	0.736	152.74	-1.88±0.03	-1.41±0.11	1092.7±17.7	0.93±0.02	64.2 ^{+6.9} _{-3.6}	Lie16
XRR 160815A	-	8.57	-1.72±0.05	-0.96±0.22	139.4±4.5	0.85±0.04	67.7 ^{+10.8} _{-4.8}	Lie16
XRR 160819A	-	67.20	-1.70±0.03	-1.49±0.11	765.3±12.2	0.81±0.02	133.0 ^{+432.1} _{-20.7}	Lie16
XRR 160821A	-	112.64	-1.53±0.03	-1.47 ^{+0.10} _{-0.05}	718.8±12.6	0.72±0.02	390.0	Lie16
XRR 160821B	0.16	0.48	-1.88±0.07	-0.12 ^{+0.48} _{-0.40}	10.3±0.6	1.15±0.12	46.3 ^{+3.7} _{-2.7}	Lie16
XRR 160824A	-	99.33	-1.62±0.05	-1.60 ^{+0.16} _{-0.06}	252.9±10.2	0.77±0.05	-	-
XRR 160826A	-	52.62	-1.55±0.14	-1.44 ^{+0.58} _{-0.63}	48.0±5.0	0.74±0.11	230.5	Lie16
XRR 161004A	-	1.32	-1.38±0.15	-1.39 ^{+0.14} _{-0.55}	4.3	0.99±0.17	-	-
XRR 161014A	2.823	23.00	-1.44±0.08	-1.18 ^{+0.33} _{-0.17}	103.7±15.0	0.94±0.19	175.2	Lie16
XRR 161017A	2.013	217.05	-1.57±0.03	-1.57 ^{+0.06} _{-0.03}	536.9±8.6	0.74	-	-
XRR 161108A	-	115.84	-1.79±0.08	-1.31 ^{+0.34} _{-0.28}	105.0±6.4	0.91±0.08	65.1±8.9	Lie16
XRR 161113A	-	43.46	-1.75±0.05	-1.71±0.16	153.4±5.0	0.84±0.04	355.5±139.8	Lie16
XRR 161117A	1.549	125.70	-1.83	-1.20±0.06	2021.7±16.3	0.86±0.01	73.1 ^{+2.4} _{-1.9}	Lie16
XRR 161117B	-	152.31	-2.11±0.03	-1.39 ^{+0.14} _{-0.13}	563.9±11.4	1.15±0.04	38.9 ^{+2.2} _{-3.1}	Lie16
XRR 161129A	-	35.54	-1.53±0.03	-1.40 ^{+0.11} _{-0.08}	355.4±6.4	0.72±0.02	243.4±60.5	Lie16
XRR 161202A	-	118.50	-1.57±0.03	-1.3±0.11	850.0±15.1	0.74±0.02	142.6 ^{+207.0} _{-21.9}	Lie16

Note. — α_{PL} is the power-law photon index in the simple power-law model, and the data are derived from Lien et al. (2016). α_{CPL} is the power-law photon index in the cutoff power-law model, and the data are derived from Lien et al. (2016). $S(15-150 \text{ keV})$ is the fluence of (15-150) keV band, and the data are derived from Lien et al. (2016). SR is the fluence ratio of $S(25-50 \text{ keV})/S(50-100 \text{ keV})$. Ref is the reference in which we take E_{peak}^{obs} values: Ama08 refers to Amati, et al. (2008), Ama09 refers to Amati, et al. (2009), Can07 refers to Cano, et al. (2017), Gru13 refers to Grupe et al. (2013), Lia15 refers to Liang et al. (2015), Lie16 refers to Lien et al. (2016), and Zan16 refers to Zaninoni et al. (2016).

Table 3. Statistics of the X-Ray Lightcurve Type for XRFs, XRRs, and C-GRBs

Class	Total Number	Type 0 [fraction]	Type I [fraction]	Type II [fraction]	Type III [fraction]
XRF	34	5 [(14.7 ± 6.6)%]	15 [(44.1 ± 11.4)%]	11 [(32.4 ± 9.8)%]	3 [(8.8 ± 5.1)%]
XRR	201	35 [(17.4 ± 2.9)%]	62 [(30.8 ± 3.9)%]	91 [(45.3 ± 4.7)%]	13 [(6.5 ± 1.8)%]
C-GRB	135	34 [(25.2 ± 4.3)%]	60 [(44.4 ± 5.7)%]	37 [(27.4 ± 4.5)%]	4 [(3.0 ± 1.5)%]

Table 4. Statistical Results of the Association between XRF/XRR and Supernova

Source	z	E_{peak}^{obs} (keV)	Supernova	Grade	Type	E_K	$\log(M^*/M_\odot)$	$\log(Z/Z_\odot)$	SFR
XRF 050416A	0.6528	$14.8^{+3.6}_{-7.0}$...	D	9.19	...	2.32
XRR 050525A	0.606	$80.4^{+1.7}_{-1.5}$	2005nc	B	...	$1.89^{+1.07}_{-0.75}$
XRF 050824	0.8278	80.0	...	E	...	$0.57^{+0.93}_{-0.37}$...	-0.3	...
XRF 060218	0.03342	4.7 ± 0.3	2006aj	A	Ic	1.02 ± 0.23	7.78	-0.53	0.05
XRR 060729	0.5428	201.2 ± 68.9	...	D	...	$2.44^{+1.43}_{-0.99}$
XRR 060904B	0.7029	84.1 ± 13.3	...	C	...	$0.99^{+0.51}_{-0.37}$
XRF 070419A	0.9705	$26.5^{+3.6}_{-11.2}$...	D
GRB 080319B	0.9382	650.6 ± 33.5	...	C	...	$2.27^{+1.91}_{-1.19}$
XRF 081007	0.5295	39.9 ± 9.8	2008hw	B	...	1.90 ± 1.50
XRR 090618	0.54	162.0 ± 3.0	...	C	...	$3.65^{+2.00}_{-1.42}$
XRR 091127	0.49044	34.0 ± 1.0	2009nz	B	Ic	1.35 ± 0.04	8.6	-0.29	0.22
XRF 100316D	0.0591	$9.6^{+9.3}_{-4.3}$	2010bh	A	Ic	1.54 ± 0.14	8.93	-0.39	0.14
XRR 101219B	0.55185	54.8 ± 7.8	2010ma	A/B	Ic	1.0 ± 0.6
XRR 101225A	0.847	57.0 ± 24.9	...	D	...	3.2 ± 1.6
GRB 111209A	0.677	768.8	2011kl	A/B	-0.39	...
XRR 111228A	0.71627	33.8 ± 4.1	...	E
XRR 120422A	0.28253	97.1	2012bz	A	Ic	2.55 ± 0.21	8.95	-0.4	0.4
XRR 120714B	0.3984	$71.2^{+50.9}_{-8.6}$	2012eb	C	Ic
XRR 120729A	0.8	175.9 ± 17.6	...	D/E	8.3	...	6
XRR 130215A	0.597	101.6 ± 16.9	2013ez	B	Ic
GRB 130427A	0.3399	932.9 ± 111.9	2013cq	B	Ic	6.4 ± 0.7	9.32	-0.2	0.9
XRR 130831A	0.4791	67.0 ± 4.0	2013fu	A/B	Ic	1.9 ± 0.9
XRR 150818A	0.282	99.8 ± 10.1	...	B

Note. — Grades are classified by Hjorth & Bloom (2012): (A) Strong spectroscopic evidence; (B) A clear light curve bump as well as some spectroscopic evidence resembling a GRB-SN; (C) A clear bump consistent with other GRB-SNe at the spectroscopic redshift of the GRB; (D) A bump, but the inferred SN properties are not fully consistent with other GRB-SNe or the bump was not well sampled or there is no spectroscopic redshift of the GRB; (E) A bump, either of low significance or inconsistent with other GRB-SNe. Type refers to the supernova explosion type. E_K is the supernova ejecta kinetic energy, in the unit of 10^{52} erg. M^* is the stellar mass of the GRB host galaxy. Z is the metallicity of the GRB host galaxy. SFR is the star formation rate of the GRB host galaxy, in the unit of $M_\odot \text{ yr}^{-1}$.

Table 5. Host Galaxy Properties of XRFs and XRRs

Source	z	E_{peak}^{obs} (keV)	SFR	$\log(M^*/M_{\odot})$	$\log(Z/Z_{\odot})$
XRF 050416A	0.6528	$14.8^{+3.6}_{-7.0}$	2.32	9.19	-
XRF 050824	0.8278	80.0	-	-	-0.3
XRF 060218	0.03342	4.7 ± 0.3	0.05	7.78	-0.53
XRF 061210	0.4095	-	-	9.52	-
XRF 071031	2.692	$2.1^{+187.8}_{-107.5}$	-	-	-1.85
XRF 071227	0.381	35.5 ± 5.3	0.6	10.65	-0.2
XRF 090205	4.6497	$38.4^{+5.0}_{-3.8}$	-	10.83	-
XRF 100316D	0.0591	$9.6^{+9.3}_{-4.3}$	0.14	8.93	-0.39
XRR 050223	0.584	68.1	1.44	9.73	-
XRR 050724	0.257	11.5	-	10.64	-
XRR 060614	0.125	$98.5^{+29.9}_{-1.8}$	0.01	7.95	-
XRR 061006	0.4377	-	0.17	8.86	-
XRR 070306	1.4959	-	13	10.36	-0.29
XRR 070429B	0.9023	72.9 ± 13.0	-	10.42	-
XRR 070612	0.671	137.7	81	-	-0.4
XRR 070724	0.4571	45.9 ± 8.6	15.3	9.92	-
XRR 070802	2.4541	58.3	-	9.85	-
XRR 080123	0.495	8.2	-	10.02	-
XRR 080325	1.78	-	9	10.8	-
XRR 081109	0.979	169.7 ± 42.3	9.9	9.82	-
XRR 090417B	0.345	112.9	-	10.14	-
XRR 090426	2.609	55.1 ± 8.1	-	10.81	-
XRR 091127	0.49044	34.0 ± 1.0	0.22	8.6	-0.29
XRR 100621A	0.542	83.0 ± 9.0	-	8.98	-
XRR 111008A	4.9907	122.6 ± 29.7	-	-	-1.7
XRR 120422A	0.28253	97.0	0.4	8.95	-0.4
XRR 120729A	0.8	175.9 ± 17.6	6	8.3	-
XRR 130606A	5.9134	150.3 ± 36.2	-	-	-1.1

Note. — SFR is star formation rate of GRB host galaxy, in the unit of $M_{\odot} \text{ yr}^{-1}$. M^* is stellar mass of GRB host galaxy. Z is metallicity of GRB host galaxy. All data are taken from GRB Host Studies (GHostS) database.